SEMMELWEIS EGYETEM

DOKTORI ISKOLA

Ph.D. értekezések

3383.

BARTA BÁLINT ANDRÁS

Szív-és érrendszeri betegségek élettana és klinikuma

című program

Programvezető: Dr. Merkely Béla, egyetemi tanár

Témavezetők: Dr. Radovits Tamás, egyetemi tanár

Dr. Oliver Schilling, tudományos főmunkatárs

SEX-SPECIFIC CARDIAC REMODELING AND FUNCTIONAL RECOVERY:
INSIGHTS INTO PROTEOMIC MECHANISMS

Doctoral dissertation

Bálint András Barta MD

Albert-Ludwigs University, Freiburg, Germany
Semmelweis University, Budapest, Hungary

universität freiburg
Semmelweis University

Chair of Doctoral Programme:
Prof. Dr. Béla Merkely, Semmelweis University
Prof. Dr. Andreas Hiltbrunner, University of Freiburg
Supervisors:
Prof. Dr. Tamás Radovits, Semmelweis University
Prof. Dr. Oliver Schilling, University of Freiburg

Freiburg
2026

Doctoral Dissertation

Submitted in March 2026 by

Bálint András Barta MD
Born in Budapest, 7th of July, 1994

For the attainment of the title of Dr. rer. nat.
at the Faculty of Biology
at Albert Ludwig University of Freiburg
Freiburg im Breisgau, Germany

Dean of the Faculty of Biology:	Prof. Dr Sonja-Verena Albers
Chair of the Doctoral Board:	Prof. Dr Andreas Hiltbrunner
Supervisor of the Doctorate:	Prof. Dr Oliver Schilling

for the attainment of the title of PhD
in the framework of the Cardiovascular Disorders: Physiology and Medicine of Ischaemic Circulatory Diseases Program
at the Cardiovascular Medicine and Research Division of the Doctoral College
at Semmelweis University (SU)
Budapest, Hungary

Rector of the University:	Prof. Dr Béla Merkely
Chair of the Doctoral College:	Prof. Dr Zoltán Benyó
Chair of the Research Division:	Prof. Dr. Béla Merkely
Head of the Complex Examination Committee at SU:	Prof. Dr. István Karádi
Members of the Complex Examination Committee at SU:	Prof. Dr. Henriette Farkas
	Prof. Dr. Péter Andréka
Supervisor of the Doctorate:	Prof. Dr. Tamás Radovits

Official reviewers: Dr. Éva Rui-Sanchez

Dr. Balázs Ördög

Declaration

I hereby declare in lieu of oath that I

✓ have prepared the dissertation independently and am responsible for its content.

✓ have accepted and complied with the regulations of the University of Freiburg to ensure honesty in science, have not committed any scientific misconduct and have no previous convictions in relation to scientific work.

✓ accept the doctoral regulations of the Faculty of Biology of the University of Freiburg. In particular, I am aware that before the awarding of the final doctoral degree, I am not entitled to use the title of Dr.

✓ have clearly labelled the works, contributions and intellectual property of all authors.

✓ have prepared this thesis without the unauthorised assistance of third parties and without the use of aids other than those specified. Data and concepts taken directly or indirectly from different sources are labelled with their source. In particular, I have not made use of the paid assistance of mediation or counselling services (doctoral advisors or other persons). No one has received any direct or indirect monetary benefits from me for work related to the content of this dissertation.

✓ if AI was used for the preparation of the dissertation, I have clearly identified the purpose and extent to which it was used and which programmes were used for this purpose.

✓ have not previously submitted the work in the same or a similar form to another examination authority, either in Germany or abroad.

Budapest, 22.03.2026

Bálint András Barta

Contribution to Manuscripts (published or unpublished)

I confirm that I have contributed to the manuscripts as stated in the tables below and have accurately acknowledged contributions by others according to the guidelines of the University of Freiburg and the German Research Foundation (DFG):

Budapest, 01.10.2025 Signature: 

Manuscript 1

Title of the manuscript: Sex-related differences of early cardiac functional and proteomic alterations in a rat model of myocardial ischemia.

I am, X the first author

☐ co-first author

☐ co-author

X corresponding author

☐ co-corresponding author

The manuscript is

X published (peer-reviewed)

☐ published as preprint

☐ not yet published

Writing draft	I have written all parts of the draft version of this manuscript. Tamás Radovits and Oliver Schilling revised it.
Writing the final version	I have written the final version of this manuscript.
Figure 1	All panels in this figure are the result of my work.
Figure 2	All panels in this figure are the result of my work. The help and technical expertise of Mihály Ruppert were invaluable during in vivo pressure-volume analysis.
Figure 3	All panels in this figure are the result of my work.
Figure 4	All panels in this figure are the result of my work. Hormone measurements were performed by our research collaborator Gellért Karvaly.
Figure 5	The panel in this figure are the result of my work.
Table 1	All data in this table is the result of my work. The help and technical expertise of Mihály Ruppert were invaluable during in vivo pressure-volume analysis.
Figure S1	All panels in this figure are the result of my work.
Other contributions	Planning, design, supervision, and project coordination were carried out by Klemens Fröhlich, Tamás Radovits, and Oliver Schilling.

Manuscript 2

Title of the manuscript: Sex similarities and differences in the reverse and anti-remodeling effect of pressure unloading therapy in a rat model of aortic banding and debanding

I am ☐ first author
X co-first author
☐ co-author
☐ corresponding author
☐ co-corresponding author

The manuscript is X published (peer-reviewed)
☐ published as preprint
☐ not yet published

Writing draft	I have written all proteomics-related parts of the draft version of the introduction, methods, results, and discussion of this manuscript. Hemodynamics, histology and PCR results were summarised by Mihály Ruppert. It was revised by Oliver Schilling, Sevil Korkmaz-Icöz, Gábor Szabó, and Tamás Radovits.
Writing the final version	I and Mihály Ruppert wrote the final version of this manuscript.
Figure 1	All panels of this figure are the result of the work by Mihály Ruppert.
Figure 2	All panels of this figure are the result of the work by Mihály Ruppert.
Figure 3	All panels of this figure are the result of the work by Mihály Ruppert.
Figure 4	All panels of this figure are the result of the work by Mihály Ruppert.
Figure 5	All panels in this figure are the result of my work.
Figure 6	All panels in this figure are the result of my work.
Figure 7	All panels in this figure are the result of my work.
Table 1	The table is based on work performed by Mihály Ruppert
Table 2	The table is based on work performed by Mihály Ruppert.
Table 3	The table is based on work performed by Mihály Ruppert.
Table 4	The table is based on work performed by Mihály Ruppert.
Table 5	The table is based on work performed by Mihály Ruppert.
Other contributions	Planning, design, supervision, and project coordination were carried out by Tamás Radovits, Sevil Korkmaz-Icöz, and Gábor Szabó.

Manuscript 3

Title of the manuscript: Myocardial Active Relaxation Mirrors the Myocardial Proteome in Remodelling and Reverse Remodelling

I am
- X first author
- ☐ co-first author
- ☐ co-author
- ☐ corresponding author
- ☐ co-corresponding author

The manuscript is
- X published (peer-reviewed)
- ☐ published as preprint
- ☐ not yet published

Writing draft	I have written all parts of the draft version of this manuscript. It was revised by Tamás Radovits and Oliver Schilling.
Writing final version	I have written the final version of this manuscript
Figure 1	Illustration of the analysis pipeline was prepared by Sylvia Spiesshofer
Figure 2	All panels in this figure are the result of my work.
Figure 3	All panels in this figure are the result of my work.
Figure 4	All panels in this figure are the result of my work.
Figure 5	All panels in this figure are the result of my work.
Figure 6	All panels in this figure are the result of my work.
Figure 7	Interaction networks were visualized by Sylvia Spiesshofer
Figure 8	Correlation subnetworks were visualized by Sylvia Spiesshofer
Figure 9	All panels in this figure are the result of my work.
Other contributions	LASSO analysis pipeline that was applied for feature selection on the proteomic dataset was set up by Eva Brombacher and was futher refined by Niko Pinter. Statistical aspects were supervised by Clemens Kreutz. Tamás Radovits and Oliver Schilling were responsible for planning, design and supervision of the project.

Table of Contents

List of Abbreviations

16-OHE1 – 16 Hydroxyestrone

16OE2 – 16 Ketoestradiol

2-MeE1 – 2 Methoxyestrone

2-MeE2 – 2 Methoxyestradiol

2-OHE1 – 2 Hydroxyestrone

4-MeE2 – 4 Methoxyestradiol

4-OHE1 – 4 Hydroxyestrone

A1BG – Alpha-1-B-glycoprotein

AB – Abdominal Aortic Banding

ACO2 – Aconitase 2 (Mitochondrial)

ACOT2 – Acyl-CoA Thioesterase 2

ACTL6A – Actin-Like Protein 6A

AD – Anderson-Darling (test)

ADInstruments – (company name)

AHSA1 – Activator of Heat-Shock 90 kDa Protein 1

ALDO – Aldosterone

ANOVA – Analysis of Variance

ANXA5 – Annexin A5

APOOL – Apolipoprotein O-Like

ARPC1A – Actin-Related Protein 2/3 Complex Subunit 1A

ARRIVE – Animals in Research: Reporting in Vivo Experiments

ATF3 – Activating Transcription Factor 3

ATP2A2 – Sarcoplasmic/Endoplasmic Reticulum Ca^{2+} ATPase 2 (SERCA2)

ATP5ME – ATP Synthase Fo Complex Subunit e, Mitochondrial

AUC – Area under the ROC Curve

AWTd – Anterior Wall Thickness in Diastole

AWTs – Anterior Wall Thickness in Systole

BCA – Bicinchoninic Acid Assay

BER – Balanced Error Rate

BIP – Binding Immunoglobulin Protein (HSPA5/GRP78)

BSA – Bovine Serum Albumin

BW – Body Weight

C1 – Component 1 (PLS Axis)

C2 – Component 2 (PLS Axis)

CAD – Coronary Artery Disease

CALR – Calreticulin

CAMK2D – Calcium/Calmodulin-Dependent Protein Kinase II Delta

CAVIN2 – Caveolae-Associated Protein 2 (SDR)

CD – Cardiomyocyte Diameter

ChEA3 – ChIP-X Enrichment Analysis Version 3 Algorithm

CISD1 – CDGSH Iron-Sulfur Domain-Containing Protein 1 (mitoNEET)

Co – Control

CO – Cardiac Output

COQ8A – Coenzyme Q8 A (Atypical Kinase COQ8A)

COQ9 – Coenzyme Q9 Homolog

CORT – Corticosterone

CPT2 – Carnitine Palmitoyltransferase 2

CRKL – CRK-Like Proto-Oncogene Adaptor Protein

CSRP3 – Cysteine- & Glycine-Rich Protein 3 (Muscle LIM Protein)

CST3 – Cystatin C

CTSB – Cathepsin B

CVDs – Cardiovascular Disorders

DABP – Diastolic Arterial Blood Pressure

DB – Debanded

DBT – Dihydrolipoamide Branched-Chain Transacylase E2

DDA – Data-Dependent Acquisition

DDX3X – DEAD-Box Helicase 3 X-Linked

DHT – Dihydrotestosterone

DOC – 11-Deoxycorticosterone

dP/dt_{max} – Maximal Rate of Pressure Increase in the LV

dP/dt_{min} – Maximal Rate of Pressure Decrease in the LV

DUSP3 – Dual-Specificity Phosphatase 3

E1 – Estrone

E2 – Estradiol

ECI1 – Enoyl-CoA Δ^3–Δ^2 Isomerase 1

EDPVR – End-Diastolic Pressure–Volume Relationship

EDV – End-Diastolic Volume

EF – Ejection Fraction

EHBP1L1 – EH-Domain-Binding Protein 1-Like 1

ENCODE – Encyclopedia of DNA Elements

ESPVR – End-Systolic Pressure–Volume Relationship

EU – European Union

F-Co – Female Control

F-Isch – Female Ischemic

FDR – False Discovery Rate

FH – Fumarate Hydratase

FLNC – Filamin C

FKBP7 – FK506-Binding Protein 7

FS – Fractional Shortening

GAPDH – Glyceraldehyde-3-Phosphate Dehydrogenase

GO – Gene Ontology

GO:BP – Gene Ontology – Biological Process

GPX4 – Glutathione Peroxidase 4

GSTK1 – Glutathione S-Transferase Kappa 1

H&E / HE – Hematoxylin & Eosin

HEPES – 4-(2-Hydroxyethyl)-1-Piperazineethanesulfonic Acid

HIST2H4 – Histone Cluster 2, H4 (Core Histone H4)

HPLC – High-Performance Liquid Chromatography

HR – Heart Rate

HSP90AA1 – Heat-Shock Protein 90 α Class A Member 1

HSP90AB1 – Heat-Shock Protein 90 α Class B Member 1

HW – Heart Weight

HW/TL – Heart Weight Normalised to Tibia Length

IHC – Immunohistochemistry

IDH2 – Isocitrate Dehydrogenase ($NADP^+$) 2, Mitochondrial

IDH3A – Isocitrate Dehydrogenase 3 (NAD^+) Alpha Subunit

IF – Immunofluorescence

ISO – Isoproterenol

ITGA5 – Integrin Subunit Alpha 5

ITGA9 – Integrin Subunit Alpha 9

JPH2 – Junctophilin-2

KNG2 – Kininogen 2 (T-Kininogen)

KO – Knock-Out

LabChart Pro – (software name)

LC MS/MS – Liquid Chromatography–Tandem Mass Spectrometry

LC-MS/MS – Liquid Chromatography–Mass Spectrometry/Mass Spectrometry

LIFR – Leukaemia Inhibitory Factor Receptor Alpha

Limma – Linear Models for Microarray Data

LMCD1 – LIM & Cysteine-Rich Domains 1

LV – Left Ventricle

LVEDD – LV End-Diastolic Diameter

LVEDP – Left Ventricular End-Diastolic Pressure

LVEDV – LV End-Diastolic Volume

LVESD – LV End-Systolic Diameter

LVESP – Left Ventricular End-Systolic Pressure

LVESV – LV End-Systolic Volume

LVH – Left Ventricular Hypertrophy

LVIDd – LV Internal Diameter in Diastole

LVIDs – LV Internal Diameter in Systole

MAFF – MAF bZIP Transcription Factor F

MAP – Mean Arterial Pressure

MAX – MYC-Associated Factor X

MaxQuant – (software name)

MCODE – Molecular Complex Detection

MI – Myocardial Infarction

M-Co – Male Control

mL/ml – Millilitre

mL/min – Millilitres per Minute

mRNA – Messenger RNA

MRRF – Mitochondrial Ribosome Recycling Factor

MS – Mass Spectrometry

MSstatsTMT – (R package)

M-Isch – Male Ischemic

MYC – MYC Proto-Oncogene, bHLH Transcription Factor

MYH6 – Myosin Heavy Chain 6 (Cardiac α-Myosin)

MYH7 – Myosin Heavy Chain 7 (Cardiac β-Myosin)

MYOD1 – Myogenic Differentiation 1

MYOG – Myogenin

NaCl – Sodium Chloride

NanoDrop 2000 – (instrument name)

NIH – National Institutes of Health

NPPA – Natriuretic Peptide A (Atrial Natriuretic Factor)

NRAP – Nebulin-Related Anchoring Protein

NS – Not Significant

OD – Optical Density

OGDH – Oxoglutarate Dehydrogenase (E1 Component)

OPN / SPP1 – Osteopontin (Secreted Phosphoprotein 1)

O_2 – Molecular Oxygen

P-V / PV – Pressure–Volume

PCCA – Propionyl-CoA Carboxylase A Subunit

PDIA3 – Protein Disulfide Isomerase Family A Member 3

PDLIM4 – PDZ & LIM Domain 4

PDLIM5 – PDZ & LIM Domain 5

PLS – Projection to Latent Structures

PLS-DA – Partial Least Squares Discriminant Analysis

PO – Pressure Overload

POSTN – Periostin

PPI – Protein–Protein Interaction

PRSW – Preload-Recruitable Stroke Work

PSM – Peptide-to-Spectrum Match

PSME1 – Proteasome Activator Subunit 1 (PA28-α)

PVAN – (software name)

qRT-PCR – Quantitative Real-Time Polymerase Chain Reaction

RAP1A – RAS-Related Protein Rap-1A

RAP1B – RAS-Related Protein Rap-1B

RCN3 – Reticulocalbin 3

REST – RE1-Silencing Transcription Factor

RIPA – Radio-Immunoprecipitation Assay Buffer

ROC – Receiver-Operating Characteristic

rpm – Revolutions per Minute

RT – Room Temperature

SABP – Systolic Arterial Blood Pressure

SAVR – Surgical Aortic Valve Replacement

SBP – Systolic Blood Pressure

SD – Standard Deviation

SEM – Standard Error of the Mean

Sham – Sham Operation

SMARCC2 –

SWI/SNF-Related Matrix-Associated Actin-Dependent Regulator of Chromatin Subfamily C Member 2

SMTN – Smoothelin

SORBS2 – Sorbin & SH3 Domain-Containing Protein 2

SPARC – Secreted Protein Acidic & Rich in Cysteine

SPR 838 – (catheter model)

sPLS-DA – Sparse Partial Least Squares Discriminant Analysis

SUCLG2 – Succinate-CoA Ligase GDP-Forming Subunit B, Mitochondrial

SV – Stroke Volume

SW – Stroke Work

TBST – Tris-Buffered Saline Tween 20

TCEP – Tris(2-Carboxyethyl)-Phosphine Hydrochloride

TF – Transcription Factor

TL – Tibial Length

TMOD4 – Tropomodulin 4

TMT – Tandem Mass Tag

TMT 11-plex – Tandem Mass Tag 11-plex

TMT 16-plex – Tandem Mass Tag 16-plex

TMTpro – Tandem Mass Tag Pro

TOF – Time of Flight

TST – Thiosulfate Sulfurtransferase (Rhodanese)

UPL – Universal Probe Library

USF1 – Upstream Transcription Factor 1

VAC – Ventricular-Arterial Coupling

VASP – Vasodilator-Stimulated Phosphoprotein

VEVO 2100 – (imaging system)

VIP – Variable Importance in the Projection

wk – Week

τ (Tau) – Time Constant of LV Pressure Decay

1. Introduction

Cardiovascular disease occupies an unenviable position at the peak of the global mortality table, eclipsing infectious illnesses, cancers, and traumatic injuries. Recent estimates indicate that in 2021, roughly 20.5 million individuals succumbed to one or another manifestation of cardiovascular pathology, approximately one in every three deaths recorded worldwide (1). In most high-income nations, the age-standardised death rate attributable to myocardial infarction, stroke, and heart failure has fallen steadily for more than half a century, a dividend of evidence-based pharmacotherapies, safer surgical techniques, advances in public-health legislation, and aggressive tobacco-control measures (2-4). Nevertheless, due to the rapid ageing of the general population, the aggregate burden continues its relentless rise (2-5). Health-services researchers now estimate the annual direct cost of treating cardiovascular complications in the European Union (EU) at €282 billion, a figure that balloons past $350 billion in the United States when hospitalisations, pharmacotherapy, outpatient care, and rehabilitation are aggregated (3, 5). When productivity losses from premature mortality, and disability are considered, the cost approaches $1 trillion each year. These numbers, however, fail to convey the granular inequities that underlie population averages. Most relevant to the present thesis, outcomes are not evenly distributed between the sexes. Men and women differ not only in their exposure to behavioural risk factors but also—and more importantly—in the biology that governs myocardial development, cardiomyocyte survival, extracellular-matrix architecture, and vascular reactivity (6).

Molecular and epidemiological data substantiate distinct trajectories of cardiovascular pathologies in males and females. From the earliest stages of embryogenesis, XX and XY genomes determine divergent trajectories of cardiac morphogenesis (7, 8). Genes such as Ddx3y and Uty, located on the Y chromosome, encode histone demethylases that modulate chromatin accessibility. In contrast, escapees from X-chromosome inactivation, including Kdm6a and Eif2s3x, confer an epigenetic landscape uniquely permissive to female-specific transcriptional networks (9, 10). Layered atop this chromosomal scaffold, cyclic surges of ovarian steroids during puberty and adulthood influence myocardial phenotype through both genomic and rapid non-genomic signalling pathways. Clinical registries therefore report that women experience their first ST-segment-elevation

myocardial infarction roughly seven to ten years later than men and, on average, manifest obstructive coronary artery disease about a decade later still (6, 11, 12). Yet the apparent female advantage in primary prevention is offset by a disproportionate early-mortality penalty (13) once infarction strikes, a paradox partially attributable to atypical symptomatology—jaw pain, dyspnoea, fatigue, indigestion—that delays presentation and complicates diagnosis, but also driven by intrinsic molecular differences in platelet reactivity, endothelial inflammation, and microvascular dysfunction (14, 15). Moreover, sex-specific differences in myocardial remodeling after myocardial infarction have been observed, with males typically exhibiting cavity dilation, eccentric hypertrophy, and scar thinning. At the same time, females tend to maintain cavity dimensions and stable scar formation, often through concentric hypertrophy (16).

Pressure-overload states, such as aortic stenosis and long-standing systolic hypertension, show similar sex-specific patterns. Whereas male hearts commonly respond to chronic afterload elevation by dilating eccentrically and progressively depressing ejection fraction—a trajectory that culminates in "classic" heart failure with reduced ejection fraction—female hearts more often develop concentric wall thickening, preserved stroke volume, and diastolic stiffness, a phenotype prototypical of heart failure with preserved ejection fraction (HFpEF) (17-19). Women with aortic stenosis tend to have a more concentric LV, with smaller diameters and better-preserved cardiac function than men (20-23). Based on myocardial biopsies from hypertrophied hearts, marked cardiac fibrosis was more prevalent in females (22, 24). Fibrotic infiltration in female myocardium tends to be more homogeneous, while male fibrosis frequently adopts a patchy, replacement-type pattern (25). Transcriptomic profiling corroborates these macroscopic observations by revealing sex-biased signatures in metabolic flexibility, oxidative-stress buffering, immune-cell chemotaxis, and extracellular-matrix remodelling (24, 26). A landmark directive from the U.S. National Institutes of Health (NIH) therefore enjoined grant recipients to "consider sex as a biological variable," obligating modern bench scientists and clinician-investigators to relinquish male-only paradigms that had dominated pre-clinical cardiovascular research for decades (27).

Cardiac remodeling, first coined in the wake of early post-infarction ventricular-aneurysm surgeries, encompasses the entire continuum of structural, functional, and

molecular adaptations that the myocardium deploys in response to pathological stimuli (28). After an acute coronary occlusion, the remodeling cascade unfolds in overlapping phases. Minutes to hours after reperfusion, necrotic cardiomyocytes release danger-associated molecular patterns—DNA fragments, heat-shock proteins, cardiac-specific isoforms of troponin—which recruit neutrophils and monocyte-derived macrophages (29). Matrix metalloproteinases degrade collagen, loosening the pericellular scaffold and enabling inflammatory infiltration (30). Days later, fibroblasts proliferate and transition to myofibroblasts, laying down type I and III collagen that gradually coalesces into an infarct scar (31). Throughout subsequent weeks, surviving myocytes elongate and slide, ventricular cavity volume increases, wall stress rises, and compensatory neuro-humoral circuits—renin-angiotensin-aldosterone, sympathetic adrenergic, natriuretic peptide—activate in an attempt to preserve stroke work. Chronically elevated catecholamines and angiotensin II, however, further aggravate apoptosis, oxidative stress, and mitochondrial dysfunction, locking the heart into a vicious downward spiral (32).

Pressure overload composes a different score. Instead of immediate ischaemic myocyte death, afterload elevation triggers a mechanotransductive signalling web mediated by integrins, stretch-activated ion channels, and sarcomeric Z-disc proteins such as titin (33-35). Within hours, transcriptional complexes centred on nuclear factor of activated T-cells (NFAT), myocyte enhancer factor-2 (MEF2), and histone deacetylases orchestrate a genetic programme that favours sarcomeric protein synthesis, re-expression of foetal myosin heavy-chain isoforms, and hypertrophic growth (36-38). Initially adaptive—because thicker walls normalise Laplacean wall stress—the concentric geometry eventually proves maladaptive if the stimulus persists, as capillary density fails to keep pace with myocyte enlargement, mitochondrial ATP production lags, and interstitial collagen stiffens the chamber (39-41). Remodeling eventually devolves into dilatation, systolic dysfunction, and heart failure (32).

Crucially, the remodeling process is not unidirectional. Decades of surgical and pharmacological innovation have demonstrated that timely unloading can reverse maladaptive changes—a phenomenon now codified as “reverse remodeling” (42). In the pressure-overload state, surgical valve replacement or transcatheter aortic valve implantation immediately drops afterload, allowing wall stress to fall and myocytes to

partially regress in size (43). Likewise, the strategic use of renin-angiotensin system inhibitors, β-blockers, and mineralocorticoid receptor antagonists promotes scar shrinkage, collagen cross-link breakdown, and partial restoration of ejection fraction (44, 45). When unloading is instituted even earlier—before gross structural changes have crystallised—so-called "anti-remodeling" can prevent deleterious hypertrophy altogether (46, 47). Despite their clinical relevance, RR and AR responses vary among patients matched for age, comorbidity, and surgical result, implying that genomic, proteomic, and endocrine determinants have yet to be fully elucidated (48).

Sex steroids loom large among those determinants. Cardioprotection of pre-menopausal women derives in part from the pleiotropic properties of 17β-estradiol (10) (49-52). Classical genomic signalling operates via oestrogen-receptor-α and -β: ligand binding induces receptor dimerisation, nuclear translocation, and transcription of anti-apoptotic and anti-oxidant genes such as Bcl-2, superoxide-dismutase-2, and eNOS (52, 53). Equally important, membrane-bound G-protein-coupled oestrogen receptor-1 (GPER-1) triggers rapid, non-genomic cascades that activate PI3K–Akt and ERK1/2, thereby modulating calcium handling, mitochondrial permeability-transition-pore opening, and nitric-oxide bioavailability within seconds (54-56). Testosterone and its potent derivative dihydrotestosterone (DHT) wield more ambiguous influence. While androgens promote anabolic skeletal-muscle growth, they can accelerate cardiomyocyte hypertrophy, stimulate fibrotic gene expression via the androgen receptor, and potentiate sympathetic nervous-system activity (57-59). Leaving canonical hormones aside, ovarian and adrenal steroidogenesis produces dozens of metabolites—2-hydroxyestrone, 4-methoxyestradiol, 16α-hydroxyestrone—that exhibit distinct receptor affinities (60). Aldosterone and progesterone intersect the remodeling narrative through mineralocorticoid- and progesterone-receptor pathways, exerting context-dependent pro- or anti-fibrotic effects (61, 62). Comprehensive "steroid-omics" therefore promises a panoramic view of the circulating milieu and its intracellular echoes, yet remains strangely under-represented in mainstream remodeling research (63).

The scientific discipline that strives to quantify proteins expressed by a cell, tissue, or organism at a given moment was named proteomics. Whereas genomics identifies what could happen and transcriptomics depicts what the nucleus intends to happen, proteomics

reveals what is actually happening in the cytoplasm, mitochondria, sarcomere, and extracellular matrix (64, 65). Proteins catalyse reactions, transduce signals, generate force, and scaffold the architectural integrity of the heart. State-of-the-art proteomics relies on mass spectrometry (MS) (66) and is pursued via three approaches: top-down, targeted, and bottom-up. In top-down ("native") proteomics, intact proteins are introduced into the mass spectrometer (67). It excels at detecting and characterizing post-translational modifications (PTMs) and can quantify their stoichiometries, but many PTMs yield spectra that are hard to interpret (68). Targeted proteomics quantifies predefined proteins or peptides with high sensitivity and specificity, providing reproducible quantitative data for biomarker validation and diagnostics (69) though it is not comprehensive and demands substantial optimization. In bottom-up proteomics, proteins are enzymatically digested (e.g., LysC, GluC) into peptides, and the peptide mixture is analyzed (66, 70). Before MS, peptides are separated by LC or CE according to hydrophobicity or electrophoretic mobility, then ionized and detected by m/z. Because different sequences can share mass, proteomics employs MS/MS: precursor ions are fragmented and fragment ions measured, yielding spectra that enable peptide-sequence determination (71). During digestion we use proteases (e.g., LysC) that cleave at defined residues (the C-terminal side of lysine), so only peptides with predictable sequences reach the instrument. Identification relies on prior knowledge of peptide and fragment m/z values (in silico predictions or databases). Although digestion creates a more complex sample than intact proteins, peptides lack secondary structure and have more uniform masses, producing clearer peaks and enabling more accurate qualitative and quantitative analyses than with intact proteins (66, 69, 72). Bioinformatics infers protein composition by matching mass spectra of observed peptides to those theoretically generated from known proteins; overlaps support the presence of specific proteins. Proteotypic peptides arise from a single protein and therefore identify it unambiguously (73), whereas shared peptides map to protein groups. Full processing details lie beyond this thesis, but with these principles and statistical controls (e.g., FDR) the sample's protein composition can be determined (66). Advances in nano-flow liquid chromatography coupled to high-resolution Orbitrap tandem mass spectrometry have enabled routine quantification of thousands of distinct proteins per run (74). Isobaric tagging with tandem-mass tags (TMT) or the newer TMT-pro chemistry allows multiplexing of sixteen to eighteen

biological replicates, drastically reducing batch effects and missing values (75). Statistical pipelines—FragPipe, MSFragger, Philosopher—align spectra to reference databases, infer peptide sequences, and roll up quantification to the protein level with stringent false-discovery controls (76). Cardiac proteomics has already illuminated the rewiring of mitochondrial metabolism in end-stage heart failure (77), unveiled unexpected collagen cross-linkers that stiffen failing ventricles (78), and charted sex-specific proteomic fingerprints in hypertrophic cardiomyopathy (65). Yet few investigations link such high-density molecular maps to pre- and afterload independent left ventricular functional profiles, determined by the gold-standard pressure-volume metrics for contractility and relaxation.

Achieving that linkage demands experimental platforms that permit both invasive haemodynamic interrogation and harvest of myocardial tissue under tightly controlled conditions. Rodents—principally mice and rats—offer unparalleled utility in this regard (79). Their diet, housing temperature, and light–dark cycles can be standardised; and their brief lifespans compress longitudinal studies that would span decades in humans (80). The present thesis therefore hinges on two complementary rodent paradigms that recapitulate diffuse ischaemia and pressure overload.

Isoproterenol (ISO), a synthetic β-adrenergic agonist, is administered to rats via subcutaneous injection at doses of 25–85 mg kg-1 day-1 for two consecutive days (81). The supra-physiological catecholaminergic surge precipitates a mismatch between myocardial oxygen (O_2) demand and supply, particularly in the vulnerable sub-endocardial layers endowed with the poorest perfusion reserve. Necrosis is patchy, interspersed with viable fibres and exuberant inflammatory infiltrate, mirroring the diffuse injury pattern observed in stress-induced cardiomyopathy and catecholamine toxicity (82). Unlike permanent coronary-artery ligation, which addresses only a single vascular territory, the ISO model recruits the entire ventricular mass, thereby exposing global remodeling signals and systemic endocrine crosstalk. Moreover, the time course is well known: within six hours, plasma troponin escalates; by forty-eight hours, macrophages supplant neutrophils; day seven heralds granulation; and week four yields a spectrum of hypertrophic, fibrotic, and dilatory phenotypes (83-86).

Pressure overload, by contrast, is induced through abdominal aortic banding (87). Under inhalational anaesthesia, a 22-gauge needle is placed parallel to the infra-renal aorta; a 4-0 silk ligature is tied snugly around both structures; the needle is removed, leaving a calibrated stenosis that raises systolic blood pressure proximal to the band by approximately 50 mmHg. Echocardiography at week six confirms concentric left-ventricular hypertrophy in nearly all banded rats, while sham-operated controls remain normotensive and structurally unremarkable (88). Crucially, the ligature can be surgically excised six weeks later—a manoeuvre termed "debanding"—instantaneously relieving afterload and enabling study of both reverse remodeling (if debanding occurs after hypertrophy has entrenched) and anti-remodeling (if debanding precedes irreversible structural damage) (89). In both models, conductance-catheter pressure–volume analysis under light anaesthesia or conscious restraint quantifies seminal indices: the slope of the end-systolic pressure–volume relationship (ESPVR) and preload-recruitable stroke work (PRSW) gauge contractility independently of loading conditions; the isovolumic relaxation constant, Tau (τ), captures lusitropic efficiency; diastolic stiffness modulus derives from the slope of the end-diastolic pressure–volume relationship (EDPVR); and stroke-work efficiency integrates pressure, volume, and heart-rate variables (79, 90). Echocardiography, Doppler tissue imaging, myocardial strain analysis, and invasive blood-pressure telemetry provide complementary, albeit load-dependent, snapshots of ventricular anatomy and performance (91, 92). The question of whether the distinct adaptation of the LV to PO in females results in a better response to pressure unloading therapy, is an area of active research. Clinical studies on patients undergoing surgical or transcatheter aortic valve replacement (SAVR and TAVR) for aortic stenosis have yielded conflicting results regarding sex-related differences. Some studies suggest that female sex is associated with a greater regression of LVH (93, 94) and myocardial fibrosis (95). The latter study however, has not found a sex-related divergence in the regression of LVH (95). The inconsistency in clinical findings may be due to factors unrelated to the pathophysiology of LVH, such as anatomical differences and comorbidities, particularly coronary artery disease (CAD). CAD is more prevalent in men and can impede myocardial restitution (96). Additionally, female patients with aortic stenosis are often older and have higher aortic valve gradients than their male counterparts (94, 95, 97),

further confounding comparisons. Whether male or female patients could potentially benefit more from TAVR/SAVR is thus still up for debate (98, 99).

Robust as these methodologies appear, some limitations still apply. Rodents possess a basal heart rate exceeding 350 beats per minute, accelerate to 600 bpm under stress, and exhibit a myocardial extracellular-matrix composition richer in glycosaminoglycans than humans (100-102). Their endocrine cycles—oestrogen surges every four to five days—diverge from the monthly fluctuations of pre-menopausal women (103). Anaesthesia can prolong ventricular relaxation, depress contractility, and modify systemic vascular resistance; yet open-chest surgery without anaesthesia is ethically untenable (104). Genetic homogeneity, while beneficial for reducing variance, obscures the polygenic complexity of human populations (105). Nevertheless, the strategic integration of multiple read-outs—haemodynamics, histology, omics—across both sexes mitigates these caveats and promises translational insights unattainable by a single technique.

Gaps in our current understanding are still prevalent. First, the field lacks an integrated, sex-stratified analysis of haemodynamics, proteomics, and steroid-omics in the immediate aftermath of global ischaemia. The earliest hours are a decisive for molecular fate: decisions concerning apoptosis versus necrosis, glycolysis versus fatty-acid oxidation, and resolution versus propagation of inflammation are made rapidly and may differ between sexes. Second, no study has juxtaposed reverse and anti-remodeling trajectories in male and female rodents subjected to an identical pressure-overload insult and an identical unloading protocol. Without such head-to-head comparisons, it remains challenging to determine whether sex modulates intrinsic reparative capacity, responsiveness to unloading, or both. Third, the molecular correlates of systolic or diastolic functional indices remain poorly characterised. Finally, clinicians crave surrogate biomarkers that predict an individual's propensity for beneficial reverse remodeling or malignant progression, thereby tailoring early intervention; yet candidate proteins and metabolites remain exploratory.

The present work is driven by the hypothesis that biological sex shapes the endocrine and proteomic programs that govern ventricular remodeling (9), and that these molecular differences can be detected in load-independent haemodynamic indices. While most

studies focus on changes in LV volumes and mass reduction as indicators of reverse remodeling (106-110), these approaches do not fully capture the molecular mechanisms at play (111, 112). To establish a connection between the molecular landscape and functional profiles, we must transcend descriptive statistics by integrating proteomics with haemodynamic indices via LASSO regression (113), receiver-operating-characteristic modelling (114), STRING/MCODE interactomics (115, 116), and transcription factor analysis (117) to extract protein modules that predict contractile or lusitropic recovery.

Mechanistically, the work promises to illuminate how sex alongside gonadal hormones modulate mitochondrial substrate preference, cytoskeletal isoform switching, and collagen dynamics under stress. Clinically, discovery of a concise, ventricular function-centric protein panel could revolutionise how heart-failure specialists monitor therapeutic efficacy, enabling them to detect early responders, escalate treatment in "slow proselytes," or de-escalate therapy in super-responders. Regulatory agencies have already signalled strong enthusiasm for personalised, sex-aware drug-development pipelines; indeed, the U.S. Food and Drug Administration and the European Medicines Agency now encourage sex-disaggregated pre-clinical data as part of Investigational New Drug submissions (27). By supplying the mechanistic scaffolding and candidate biomarkers necessary for such pipelines, the present research aligns squarely with the imperatives of precision medicine.

In sum, the 20.5 million annual deaths attributed to cardiovascular disease are not merely a statistic (2); they reflect biological variability in which sex is a dominant theme. Unravelling its effect on cardiac remodeling demands a multidisciplinary approach that integrates deep proteomics, endocrine profiling, and gold-standard haemodynamic phenotyping.

2. Objectives

The main aims of the study can be formulated as follows:

- To provide a comprehensive and unbiased characterization of early sex-specific cardiac functional and proteomic changes in a rat model of myocardial ischemia induced by ISO.

- To analyse steroid hormone profiles and their effect on cardiac functional outcome in ischemic female rats.

- To investigate the role of sex in pressure unloading-induced anti-remodeling and reverse remodeling under standardized laboratory conditions using aortic banding-debanding in a rat model.

- To establish unifying molecular and functional parameters that can quantify reverse remodeling and predict clinical outcomes, with the ultimate goal of contributing to improved treatment strategies for heart failure and other cardiovascular conditions.

The overarching aim is to delineate the mechanistic pathways through which biological sex shapes ventricular function, thereby informing the design of sex-aware cardioprotective strategies.

3. Methods

Animals

The investigation conformed to the EU Directive 2010/63/EU and the Guide for the Care and Use of Laboratory Animals by the National Institutes of Health (NIH Publication No. 85-23, Revised 1996) (118). The study is interpreted in accordance with the Animals in Research: Reporting in Vivo Experiments (ARRIVE) guidelines (119). The investigations of myocardial ischemia and pressure unloading were approved by the Ethics Committee of Hungary for Animal Experimentation, Semmelweis University, Budapest (PEI/001/2374-4/2015) and by the regional authorities in Karlsruhe, Germany for Animal Experimentation (G-198/16) respectively. Animals were kept in standard conditions (22 ± 2 °C with 12-h light/dark cycles) and were allowed access to laboratory rat diet and water ad libitum during the whole experiment. All animals received humane care.

3.1. Study Protocol of Myocardial Ischemia Study

After 1 week of acclimatization, young adult (fertile) male and female Wistar rats (180 to 220 g) were assigned to matched control (Co) and ischemic (Isch) groups (Fig. 1):

- Male control (M-Co, n = 8)
- Male ischemic (M-Isch, n = 20)
- Female control (F-Co, n = 8)
- Female ischemic (F-Isch, n = 17)

All animals underwent body weight measurement (BW) and were briefly anaesthetized using 5% isoflurane. Rats from the ischemic groups were injected with ISO (ISO, 85 mg/kg, subcutaneous, Sigma-Aldrich) daily for 2 consecutive days to induce diffuse subendocardial ischemia as previously described (120), while Co rats received equivalent volumes of subcutaneous saline (NaCl 0.9%) injections at the same timepoints. Electrocardiograms were recorded 2 min after injections to assess the acute effect of the drug by a computer-based data acquisition system (PowerLab 16/30 and LabChart Pro software v7; AD Instruments, Colorado Spring, US). Pressure-volume (PV) analysis was performed at the end of the observational period, 48 hours after the first injection of ISO.

3.2. Study Protocol of Aortic Banding-Debanding Study

After a 1-wk acclimatization period, abdominal aortic banding (AB) or sham operations were performed as described elsewhere (88) on male (n = 49) and female (n=45) Sprague-Dawley rats (at the age of 5 wk; Janvier Labs, Saint Berthevin, France). Female rats used in this study were at prepubertal stage at the start of the experiment, and the investigation concluded during the premenopausal stage. At the time of AB, the body weight (BW) of the male and female animals did not differ from each other [BW: 154 ± 2 g male AB week 6 vs. 147 ± 4 g female AB week 6, not significant (NS); 157 ± 5 g male AB week 12 vs. 145 ± 3 g female AB week 12, NS; 155 ± 4 g male debanded vs. 146 ± 4 g female debanded NS].

In brief, general anesthesia was induced with 5% isoflurane gas in a chamber and maintained by inhalation from a connected tube with 1.5%–2% isoflurane in O_2. The animals were placed in a supine position on a heating pad to maintain the core temperature at 37°C measured via a rectal probe. The surgery was performed in midline laparotomy under sterile conditions. After dissecting the peritoneal layer, the abdominal aorta between the right renal artery and the superior mesenteric artery was prepared and subsequently constricted to the size of the external diameter of a 22-gauge needle. The same needle size was used for the creation of AB in both male and female sexes. Analgesia was provided by subcutaneously administering buprenorphine at the dose of 0.05 mg/kg. Furthermore, postoperative dehydration was prevented by subcutaneous injection of 1 mL physiological saline. Sham-operated animals were subjected to the same surgical procedure except for aortic constriction. At the end of the experimental period (weeks 6 or 12), PO was confirmed in AB rats by invasive blood pressure measurements. Only AB rats where PO was confirmed were included in the study, which was defined as a systolic blood pressure of 180 mmHg or higher.

At week 6, a proportion of the male and female AB animals underwent a second operation under identical surgical conditions, during which the aortic constriction was reversed by removal of the suture and the reactive fibrotic tissue surrounding the aorta (termed debanding). Only debanded (DB) rats in which the constricting suture was completely removed were included in the study.

After AB or sham operation, rats were randomized into the following 10 experimental groups (121):

- Groups 1 and 2: male (n = 9) and female (n = 8) sham week 6 groups: these rats underwent sham operation and a 6-wk-long follow-up period,
- Groups 3 and 4: male (n = 10) and female (n = 8) AB week 6 groups: these rats underwent AB and a 6-wk-long follow-up period,
- Groups 5 and 6: male (n = 9) and female (n = 9) sham week 12 groups: these rats underwent sham operation and a 12-wk-long follow-up period,
- Groups 7 and 8: male (n = 10) and female (n = 8) AB week 12 groups: these rats underwent AB and a 12-wk-long follow-up period, and
- Groups 9 and 10: male (n = 11) and female (n = 12) DB groups: these rats underwent AB operation. After week 6, the banding suture was removed and rats were followed up until week 12.

3.3. Echocardiography

Echocardiography was performed at baseline (before AB/sham operation) and 3, 6, 9, and 12 wk after AB/sham operation according to the previously published protocol (122). For the sonographic measurements, the Vevo 2100 imaging system (FujiFilm VisualSonics, Inc., Toronto, ON, Canada) equipped with a 21-MHz linear probe was used. Briefly, rats were anesthetized with 5% isoflurane in a chamber. After induction of anesthesia, rats were placed on an automatic heating pad in a supine position and core temperature was maintained at 37°C. To obtain an optimal acoustic window, the thorax of the animals was shaved. Anesthesia was maintained by inhalation of 1%–1.5% isoflurane gas in pure O_2. Images in two-dimensional parasternal long-axis and short-axis views as well as M-mode recordings at the midpapillary level were recorded. The study was completed by analyzing the digital images in a blinded fashion. On M-mode recorded images, LV internal diameters as well as anterior and posterior wall thicknesses in diastole (d) and systole (s) were measured. All values were calculated as the average of three consecutive cardiac cycles. LVmass was calculated from the measured parameters (121).

3.4. Hemodynamic Measurements

Detailed invasive LV-PV analysis was conducted to assess cardiac function in rats subjected to myocardial ischemia or pressure overload (122). The procedures began with anesthesia induction using 5% isoflurane in a chamber, followed by maintenance with 1-

1.5% isoflurane delivered through an intubation system. Tracheotomy was performed to facilitate mechanical ventilation, ensuring consistent delivery of anaesthetic gases and O_2 throughout the procedure. The animals were positioned supine on an automatic heating pad equipped with a rectal probe to maintain their core body temperature at 37°C, ensuring optimal physiological conditions.

A polyethylene catheter was inserted into the left external jugular vein to allow for the continuous administration of fluids during the procedure. To initiate the hemodynamic measurements, a 2F microtip pressure-conductance catheter (SPR-838, Millar Instruments, Houston, TX) was carefully inserted into the right carotid artery and advanced into the ascending aorta. This catheter was designed to simultaneously measure pressure and volume within the LV, providing a comprehensive assessment of cardiac function (123).

After a stabilization period of 5 minutes, arterial blood pressure was recorded at a high sampling rate of 1000 datapoints per second, ensuring precise and accurate data collection. The catheter was then advanced further through the aortic valve into the left ventricle to record pressure-volume (PV) loops. These loops were essential for evaluating both systolic and diastolic function under steady-state conditions.

The recorded PV loops were analyzed using the PVAN software (Millar Instruments) for the AB-Debanding study and Labchart 7 Pro (ADInstruments) for the myocardial ischemia study, which provided detailed calculations of a variety of hemodynamic parameters. These included systolic arterial blood pressure (SABP), diastolic arterial blood pressure (DABP), mean arterial pressure (MAP), LV end-systolic pressure (LVESP), LV end-diastolic pressure (LVEDP), heart rate (HR), stroke volume (SV), cardiac output (CO), ejection fraction (EF), and stroke work (SW). Additionally, dynamic measures such as the maximal rate of pressure increase in the LV (dP/dt_{max}) and the maximal rate of pressure decrease in the LV (dP/dt_{min}) were calculated to assess the contractile and relaxation properties of the myocardium. The time constant of LV pressure decay (τ, Tau) was computed using the Glantz method (124), providing insights into diastolic function.

To assess load-independent parameters of myocardial contractility and stiffness, PV loops were recorded during transient reductions in preload, achieved by temporarily occluding the inferior vena cava. This manoeuvre allowed for the calculation of the preload

recruitable stroke work (PRSW), a sensitive index of contractility, and the maximal slope of the dP/dt_{max}-end-diastolic volume (EDV) relationship, which further detailed the contractile function. The slope of the LV EDPVR was also determined as a measure of LV diastolic stiffness. Ventriculo-arterial coupling (VAC) was evaluated by calculating the ratio of arterial elastance (Ea) to the slope of the end-systolic PV relationship (ESPVR, using the parabolic – curvilinear model (125)), providing an integrated assessment of the interaction between the heart and the vascular system (126).

To ensure accurate volume measurements, parallel conductance was measured, and volume calibration of the conductance system was performed as described in previous protocols (90). These calibrations were critical for adjusting the PV data to reflect true LV volumes, accounting for the influence of surrounding tissues and ensuring precise quantification of cardiac function.

Following the completion of hemodynamic measurements, the animals were humanely euthanised by exsanguination. The hearts were perfused with oxygenated Ringer's solution to remove blood and preserve tissue integrity. The hearts were then excised, and heart weight (HW) and tibial length (TL) were measured. The heart weight-to-tibial length ratio (HW/TL) was calculated as an indicator of LVH, allowing for the assessment of the extent of hypertrophic remodeling in response to PO or ischemia.

At the time of euthanasia and PV analysis, rats of the AB-Debanding study in the male/female sham week 6 groups and male/female AB week 6 groups were at 11 wk of age, whereas rats in the male/female sham week 12 groups, the male/female AB week 12 groups, and the male/female DB groups were 17 wk of age. Rats of the myocardial ischemia study were analyzed and euthanized 48 hours after the first injection of ISO.

3.4. Histology and immunohistochemistry

Mid-papillary slices of the left ventricle were excised from the explanted hearts and were stored either by snap freezing or by formalin fixation (24 h in 4% buffered paraformaldehyde solution). From the formalin-fixed paraffin-embedded tissue, 5 µm thick slices were sectioned and stained with hematoxylin and eosin (H&E) and picrosirius red. Sections of the myocardial ischemia study were then digitised using a whole slide scanner (Ventana DP 200, Roche). The percentage of areas with intact myofibers to the total myocardial area (an indirect measure of the extent of necrosis) was quantified with QuPath 0.2.3 (127) using H&E colour deconvolution following the principles set by van

Putten et al. (128). Briefly, the overall area of the myocardium is detected. Areas devoid of any myocardial tissue are outlined in yellow and are excluded from the calculation of the overall myocardial area. Then, careful thresholding on the eosin colour component can identify viable cardiomyocytes with intact myofibrillar structures. These areas (coloured red in the software) are then used to calculate intact myofibrillar areas, which are inversely proportional to and thus an indirect measure of the extent of necrosis. The percentage of picrosirius red-stained area was quantified using thresholding in QuPath (129).

Light microscopic examination in the AB-Debanding study was performed with a Zeiss microscope (Axio Observer.Z1, Carl Zeiss, Jena, Germany) and digital images were captured by a special imaging software (QCapture Pro 6.0, QImaging, Canada).

Based on our previously published method (130), HE-stained slices were used to define cardiomyocyte diameter (CD) as a cellular marker of myocardial hypertrophy. Accordingly, 100 longitudinally oriented cardiomyocytes from the LV were examined in each sample at a magnification of ×400 and the diameters at transnuclear position were measured using Image J software (NIH, Bethesda, MD). The mean value of 100 measurements represented one sample. The extent of interstitial myocardial fibrosis was assessed on picrosirius-stained sections (130). Applying ×50 magnification, three transmural images (from the anterior, posterior, and free wall of the LV) were collected from each sections. ImageJ software (NIH, Bethesda, MD) was used to identify the picrosirius red-positive area. After background subtraction, eye-controlled autothreshold was determined to detect positive areas. The collagen area (picrosirius red-positive area–to–total area ratio) was determined on each image, and the mean value of three images represents each animal.

3.5. Quantitative Real-Time Polymerase Chain Reaction

LV mRNA analysis was performed according to the previously described protocol (122). Briefly, LV myocardium was homogenized in a lysis buffer (RLT buffer; Qiagen, Hilden, Germany). RNA was isolated using the RNeasy Fibrous Tissue Mini Kit (Qiagen) according to the manufacturer's instructions. The quality and concentration of the isolated RNA were assessed by the NanoDrop 2000 Spectrophotometer (Thermo Scientific, Waltham, MA). Accordingly, optical density at 230, 260, and 280 nm was measured. The

ratios of 230/260 and 230/280 nm were defined for quality control. Reverse transcription reaction (1 μg total RNA of each sample) was completed using the QuantiTect Reverse Transcription Kit (Qiagen). Quantitative real-time PCR (qRT-PCR) was performed with the LightCycler 480 system using LightCycler 480 Probes Master and the Universal Probe Library Probes (Roche, Mannheim, Germany). Forward and reverse primers for atrial natriuretic peptide (nppa: forward 5′-CAACACAgATCTgATggATTTCA-3′ and reverse 5′-CgCTTCATCggTCTgCTC-3′), β-type myosin heavy chain (myh7: forward 5′-gCTgCAgAAgAAgCTCAAAgA-3′ and reverse 5′-gCAgCTTCTCCACCTTgg-3′), and α-type myosin heavy chain (myh6: forward 5′-ggAggTggAgAAgCTggAA-3′ and reverse 5′-ATCTTgCCCTCCTCATgCT-3′) were obtained from TIB Molbiol (Berlin, Germany). For the measurement of nppa, myh7, and myh6 the UPL probe no. 65 was used. Gene expression data were normalized to glyceraldehyde 3-phosphate dehydrogenase (gapdh: forward 5′- CTACCCACGGCAAGTTCAAT-3′ and reverse 5′-ATTTGATGTTAGCGGGATCG-3′). For the measurement of gapdh, the UPL probe no. 111 was used. Expression levels were calculated using the CT comparative method ($2^{-\Delta CT}$). All results are expressed as values normalized to a positive calibrator [a pool of cDNA from all samples of the sham week 6 group ($2^{-\Delta\Delta CT}$)].

3.6. Hormone measurements

The concentrations of circulating endogenous steroid hormones (ALDO aldosterone, PROG progesterone, 2-OHE1 2-hydroxyestrone, 4-OHE1 4-hydroxyestrone, 4-MeE2 4-methoxyestradiol, DHT dihydrotestosterone, 2-MeE1 2-methoxyestrone, 2-MeE2 methoxyestradiol, 16-OHE1 + 16OE2 16-hydroxyestrone + 16-ketoestradiol, E2 estradiol, CORT corticosterone, DOC 11-deoxycorticosterone, E1 estrone) were quantitated using in-house methods developed and validated at the Department of Laboratory Medicine, Semmelweis University, relying on ultra-high performance liquid chromatography-triple quadrupole mass spectrometry with positive electrospray ionization and multiple reaction monitoring (Shimadzu Nexera X2-LCMS-8060, Simkon Kft., Budapest, Hungary). Isotopically labeled internal standards were added to the samples at the beginning of sample preparation to correct for random errors during preparation and analysis. Following deproteinization of 200 μL serum with 600 μL methanol containing the internal standards, ALDO, DHT, DOC, CORT and PROG were

extracted by solid phase extraction (Phenomenex Strata-X 60 mg, Gen-Lab Kft, Budapest, Hungary). E1, E2, 2-OHE1, 4-OHE1, 2-MeE1, 2-MeE2, 4-MeE2, 16OHE1 and 16OE2 were first released from their conjugates by incubating another 500-µL fraction of serum with 500 µL β-glucuronidase/aryl sulfatase in pH = 5.0 acetate buffer at 60 °C for 120 min. Subsequently, the mixture was cooled and mixed intensively with 2 × 1 mL ethyl acetate. Following the evaporation of the combined fractions of the organic solvent, 100 µL 1 mg/mL dansyl chloride in acetonitrile and 20 µL 0.5 mol/L sodium carbonate in water were added to the residue. The mixture was incubated at 45 °C for 15 min, followed by the addition of 20 µL 0.5 mol/L hydrochloric acid.

3.7. Western blot

Myocardial LV tissue samples were homogenized in RIPA buffer (Bio-Rad Laboratories, Hercules, CA, USA) containing protease and phosphatase inhibitor cocktail (Roche, Basel, Switzerland), using the Bertin Precellys 24 Tissue Homogenizer with the Bertin Cryolys cooling system (Bertin Technologies). The concentrations of the extracted proteins were measured by BCA assay (Thermo Fisher Scientific). Then, protein homogenates were suspended in sample buffer and heated at 70 °C for 10 min. A total of 20 µg protein for each sample was loaded onto 6–12% acrylamide gels and separated with a sodium dodecyl sulfate polyacrylamide gel electrophoresis system (Bio-Rad Laboratories). Gels were transferred to polyvinylidene fluoride membranes under dry conditions. Membranes were then washed and blocked for 1 h in 5% bovine serum albumin (BSA) in Tris-buffered saline Tween 20 (TBST) at room temperature. Next, membranes were incubated overnight at 4 °C with the following primary antibodies diluted in 2.5% BSA in TBST. The following primary antibodies were used: from Cell Signaling (Cell Signaling Technology, Danvers, MA, USA): VASP (1:1000, ID:#3112), ATP2A2 (1:1000, ID:#4388) and the housekeeping GAPDH (1:5000; ID: #5174); from R&D Systems (R&D Systems Inc., Minneapolis, MN, US): POSTN (1:1000, ID: AF3548); from Abcam (Abcam Inc., Toronto, ON, Canada): OPN (1:1000, ID: ab63856). The blots were washed and incubated with horseradish peroxidase-conjugated secondary antibody (1:5000, 2.5% BSA in TBST) for 2 h at room temperature. The immunoreactive protein bands were developed using Super Signal West Pico Plus (Thermo Fisher Scientific) or SuperSignal West Femto chemiluminescent substrate. The intensity of the immunoblot bands was analyzed with Image J (NIH, Bethesda, MD, USA). The intensity

of the bands of the primary targets was normalized to that of the housekeeping GAPDH on the same blot.

3.8. Proteomics

3.8.1. Proteomics of the Myocardial Ischemia Study

Cryopreserved myocardial samples of 40 rats of the myocardial ischemia study were homogenized in 0.1% Rapigest and 100 mM HEPES (pH 7.5) solution. Reductive alkylation was performed using 5 mM tris(2-carboxyethyl)phosphine-hydrochloride (TCEP, Sigma-Aldrich) and 20 mM iodoacetamide (Sigma-Aldrich). Proteins were digested overnight by Trypsin (Worthington, Lakewood, NJ, sequencing grade), and the resulting peptides were desalted on PreOmics columns (PreOmics, Bavaria, Germany). Further steps were performed as described previously (131). Briefly, peptides were labeled with TMT11plex isobaric label reagents (Thermo Fisher Scientific) and combined into four batches including a cohort-wide normalization channel. Reverse-phase prefractionation (pH = 10) was performed on an XBridge C18 column, 150 mm × 1 mm column containing 3.5 µm particles (Waters) inserted into an Agilent 1100 high performance liquid chromatography system (HPLC). Fractions were analyzed on a Q-Exactive Plus (Thermo Scientific, Bremen, Germany) operating in a data-dependent acquisition (DDA) mode. (For the detailed distribution of samples over batches, we refer to the MSV000088184 entry on the MassIVE repository.) Mass spectra were analyzed using MaxQuant version 1.6.17.0 (132) with the Uniprot rat database downloaded in November 2020. Quantified peptide intensities were then summarized by MSstatsTMT (R package (133)).

3.8.2. Proteomics of the AB-DB Study

Cryopreserved myocardial samples of 44 rats were homogenized in lysis buffer containing 0.5% SDS and 0.1 M HEPES (pH = 8.0). Reductive alkylation was performed using 5 mM Tris (2-carboxyethyl) phosphine-hydrochloride (TCEP, Sigma-Aldrich) and 20 mM chloroacetamide (Sigma-Aldrich) for 30 min at room temperature. Overnight digestion was carried out in line with the “single-pot, solid-phase-enhanced sample preparation” (SP3) protocol (134). Briefly, an equal mixture of prewashed hydrophilic and hydrophobic SP3 beads were added to the sample. A volume of acetonitrile equal to the volume of the sample-bead mix was added to ensure the binding of proteins to the

beads during a 10-min incubation period at room temperature with 1,000 rpm shaking applied. Protein bound beads were washed on a magnetic rack with ethanol and acetonitrile. Beads were resuspended in 100 mM ammonium bicarbonate buffer to ensure pH 8.0–8.5 for optimal digestion with trypsin and LysC overnight. Peptides were released from the beads by sonication. Further steps were performed as described previously (131). Briefly, 16-plex TMT labeling (Thermo Fisher Scientific) enabled formation of three measurement pools, each encompassing cardiac samples from up to 15 animals and one master sample for comparability. Accordingly, peptides were labeled with TMT16plex isobaric label reagents and combined into three batches, including a cohort-wide normalization channel. Samples from all experimental groups, and thus sexes, were divided equally among measurement pools and TMT reagents to account for potential batch effects. (For the detailed distribution of samples over batches, we refer to the MSV000089077 entry on the MassIVE repository.) On an XBridge C18 column, 150 mm × 1-mm column containing 3.5-µm particles (Waters), reverse-phase prefractionation (pH 10) was performed with an Agilent 1100 high-performance liquid chromatography system (HPLC). Fractions were analyzed on a Q-Exactive plus (Thermo Scientific, Bremen, Germany) in a data-dependent acquisition (DDA) mode. Mass spectra were analyzed using MaxQuant version 1.6.17.0 (132) with the Uniprot rat database downloaded in June 2021 using a false discovery rate (FDR) of 1% on both peptide and protein levels. Quantified peptide intensities were summarized by MSstatsTMT [R package (133)]. Protein quantification was based on intensities of peptides that are unique to their corresponding protein. Only proteins that were identified in at least two of the three batches, thus in at least 2/3 of all animals measured with mass spectrometry, were included in our study. Missing value imputation was performed with missForest [R package (135)] whereas batch-effect correction was carried out with the sva package [ComBat algorithm (136)].

3.8.3. Proteomics Reanalysis of Data of the AB-DB Study

Due to recent advancements in proteomics software, it was advantageous to extensively reanalyse the proteomics data from the AB-Debanding (121), which were made available on the MassIVE repository (MSV000089077). The cohort, as described before included several experimental groups: a sham-operated group (n = 10, Co), aortic banded groups observed for 6 or 12 weeks (n = 12 each, AB) and a DB group (n = 10, DB) that underwent

the AB operation, was observed for 6 weeks, then underwent debanding after which they were followed up until week 12. Each group included an equal number of male and female rats.

The FragPipe pipeline 19–21 (v17) was used for peptide/protein identification and quantitation (137). In brief, spectral data were searched against an in-silico-digested protein sequence database (EBI Rat canonical proteome, version 2021_03, appended with common contaminants and iRT peptides), assuming experimental tryptic digestion to generate in-silico-digested peptides and precursor candidates with a mass tolerance of -20/20 ppm. Peptide N-terminal acetylation and peptide N-terminal TMT labeling were set as variable modifications. MSBooster was used for deep learning-based predictions of retention time and spectra. Predicted features were used by Percolator 4 for post-processing scoring and false discovery rate (FDR) control via target-decoy competition of all peptide-to-spectrum matches (PSMs) obtained from MSFragger search. Relative quantitation of identified peptides within each sample was performed via their reported ion intensities using TMT-Integrator. Only PSMs derived from unique peptides with a minimum probability of 0.9 and an isotopic purity of at least 50% were considered for quantitation. Quantitative values were normalized via median centering and summarized by protein/gene and peptide using a virtual reference channel, to finally generate protein and peptide normalized matrices of abundance, which then underwent statistical processing.

3.9. Statistics and bioinformatics

3.9.1. Statistics of the Myocardial Ischemia Study

The data are presented as mean ± SEM. Normal distribution was confirmed by the Shapiro-Wilks method. Two-way analysis of variance (ANOVA) on the factors of "sex" and "ischemia", followed by a Tukey HSD post hoc test to examine intergroup differences. Contingency tables were analyzed with Fisher's exact test. Correlations were tested using Pearson's method. Two-sample T-test was used to compare the area of intact myofibers in the F-isch subgroups. Relationships of functional, proteomic and hormonal profiles were established using log- transformed and quantile normalized values to account for differences among datasets obtained with different methodologies in a subgroup analysis of F-Isch animals. A P value of < 0.05 was deemed significant for all

but gene ontology enrichment analyses (executed with clusterProfiler (138)), where an adjusted P value of < 0.01 was defined as the threshold.

Differential expression analysis was performed with Linear Models for Microarray Data (Limma R package (139)) by setting up a 2×2 factorial design. Significantly changed proteins were grouped into functional groups based on an extensive literature search. Supervised algorithms from the MixOmics R package (140) were utilized to establish associations among functional, proteomic and hormonal datasets. Partial Least Squares Discriminant Analysis (PLS-DA) was employed to examine hormonal-functional relationships where a Variable Importance in the Projection (VIP) score of more than one was considered influential in feature selection. sparse PLS-DA (sPLS-DA) was utilized to provide a visual overview of the extent of inter-sex and Isch-Co differences. Projection to Latent Structure (PLS) analysis was performed to screen for hormone-protein associations, where a VIP score of more than 1.3 was considered influential in feature selection. K-fold cross-validation from MixOmics was used to test the classification efficiency of the models. As a measure of model performance, balanced error rate (BER) was calculated. The number of components to be included in the models was based on the lowest BER and lowest SEM of BER that was achievable.

3.9.2. Statistics of the AB-Debanding Study

All values are expressed as means ± SE. The distributions of the data sets were analyzed with D'Agostino Pearson omnibus and Shapiro–Wilk (if the number of samples were seven or less) normality tests.

Two-way analysis of variance (ANOVA) with the factors of "sex" and "time" was used to compare the four sham (male and female sham week 6 groups and male and female sham week 12 groups) and the four AB (male and female AB week 6 groups and male and female AB week 12 groups) groups separately. Before two-way ANOVA, data sets that failed to show normal distribution were logarithmically transformed. Tukey's post hoc test was used to detect intergroup differences.

An unpaired two-sided Student's t test in case of normal distribution or Mann–Whitney U test in case of nonnormal distribution was used to compare means of two independent groups.

Furthermore, the male and female AB week 6, AB week 12, and DB groups were normalized to the corresponding age- and sex-matched sham groups (expressed as Δ) to

eliminate any differences which could have originated from the differences in age and body weight. The normalized male AB week 6, AB week 12, and DB groups and the normalized female AB week 6, AB week 12, and DB groups were compared in two separate analyses by one-way ANOVA. Finally, the percent of change in the normalized DB groups compared with the normalized AB week 6 (to detect the reverse-remodeling effect) and AB week 12 (to detect the anti-remodeling effect) groups was calculated in both sexes. These values (expressed as ΔΔ) were used to directly assess sex similarities or differences during pressure unloading induced reverse and anti-remodeling.

sPLS-DA from the MixOmics R package (140) was used to distinguish the proteomic profiles of experimental groups and animals. The first 15-15 proteins with the greatest contribution to the separation of proteomes in the experimental groups along component 1 (C1) and component 2 (C2), the two axes of the two-dimensional projection, were extracted from the model. Differential expression analysis of the proteomic data set was carried out using Linear Models for Microarray Data [Limma R package (139)] with incorporation of the Benjamini-Hochberg procedure to account for the pitfalls of multiple testing. Sex-related differences in numbers of differentially regulated proteins were investigated with $\chi 2$ test. Gene ontology biological process enrichment analysis (GO:BP) was performed with clusterProfiler (138) on proteins that showed a significant change in relative abundance. A P value of <0.05 was used as a criterion for statistical significance.

3.9.3. Bioinformatics of the Proteomic Reanalysis of the AB-DB Study

Feature selection of clinical parameters was performed using the Least Absolute Shrinkage and Selection Operator (LASSO) regression to identify the minimum set of associations between protein abundances and LV parameters. The best lambda, i.e., the best regularisation parameter controlling the strength of the penalty applied to regression coefficients, was determined following the application of LASSO to all predictors by k-fold cross-validation (with k=10) as implemented in the cv.glmnet function of the glmnet package (141). Subsequently, for all proteins with non-zero coefficients, Linear Models for Microarray Data (limma) was run on PV and echocardiographic parameters obtained by LASSO to estimate coefficients without regularisation. A protein was deemed significantly associated with a PV or echocardiographic parameter if the limma P value was less than 0.05. The highest-performing PV and echocardiographic parameters, were then selected for subsequent investigation. The term “highest-performing” denotes the

PV and echocardiographic parameters with the largest number of associated proteins. Gene Ontology (GO) enrichment analysis (GO over-representation analysis), facilitated by clusterProfiler (138), was conducted on proteins associated with selected parameters of the left ventricle. To offer a comprehensive overview of enriched biological processes, GO: BP terms were grouped hierarchically based on semantic similarity (rrvgo). Sensitivity and specificity of τ and LVmass-associated proteins were calculated across different thresholds to identify the best biomarker candidates, the relative abundance of which can best discriminate non-banded (either sham-operated or DB) animals from ongoing myocardial remodeling (AB). Proteins with an area under the (ROC) curve (AUC) of more than 0.85 were considered good discriminators.

Network analysis

The online Search Tool for the Retrieval of Interacting Genes/Proteins online database (STRING-DB) tool (142) was used to create a protein-protein interaction (PPI) network of all τ-related proteins. The visualization allows the investigation of potential interactions among τ linked proteins (143). Subsequently, the MCODE plugin (116) of the Cytoscape software (144) was used for subnetwork extraction and re-identifying the hub genes associated with τ from the STRING network with the following settings: node score cut-off ≥0.2, degree cut-off ≥2, max depth = 100 and K-core ≥2. Subnetworks with an MCODE score >3 were selected for further evaluation. Pairwise relationship among subnetwork member proteins was investigated with Pearson correlation separately, in Co, AB, and DB conditions.

MCODE Subnetwork proteins subsequently underwent correlational analysis with AB, DB and Co and plotted in separate network plots based on edge-weighted spring-relationship, where a spring model is used to simulate relative attraction between proteins (nodes).

Both the STRING Database combined score for inter-node relationships for τ-related proteins and correlation coefficients for subnetwork proteins were used as determinants for graphically representing subnetwork proteins, node positioning and edge weight representing the edge-weighted spring-relationship. Proximity and edge weight in subnetworks were selected to be the graphical markers of increased correlation and combined score.

Correlation between inter-group proteins was used as the edge weight determinant, with shorter distances indicating greater correlation. The correlation of AB, DB and Co proteins with other proteins in each subnetwork was indicated using edge width between individual nodes. Nodes and edges were color-coded to enable visualization of those proteins identified as being related to cardiac function and / or had AUC of more than 0.85 (banded vs. non-banded rats).

Transcription factors were identified using the and "ChIP-X Enrichment Analysis 3" (ChEA3) algorithm (117) based on the "Encyclopedia of DNA Elements" (ENCODE) database (145) to export the 10 transcription factors with the lowest FDR-corrected P Values (< 0.05) and their potential τ-associated target proteins.

4. Results

4.1. Results of the myocardial ischemia study

4.1.1. Assessment of effect of ISO treatment

HR has increased after the subcutaneous injection of ISO both sexes (Fig. 1B). M-Isch and F-Isch rats experienced a mortality rate of 38% and 17% prior to PV measurement, respectively. Area of intact myofibers as quantified on the H&E stained slides decreased but the HW/TL ratio increased in ischemic animals (Fig. 1C, D, F). Collagen content on picrosirius stained slides was similar among all groups (Fig. 1E, G).

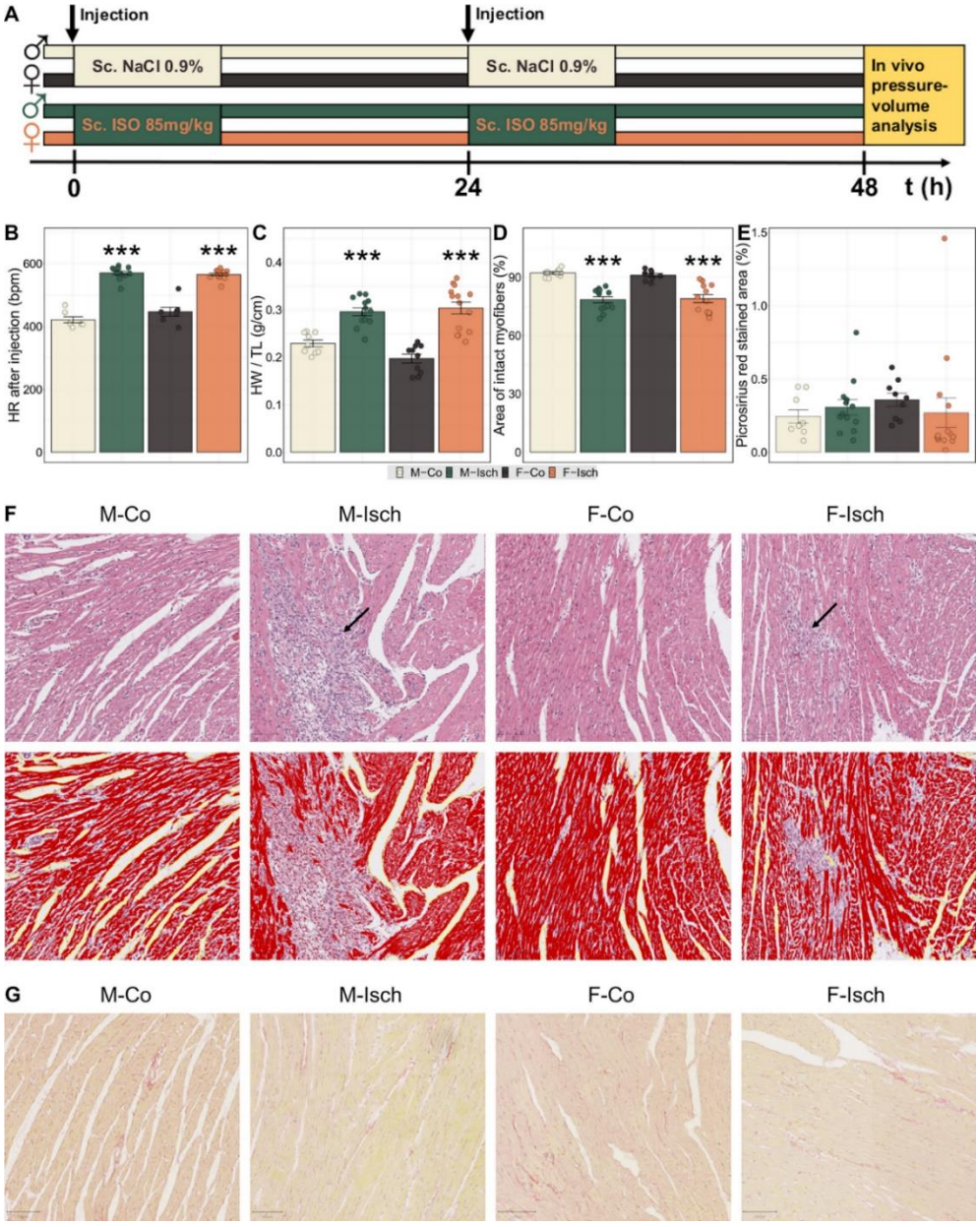

Figure 1. Experimental protocol and assessment of effect of ISO

A *Study design.* ***B*** *Heart rates recorded 2 min after injection of ISO showed a comparable increase due to β-adrenergic activation in both males and females.* ***C*** *Increments in heart weight normalized to tibia length indicated a buildup of edema in both sexes.* ***D*** *The percentage of the area of intact myofibers on histological slides of the myocardium declined due to ISO therapy in both sexes compared to Co.* ***E*** *The percentage of picrosirius red stained area was not significantly changed in response to ischemia at the end of the experimental period.* ***F*** *Representative photomicrographs of hematoxylin & eosin stained slides demonstrate diffuse necrotic areas (arrows) embedded within healthy areas of the myocardium after ISO-induced ischemia. Further images (second row) demonstrate how after H&E color deconvolution the eosin color component can be used to quantify the relative area of intact myofibers in the myocardium an indirect measure of the extent of myocardial damage, myocardial necrosis.* ***G****: representative photomicrographs of picrosirius stained slides. Statistical significance of post-hoc test compared to same sex Co is highlighted as follows: *P < 0.05, **P < 0.01, ***P < 0.001. M-Co: male control; M-Isch: male ischemic; F-Co: female control; F-Isch: female ischemic; HR: heart rate; HW/TL: heart weight normalized to tibia length* Source: *reproduced from Barta et al. (129).*

4.1.2. LV functional characterization

48 h after the first injection MAP, SABP, SADP and SW were found to be markedly diminished only in M-Isch. Concurrently contractility (EF and PRSW) declined in M-Isch animals only. Furthermore, cardiac efficiency was negatively impacted in males after ischemia (Fig. 2 and Table 1). Rats in the F-Isch group have decreased CO, partially explained by their greater, but not significant, reduction in SV compared to sex-matched Co groups. Active relaxation (T) and myocardial stiffness (LVEDP and EDPVR) were more severe in F-Isch, indicating more severe diastolic dysfunction (Fig. 2 and Table 1).

Table 1. Basic hemodynamic characteristics of experimental groups

*Statistical significance of post hoc test compared to same-sex Co is highlighted as follows: *P < 0.05, **P < 0.01, ***P < 0.001. M-Co male control, M-Isch male ischemic, F-Co female control, F-Isch female ischemic, BW body weight, SABP systolic arterial blood pressure, DABP diastolic arterial blood pressure, HR heart rate 48 h after the first injection, LVESP LV end-systolic pressure, LVEDP LV end-diastolic pressure, LVEDV LV end-diastolic volume, LVESV LV end-systolic volume, SV stroke volume, CO cardiac output, SW stroke work, dP/dt_{max} maximal rate of rise in LV pressure, dP/dt_{max}-EDV maximal slope of dP/dt_{max} – EDV relationship, dP/dt_{min} maximal rate of decrease in LV pressure. Source: reproduced from Barta et al. (129).*

Table 1				
Parameter	**M-Co**	**M-Isch**	**F-Co**	**F-Isch**
BW (g)	205.1 ± 3.3	195.2 ± 5.6	189.8 ± 2.2	193.2 ± 3
SABP (mmHg)	136.2 ± 3.5	103.4 ± 5.0**	129.7 ± 7.4	114.6 ± 7.2
DABP (mmHg)	105.4 ± 1.9	81.52 ± 4.7*	104.22 ± 4.9	91.6 ± 5.3
MAP (mmHg)	115.2 ± 2.2	88.8 ± 4.7*	112.7 ± 5.7	99.2 ± 5.9
HR (bpm)	419.2 ± 11.2	408.9 ± 7.8	416.5 ± 12.1	386.3 ± 9.2
LVESV (µL)	53.5 ± 3.3	114.2 ± 21.0	67.7 ± 11.5	89.7 ± 12.6
LVEDV (µL)	154.6 ± 9.2	207.3 ± 20.7	195.9 ± 14.0	189.4 ± 17.4
LVESP (mmHg)	124.8 ± 3.4	100.1 ± 3.5*	128.8 ± 5.3	103.6 ± 6.0**
LVEDP (mmHg)	11.0 ± 1.1	11.2 ± 0.9	8.6 ± 0.8	13.6 ± 1.7*
SV (µL)	117.5 ± 11.3	111.8 ± 5.6	141.6 ± 5.1	112. ± 11.1
CO (µL/min)	48,694 ± 4	45,785 ± 3	58,968 ± 3	43,175 ± 4*
SW (mmHg*µL)	14,316 ± 2	9455 ± 8*	15,111 ± 8	10,626 ± 1
dP/dt_{max} (mmHg/s)	7458 ± 341	6612 ± 293	8636 ± 420	7531 ± 402
dP/dt_{max}-EDV (mmHg/(s*µL))	64.8 ± 3.4	45.7 ± 4.9	59.9 ± 5.9	54.3 ± 4.7
dP/dt_{min} (mmHg/s)	− 9322 ± 542	− 6677 ± 433*	− 11,095 ± 640	− 6736 ± 598***

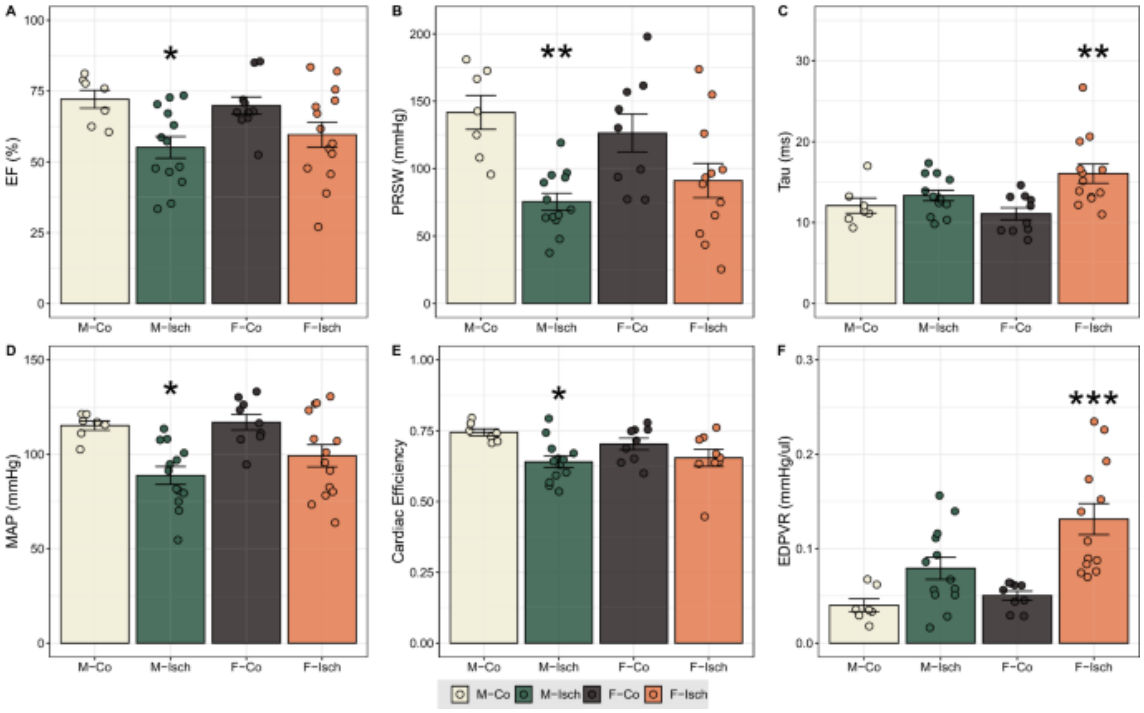

Figure 2. Assessment of systolic and diastolic function

The decline of systolic function was more pronounced in males, while diastolic function deteriorated to a greater degree in females after ISO treatment. ***A***, ***B*** *Systolic function, as assessed by EF and PRSW, markedly decreased in males after ischemia.* ***D*** *Accordingly, MAP significantly decreased in males as well.* ***E*** *The observed deterioration of systolic function of males was underlain by a marked decline in cardiac efficiency.* ***C*** *Marked increase in τ indicated a more pronounced worsening of active relaxation in females.* ***F*** *Diastolic stiffness increased only in females as determined by EDPVR. The statistical significance of the post hoc test compared to same-sex Co is highlighted as follows: *P < 0.05, **P < 0.01, ***P < 0.001. M-Co: male control; M-Isch: male ischemic; F-Co: female control; F-Isch: female ischemic; EF: ejection fraction; PRSW: preload recruitable stroke work; MAP: mean arterial pressure; EDPVR: slope of the LV end-diastolic PV relationship. Source: reproduced from Barta et al. (129).*

4.1.3. Proteomic results

Based on the relative quantification of 2224 proteins, the supervised sPLS-DA algorithm could clearly separate the samples of our experimental groups (0.0002 ± 0.0069 BER), hinting at consistent changes in protein expression patterns (Fig. 3B). The most influential proteins alongside the axis of Isch vs. Co (component 1) were JPH2, ATP5ME, KNG2, CAVIN2, APOOL, MRRF and COQ8A, while A1BG, LIFR, FKBP7, and RCN3 helped separate male vs. female groups. The distribution of sex-specific differentially regulated proteins in response to ischemia was associated with the sexes (Fisher's exact test, $p < 0.001$). Of note, the frequency of sex-specific upregulations was 56% higher in females (455 vs. 291, F-Isch vs. M-Isch), while a comparable number of downregulations were detected (603 vs 607, F-Isch vs. M-Isch; Fig. 3A). Principally, this was due to more pronounced upregulation of proteins of transcription, cytoskeleton & contraction, extracellular matrix & wound healing and inflammation in ischemic females. Metabolic and mitochondrial proteins tended to be downregulated to a greater extent in ischemic males (Fig. 3C). Western blotting has confirmed the female-specific upregulation of VASP and OPN in F-Isch, and the sex-independent upregulation of POSTN in M-Isch, as well as in F-Isch compared to the respective Co, validating the proteomics results. Furthermore, the expression of ATP2A2 was consistently unaffected by ischemia, as assessed by both Western blotting and LC–MS/MS measurements (Fig. 4).

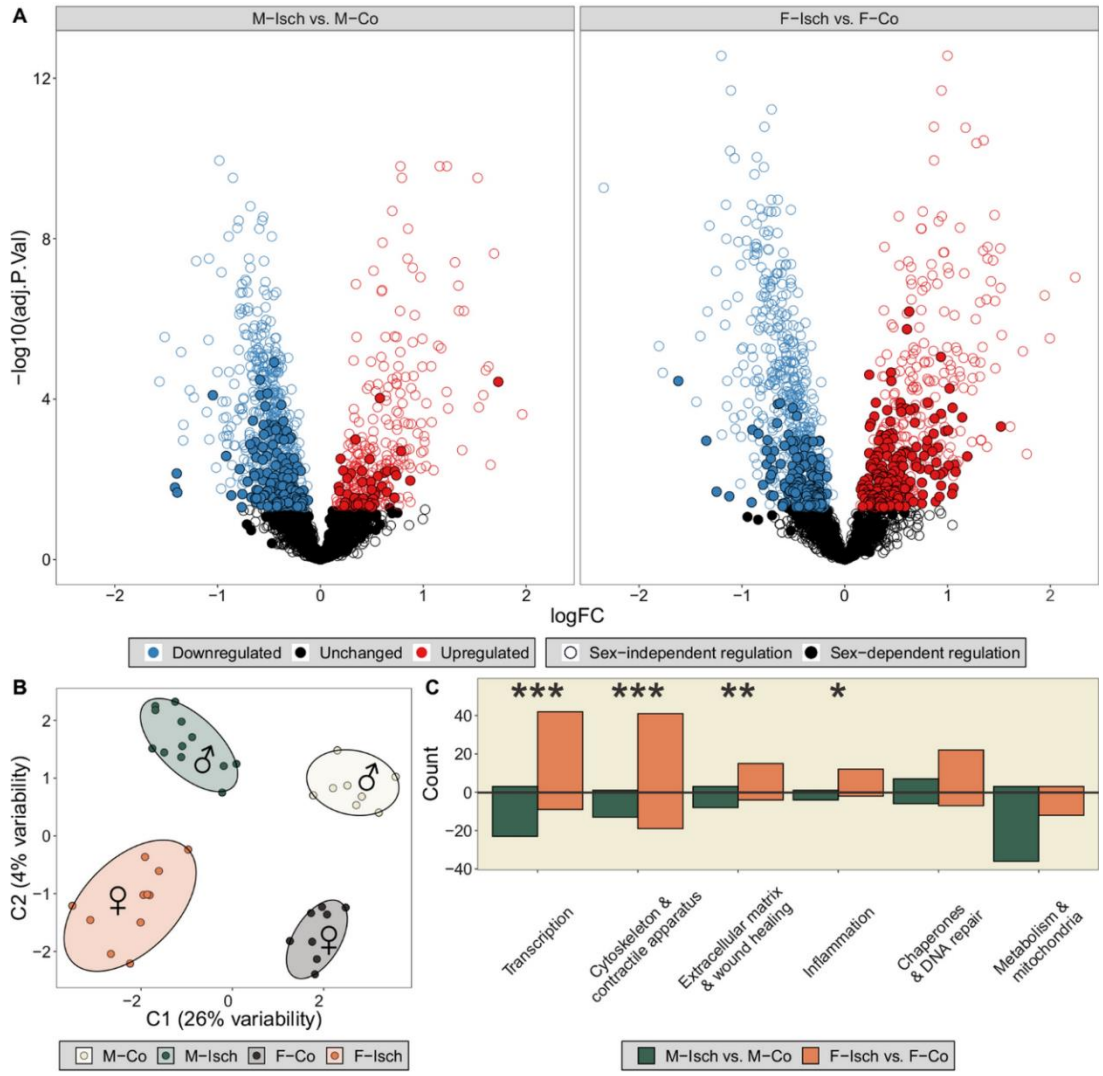

Figure 3. Proteomic comparison of sex-specific changes after ischemia

A *result of differential expression analysis. Proteins under sex-specific regulation are highlighted. An adjusted P value of < 0.05 was considered significant compared to the sex-matched Co group. The female proteomic adaptation following ischemia is characterized by a higher number of upregulated proteins compared to males.* ***B*** *The supervised sPLS-DA clearly separated all groups, proving that both sex and ischemia affect proteomic profiles.* ***C*** *Proteins under sex-dependent regulation in response to ischemia were grouped according to biological categories. Statistically significant association was found between sex and differential expression of proteins with a function in transcription, inflammation, extracellular remodeling and cytoskeletal organization. Statistical significance of Fisher's exact test is highlighted as follows: *P < 0.05, **P < 0.01, ***P < 0.001. M-Co: male control; M-Isch: male ischemic; F-Co: female control; F-Isch: female ischemic.* Source: reproduced from Barta et al. (129).

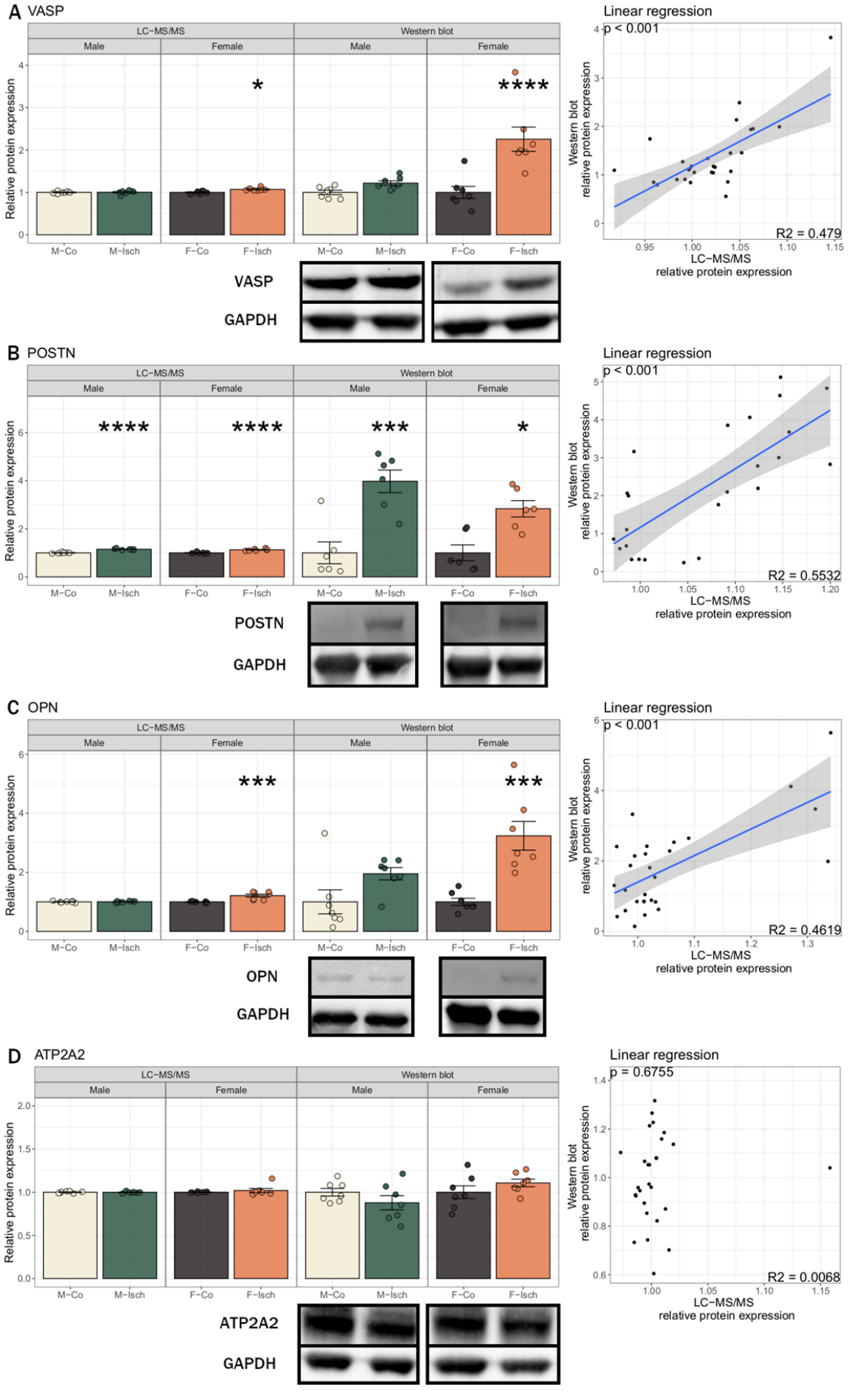
A VASP
LC−MS/MS
Western blot
Male
Female
Relative protein expression
M−Co
M−Isch
F−Co
F−Isch
VASP
GAPDH
Linear regression
p < 0.001
Western blot relative protein expression
LC−MS/MS relative protein expression
R2 = 0.479
B POSTN
POSTN
GAPDH
R2 = 0.5532
C OPN
OPN
GAPDH
R2 = 0.4619
D ATP2A2
ATP2A2
GAPDH
p = 0.6755
R2 = 0.0068

Figure 4. Validation of LC–MS/MS measurements with western blot

***A–D**: Relative protein expression of VASP, POSTN, OPN and ATP2A2 as measured by LC–MS/MS and western blot. Values were normalized to the mean of the corresponding Co group. Statistical significance of post hoc test compared to same-sex Co is highlighted as follows: *P < 0.05, **P < 0.01, ***P < 0.001, ****P < 0.0001. M-Co male control, M-Isch male ischemic, F-Co female control, F-Isch female ischemic. Source: reproduced from Barta et al. (129).*

4.1.4. Association of steroid hormones and cardiac functional outcomes

Hierarchical clustering of P–V hemodynamic parameters has divided F-Isch animals into clusters of mild and severe functional outcomes (Fig. 5A). This distinction was not directly related to the extent of myocardial damage ($79.774 \pm 2.963\%$ vs $78.259 \pm 2.953\%$, F-Isch mild vs. F-Isch severe in areas of intact myofibers). These subgroups of F-Isch rats could successfully be distinguished from each other based on just their steroid hormone profiles using supervised PLS-DA (0.307 ± 0.063 BER, Fig. 5B). Aldosterone, progesterone, 2-hydroxyestrone, 4-hydroxyestrone and 4-methoxyestradiol were found to be of particular importance in the classification of mild vs. severe outcomes based on VIP scores extracted from the model (Fig. 5C, D). 2-hydroxyestrone and crucial P–V parameters of systolic and diastolic function (PRSW, T and dP/dt_{min}, Fig. 5E–G) as well as HW/TL (Fig. 5H) were markedly correlated in the F-Isch group.

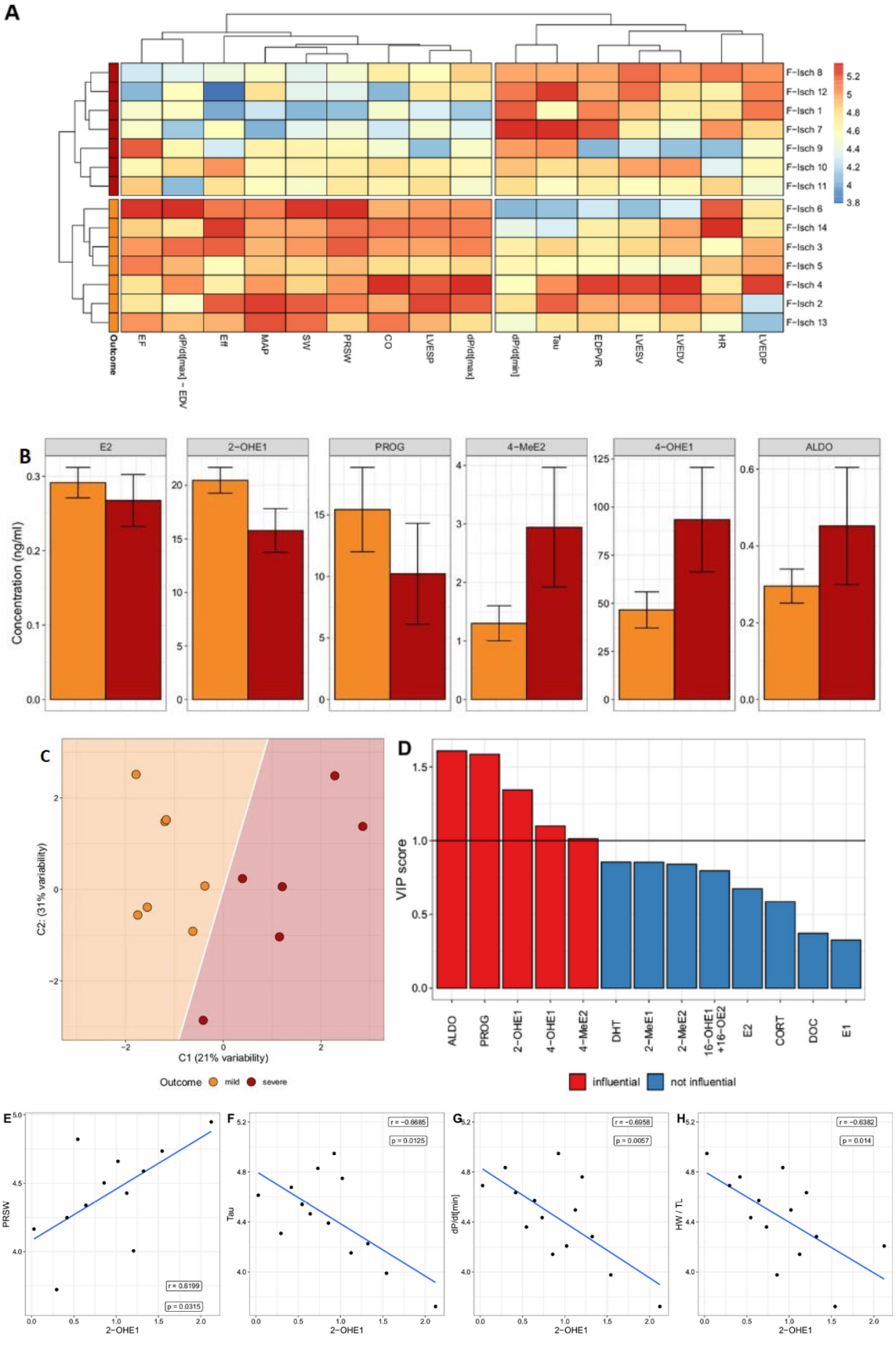
A
F−Isch 8
F−Isch 12
F−Isch 1
F−Isch 7
F−Isch 9
F−Isch 10
F−Isch 11
F−Isch 6
F−Isch 14
F−Isch 3
F−Isch 5
F−Isch 4
F−Isch 2
F−Isch 13
5.2
5
4.8
4.6
4.4
4.2
4
3.8
Outcome
EF
dP/dt[max] − EDV
Eff
MAP
SW
PRSW
CO
LVESP
dP/dt[max]
dP/dt[min]
Tau
EDPVR
LVESV
LVEDV
HR
LVEDP
B
E2
2−OHE1
PROG
4−MeE2
4−OHE1
ALDO
Concentration (ng/ml)
C
C2: (31% variability)
C1 (21% variability)
Outcome
mild
severe
D
VIP score
ALDO
PROG
2−OHE1
4−OHE1
4−MeE2
DHT
2−MeE1
2−MeE2
16−OHE1 +16−OE2
E2
CORT
DOC
E1
influential
not influential
E
PRSW
2−OHE1
r = 0.6199
p = 0.0315
F
Tau
2−OHE1
r = −0.6685
p = 0.0125
G
dP/dt[min]
2−OHE1
r = −0.6958
p = 0.0057
H
HW / TL
2−OHE1
r = −0.6382
p = 0.014

Figure 5. Assessment of influence of circulating steroid hormone levels on functional outcomes after ischemia in females

A *Hierarchical clustering identified two equally sized subgroups of female ischemic animals characterized by an overall mild or severe functional impairment based on parameters of the pressure–volume analysis.* ***B*** *Absolute concentrations of steroid hormones that were found influential on functional or proteomic profiles.* ***C*** *PLS-DA analysis performed on the concentrations of circulating steroid hormone levels in ischemic females distinguished animals with mild or severe functional outcomes.* ***D*** *VIP scores extracted from the PLS-DA model identified hormones that contributed the most to the moderate separation of mild and severe functional outcomes.* ***E***–***H*** *Out of all influential hormones 2-OHE1 showed strong significant correlations with systolic (PRSW) and diastolic (T, dP/dt_{min}) as well as HW/TL. For comparison of functional and hormonal datasets acquired by distinct methodologies values were log-transformed and quantile normalized. M-Co: male control; M-Isch: male ischemic; F-Co: female control; F-Isch: female ischemic; SABP: systolic arterial blood pressure; DABP: diastolic arterial blood pressure; HR: heart rate; LVESP: LV end-systolic pressure; LVEDP: LV end-diastolic pressure; LVEDV: LV end-diastolic volume; LVESV: LV end-systolic volume; SV: stroke volume; CO: cardiac output; SW: stroke work; dP/dt_{max} maximal rate of rise in LV pressure; EF: ejection fraction; PRSW: preload recruitable stroke work; dP/dt_{max}-EDV: maximal slope of dP/dt_{max} – EDV relationship; Eff: cardiac efficiency; dP/dt_{min}: maximal rate of decrease in LV pressure; C1: component 1; C2: component 2; ALDO: aldosterone; PROG: progesterone; 2-OHE1: 2-hydroxyestrone, 4-OHE1: 4-hydroxyestrone; 4-MeE2: 4-methoxyestradiol; DHT: dihydrotestosterone; 2-MeE1: 2-methoxyestrone; 2-MeE2: 2-methoxyestradiol; 16-OHE1 + 16OE2: 16-hydroxyestrone + 16-ketoestradiol; E2: estradiol; CORT: corticosterone; DOC: 11-deoxycorticosterone; E1: estrone; HW/TL: heart weight normalized to tibia length.* Source: reproduced from Barta et al. (129).

4.1.5. Association of hormonal and proteomic profiles

Associations of steroid hormone concentrations and protein expression values was investigated with PLS in the F-Isch group and was established if the relationship had an extracted VIP score higher than 1.3. 4-hydroxyestrone (n = 381), 2-hydroxyestrone (n = 196), estradiol (n = 141) and corticosterone (n = 93) had the most associated proteins. Subsequently, gene ontology biological process (GO) enrichment analysis was conducted on all hormone-associated protein groups to identify common biological processes that might be regulated by these hormones. Significant GO enrichment was observed in three protein groups: 4-hydroxyestrone, 2-hydroxyestrone, and estradiol (Fig. 6). Estradiol and 2-hydroxyestrone were associated with proteins involved in oxidative phosphorylation and aerobic respiration. Additionally, estradiol was linked to proteins of the tricarboxylic acid cycle, while 2-hydroxyestrone was specifically associated with proteins involved in fatty acid β-oxidation. Proteins associated with 4-hydroxyestrone were also involved in cellular respiration but showed a strong association with elements of supramolecular fibers and the cytoskeleton, particularly actin filament-related proteins.

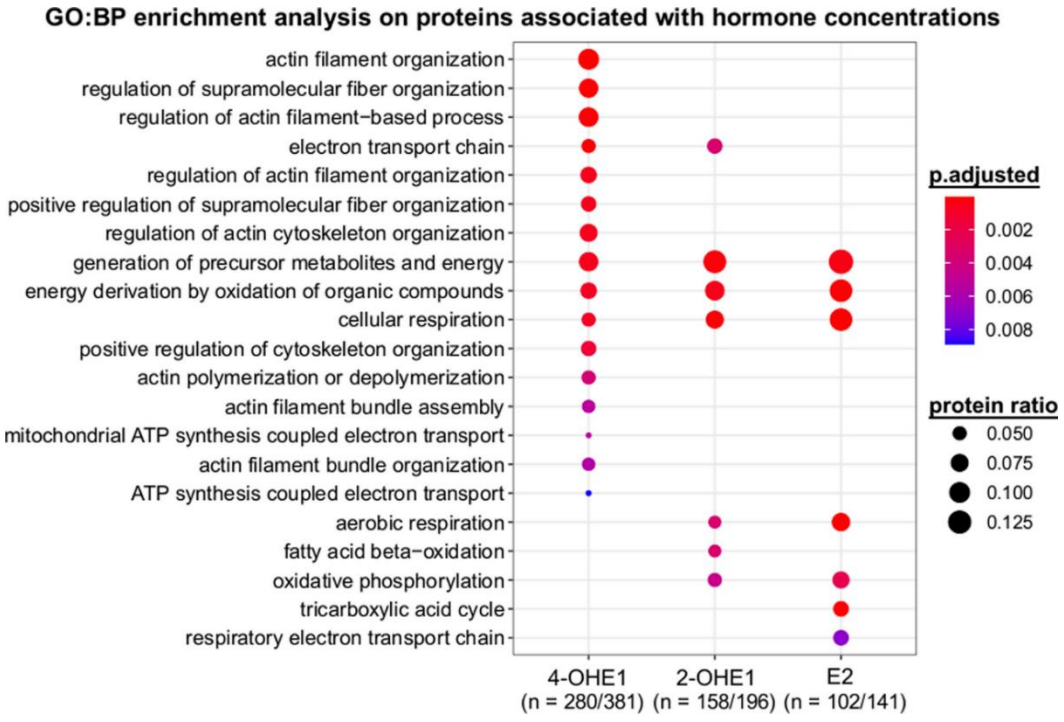

Figure 6. Gene ontology biological process enrichment analysis on proteins associated with hormone concentrations after ischemia in females

2-OHE1: 2-hydroxyestrone; 4-OHE1: 4-hydroxyestrone; E2: estradiol. Source: reproduced from Barta et al. (129).

4.2. Results of the AB-Debanding Study

4.2.1. Sex Differences and Similarities under Control and Pressure Overloaded States

In the sham groups, notable sex-specific differences were observed. Male rats in both week 6 and week 12 had significantly higher body weights compared to their female counterparts. This difference in body weight was mirrored by a greater LVmass in males. Additionally, male rats showed thicker AWTd and larger chamber dimensions, specifically in LVEDD and LVESD. The cardiomyocyte diameter CD was also greater in males, alongside a higher HW/TL, reflecting their larger overall heart size. One of the key molecular differences was observed in the ratio of myh7/myh6 mRNA expression, which was higher in male rats, indicating differences in myocardial gene expression. On the other hand, female rats exhibited higher LVESP, Ea, and ESPVR, alongside a shorter τ (Table 2).

In the AB groups, similar to the Co groups, male rats displayed significantly higher BW, LVmass, cardiomyocyte diameter CD, chamber dimensions LVEDD, LVESD, and myh7/myh6 mRNA expression ratio compared to their age-matched female counterparts. Over time, from week 6 to week 12, male rats experienced a reduction in LV contractility, as indicated by a decrease in PRSW, which did not occur in female rats. This reduction in contractility in males led to impaired VAC and decreased EF. Additionally, male rats exhibited more severe diastolic dysfunction, as reflected by a higher τ and elevated LVEDP. These findings indicate that male AB rats suffer more pronounced cardiac dysfunction and structural changes compared to females. (Table 3).

Table 2. Characersitics of the sham groups

*Values are expressed as mean ± SE. Two-way analysis of variance (ANOVA) was performed with the factors of sex and age. *P < 0.05 male sham week 6 vs. female sham week 6 and male sham week 12 vs. female sham week 12. #P < 0.05 male sham week 6 vs. male sham week 12 and female sham week 6 vs. female sham week 12. AWTd, anterior wall thickness measured in diastole; AWTs, anterior wall thickness measured in systole; CD, cardiomyocyte diameter; CO, cardiac output; DBP, diastolic arterial blood pressure; Ea, arterial elastance; EF, ejection fraction; EDPVR, slope of end-diastolic PV relationship; ESPVR, slope of end-systolic PV relationship; HR, heart rate; HW/TL, heart weight-to-tibial length ratio; LVEDD, LV end-diastolic diameter; LVEDP, LV end-diastolic pressure; LVEDV, LV end-diastolic volume; LVESD, LV end-systolic diameter; LVESP, LV end-systolic pressure; LVESV, LV end-systolic volume; MAP, mean arterial pressure; myh6, α-type myosin heavy chain; myh7, β-type myosin heavy chain; nppa, atrial type natriuretic peptide; PWTd: posterior wall thickness measured in diastole; PWTs, posterior wall thickness measured in systole; PRSW, preload recruitable stroke work; SBP, systolic arterial blood pressure; SV, stroke volume; τ, active relaxation time constant; VAC, ventriculoarterial coupling. Boldface values indicate significant changes. Source: reproduced from Ruppert et al. (121).*

Table 2	**Sham (W*eek 6*)**		**Sham (W*eek 12*)**		**Two-Way ANOVA**		
Parameters	**Male (n=9)**	**Female (n=8)**	**Male (n=9)**	**Female (n=9)**	***P* (sex)**	***P* (age)**	***P* (interaction)**
Body weight, g	486 ± 11	288 ± 9*	595 ± 9#	320 ± 6*	**<0.001**	**<0.001**	**<0.001**
HW/TL, g/cm	0.33 ± 0.01	0.24 ± 0.01*	0.36 ± 0.01#	0.25 ± 0.01*	**<0.001**	**0.003**	0.467
HR, beats/min	357 ± 7	357 ± 10	356 ± 5	364 ± 12	0.631	0.754	0.705
MAP, mmHg	123 ± 4	125 ± 3	118 ± 4	118 ± 4	0.779	0.133	0.743
SBP, mmHg	144 ± 5	146 ± 4	137 ± 5	138 ± 4	0.675	0.111	0.901
DBP, mmHg	112 ±	115 ± 3	109 ± 3	108 ± 5	0.833	0.172	0.656
E_a, mmHg/μL	0.79 ± 0.05	1.04 ± 0.10	0.70 ± 0.05	0.90 ± 0.05	**0.002**	0.088	0.704
LVEDP, mmHg	3.6 ± 0.4	3.6 ± 0.2	3.7 ± 0.4	3.4 ± 0.3	0.660	0.939	0.624

Table 2	**Sham (W*eek 6*)**		**Sham (W*eek 12*)**		**Two-Way ANOVA**		
Parameters	**Male (n=9)**	**Female (n=8)**	**Male (n=9)**	**Female (n=9)**	***P* (sex)**	***P* (age)**	***P* (interaction)**
LVESP, mmHg	139 ± 3	140 ± 4	128 ± 3	136 ± 3	**0.033**	0.109	0.896
LVEDV, µL	316 ± 17	269 ± 26	334 ± 20	298 ± 10	**0.035**	0.229	0.782
LVESV, µL	138 ± 13	130 ± 16	144 ± 13	139 ± 6	0.570	0.558	0.886
SV, µL	178 ± 16	140 ± 11	190 ± 11	159 ± 9	**0.008**	0.200	0.777
CO, mL/min	64 ± 6	49 ± 3	68 ± 5	57 ± 3	**0.010**	0.173	0.670
EF, %	56 ± 3	55 ± 2	58 ± 2	53 ± 2	0.253	0.898	0.509
τ, ms	14.1 ± 0.4	12.5 ± 0.6	13.1 ± 0.4	12.1 ± 0.4	**0.007**	0.143	0.503
ESPVR, mmHg/µL	1.73 ± 0.21	2.03 ± 0.26	1.48 ± 0.21	2.08 ± 0.15	**0.036**	0.639	0.468
PRSW, mmHg	79 ± 4	91 ± 7	75 ± 6	85 ± 7	0.083	0.466	0.836
EDPVR, mmHg/µL	0.037 ± 0.005	0.043 ± 0.006	0.028 ± 0.004	0.032 ± 0.003	0.326	**0.041**	0.816
VAC	0.52 ± 0.07	0.55 ± 0.07	0.53 ± 0.06	0.45 ± 0.04	0.731	0.519	0.367
LV_{mass}, mg	1,057 ± 52	694 ± 37*	1,199 ± 40	748 ± 27*	**<0.001**	**0.021**	0.277
AWT_d, mm	1.97 ± 0.04	1.74 ± 0.05*	1.93 ± 0.07	1.70 ± 0.06*	**<0.001**	0.560	0.994
AWT_s, mm	3.08 ± 0.09	2.95 ± 0.14	3.25 ± 0.08	2.95 ± 0.10	**0.044**	0.402	0.398
PWT_d, mm	1.83 ± 0.09	1.69 ± 0.09	2.05 ± 0.10	1.86 ± 0.07	0.066	**0.024**	0.879
PWT_s, mm	2.93 ± 0.13	2.82 ± 0.07	3.28 ± 0.08#	2.98 ± 0.05	0.031	**0.004**	0.299
LVEDD, mm	8.68 ± 0.21	7.17 ± 0.16*	8.86 ± 0.18	7.27 ± 0.20*	**<0.001**	0.461	0.849
LVESD, mm	5.41 ± 0.18	3.97 ± 0.23*	5.09 ± 0.13	4.01 ± 0.19*	**<0.001**	0.438	0.330
CD, µm	14.5 ± 0.5	13.3 ± 0.3	15.3 ± 0.4	13.5 ± 0.4*	0.001	0.209	0.406
Fibrosis, %	3.6 ± 0.1	3.7 ± 0.1	4.0 ± 0.18	3.9 ± 0.2	0.936	**0.049**	0.546
Nppa	1.04 ± 0.30	1.19 ± 0.23	1.64 ± 0.33	1.13 ± 0.25	0.943	0.457	0.300
myh7/myh6	2.01 ± 0.35	1.36 ± 0.29	3.24 ± 0.33#	1.93 ± 0.14*	**0.002**	**0.005**	0.297

Table 3. Characteristics of the aortic banded groups

*Values are expressed as mean ± SE. Two-way analysis of variance (ANOVA) was performed with the factors of sex and age. *P < 0.05 male AB week 6 vs. female AB week 6 and male AB week 12 vs. AB sham week 12. #P < 0.05 male AB week 6 vs. male AB week 12 and female AB week 6 vs. female AB week 12. AB, aortic banding; AWTd, anterior wall thickness measured in diastole; AWTs, anterior wall thickness measured in systole; CD, cardiomyocyte diameter; CO, cardiac output; DBP, diastolic arterial blood pressure; Ea, arterial elastance; EF, ejection fraction; EDPVR, slope of end-diastolic PV relationship; ESPVR, slope of end-systolic PV relationship; HR, heart rate; HW/TL, heart weight-to-tibial length ratio; LVEDD, LV end-diastolic diameter; LVEDP, LV end-diastolic pressure; LVEDV, LV end-diastolic volume; LVESD, LV end-systolic diameter; LVESP, LV end-systolic pressure; LVESV, LV end-systolic volume; MAP, mean arterial pressure; myh6, α-type myosin heavy chain; myh7, β-type myosin heavy chain; nppa, atrial type natriuretic peptide; PWTd: posterior wall thickness measured in diastole; PWTs, posterior wall thickness measured in systole; PRSW, preload recruitable stroke work; SBP, systolic arterial blood pressure; SV, stroke volume; τ, active relaxation time constant; VAC, ventriculoarterial coupling. Boldface values indicate significant changes. Source: reproduced from Ruppert et al. (121).*

Table 3	**AB (*Week 6*)**		**AB (*Week 12*)**			**Two-Way ANOVA**	
Parameters	**Male (n=10)**	**Female (n=8)**	**Male (n=10)**	**Female (n=8)**	***P* (sex)**	***P* (age)**	***P* (interaction)**
Body weight, g	479 ± 7	314 ± 12*	599 ± 11#	336 ± 11*	**<0.001**	**<0.001**	**<0.001**
HW/TL, g/cm	0.44 ± 0.01	0.32 ± 0.02*	0.47 ± 0.01	0.31 ± 0.02*	**<0.001**	**0.008**	0.240
HR, beats/min	371 ± 11	365 ± 12	369 ± 6	384 ± 7	0.656	0.364	0.256
MAP, mmHg	173 ± 3	186 ± 8	172 ± 5	180 ± 8	0.081	0.573	0.637
SBP, mmHg	217 ± 5	232 ± 11	213 ± 6	224 ± 10	0.107	0.446	0.835
DBP, mmHg	150 ± 3	163 ± 7	152 ± 5	158 ± 7	0.109	0.337	0.555
E_a, mmHg/μL	1.19 ± 0.09	1.23 ± 0.15	1.41 ± 0.12	1.50 ± 0.12	0.620	**0.034**	0.716
LVEDP, mmHg	5.2 ± 0.8	5.3 ± 0.8	7.7 ± 1.3	3.0 ± 0.4*	**0.020**	0.907	**0.018**

Table 3	**AB (*Week 6*)**		**AB (*Week 12*)**			**Two-Way ANOVA**	
Parameters	**Male (n=10)**	**Female (n=8)**	**Male (n=10)**	**Female (n=8)**	***P* (sex)**	***P* (age)**	***P* (interaction)**
LVESP, mmHg	199 ± 5	202 ± 9	201 ± 5	210 ± 7	0.358	0.450	0.605
LVEDV, µL	341 ± 17	301 ± 21	357 ± 18	293 ± 7	**0.005**	0.788	0.481
LVESV, µL	164 ± 9	127 ± 15	201 ± 10	148 ± 7*	**<0.001**	**0.010**	0.463
SV, µL	176 ± 12	174 ± 11	157 ± 14	145 ± 8	0.560	0.055	0.712
CO, mL/min	65 ± 4	64 ± 5	58 ± 5	56 ± 3	0.753	0.112	0.906
EF, %	52 ± 2	59 ± 3	43 ± 2#	50 ± 2	**0.006**	**<0.001**	0.838
τ, ms	18.1 ± 1.0	15.2 ± 1.0	19.6 ± 0.7	15.2 ± 1.3*	**<0.001**	0.453	0.418
ESPVR, mmHg/µL	3.23 ± 0.36	4.22 ± 0.89	1.87 ± 0.15	3.92 ± 0.46*	**0.004**	0.106	0.292
PRSW, mmHg	134 ± 12	165 ± 15	85 ± 12#	136 ± 13*	**0.002**	0.003	0.140
EDPVR, mmHg/µL	0.040 ± 0.008	0.054 ± 0.010	0.047 ± 0.007	0.047 ± 0.007	0.342	0.802	0.581
VAC	0.42 ± 0.07	0.34 ± 0.04	0.80 ± 0.10#	0.41 ± .0.05*	**0.003**	**0.003**	**0.040**
LV_{mass}, mg	1,424 ± 40	1,022 ± 53*	1,748 ± 74#	1,075 ± 86*	**<0.001**	**0.007**	**0.046**
AWT_d, mm	2.59 ± 0.09	2.23 ± 0.10	2.38 ± 0.07	2.29 ± 0.12	0.019	0.464	0.195
AWT_s, mm	3.87 ± 0.14	3.45 ± 0.16	3.40 ± 0.12	3.58 ± 0.10	0.417	0.238	**0.027**
PWT_d, mm	2.26 ± 0.07	2.25 ± 0.14	2.38 ± 0.10	2.21 ± 0.17	0.454	0.754	0.530
PWT_s, mm	3.66 ± 0.11	3.67 ± 0.19	3.50 ± 0.11	3.43 ± 0.13	0.823	0.137	0.743
LVEDD, mm	8.26 ± 0.22	7.19 ± 0.24*	9.58 ± 0.19#	7.35 ± 0.23*	**<0.001**	**0.002**	**0.014**
LVESD, mm	4.96 ± 0.27	4.10 ± 0.27	6.60 ± 0.25#	4.21 ± 0.31*	**<0.001**	**0.004**	**0.009**
CD, µm	18.0 ± 0.3	16.1 ± 0.6*	19.6 ± 0.5	18.1 ± 0.3#	**<0.001**	**<0.001**	0.621
Fibrosis, %	5.3 ± 0.6	5.5 ± 0.5	8.8 ± 0.7#	6.7 ± 0.6	0.151	**<0.001**	0.065
Nppa	8.49 ± 1.83	8.5 ± 2.9	13.9 ± 2.3	7.3 ± 1.7	0.151	0.359	0.140
myh7/myh6	5.42 ± 0.75	4.61 ± 1.29	7.87 ± 1.06	3.47 ± 0.61*	**0.010**	0.066	0.489

4.2.2. Effect of Sex on Pressure Unloading-Induced reverse and anti remodeling

Comparison of male and female DB groups are depicted in Table 4. Similar to the sham and AB groups, comparison of DB animals revealed greater BW, LVmass, wall thicknesses (AWTd, PWTd), LVEDD, HW/TL, CD, and myh7/myh6 gene expression ratio in male rats compared with their female counterparts. Furthermore, the male DB group was also associated with more severe interstitial fibrosis (Table 4).

As detailed above, the sex and age of animals greatly influenced the measured parameters even in healthy control states. Therefore, to investigate the effect of sex on the processes of reverse and anti-remodeling, the DB, the AB week 6, and the week 12 groups were normalized to their corresponding sham groups and subsequently compared within a different analysis. These comparisons are summarized in Figs. 8, 9 and 10; Tables 5 and 6.

Table 4. Hemodynamic characteristics of the DB groups

Values are means ± SE. AWTd, anterior wall thickness measured in diastole; AWTs, anterior wall thickness measured in systole; CD, cardiomyocyte diameter; CO, cardiac output; DBP, diastolic arterial blood pressure; Ea, arterial elastance; EDPVR, slope of end-diastolic PV relationship; EF, ejection fraction; ESPVR, slope of end-systolic PV relationship; HR, heart rate; HW/TL, heart weight-to-tibial length ratio; LVEDD, LV end-diastolic diameter; LVEDP, LV end-diastolic pressure; LVEDV, LV end-diastolic volume; LVESD, LV end-systolic diameter; LVESP, LV end-systolic pressure; LVESV, LV end-systolic volume; MAP, mean arterial pressure; myh6, α-type myosin heavy chain; myh7, β-type myosin heavy chain; nppa, atrial type natriuretic peptide; PRSW, preload recruitable stroke work; PWTd, posterior wall thickness measured in diastole; PWTs, posterior wall thickness measured in systole; SBP, systolic arterial blood pressure; SV, stroke volume; τ, active relaxation time constant; VAC, ventriculoarterial coupling. Boldface values indicate significant changes. Source: reproduced from Ruppert et al. (121).

Table 4			
Parameter	**Male DB *Week 12* (n=10)**	**Female DB *Week 12* (n=12)**	***P*** **(Male vs. Female)**
Body weight, g	557 ± 16	332 ± 8	**<0.001**
HW/TL, g/cm	0.38 ± 0.01	0.28 ± 0.01	**<0.001**
HR, beats/min	365 ± 6	372 ± 9	0.514
MAP, mmHg	134 ± 4	132 ± 5	0.766
SBP, mmHg	161 ± 4	159 ± 6	0.619
DBP, mmHg	121 ± 4	119 ± 5	0.855
E_a, mmHg/µL	0.96 ± 0.08	1.02 ± 0.08	0.570
LVEDP, mmHg	4.5 ± 0.7	3.5 ± 0.37	0.165
LVESP, mmHg	157 ± 4	151 ± 5	0.491
LVEDV, µL	326 ± 19	292 ± 15	0.280
LVESV, µL	154 ± 11	136 ± 11	0.283
SV, µL	173 ± 12	156 ± 10	0.267
CO, mL/min	63 ± 4	58 ± 3	0.306
EF, %	53 ± 2	54 ± 2	0.832
τ, ms	13.9 ± 0.6	12.4 ± 0.5	0.082
ESPVR, mmHg/µL	1.82 ± 0.12	2.62 ± 0.25	**0.014**
PRSW, mmHg	85 ± 9	102 ± 8	0.166
EDPVR, mmHg/µL	0.035 ± 0.004	0.040 ± 0.003	0.268
VAC	0.54 ± 0.04	0.43 ± 0.05	0.097
LV_{mass}, mg	1,285 ± 44	793 ± 37	**<0.001**
AWT_d, mm	2.09 ± 0.05	1.88 ± 0.07	**0.042**
AWT_s, mm	3.29 ± 0.13	3.11 ± 0.12	0.313
PWT_d, mm	2.14 ± 0.08	1.90 ± 0.07	**0.035**
PWT_s, mm	3.36 ± 0.13	3.10 ± 0.10	0.121
LVEDD, mm	8.78 ± 0.15	7.14 ± 0.18	**<0.001**
LVESD, mm	5.41 ± 0.23	4.05 ± 0.19	**<0.001**
CD, µm	16.1 ± 0.5	14.8 ± 0.4	**0.048**
Fibrosis, %	6.0 ± 0.4	4.6 ± 0.3	**0.015**
Nppa	3.27 ± 0.86	1.76 ± 0.40	0.129
myh7/myh6	5.11 ± 0.61	2.03 ± 0.23	**<0.001**

Table 5. Changes in echocardiographic and hemodynamic parameters during pressure overload-induced remodeling and pressure unloading-evoked reverse and anti-remodeling in male and female rats

*Values are expressed as mean ± SE. The AB- (aortic banding; at weeks 6 and 12) and debanding-associated alterations normalized to the corresponding sham groups are listed (as a Δ value). *P < 0.05 vs. AB week 6; #P < 0.05 vs. AB week 12. AWT_d, anterior wall thickness measured in diastole; AWT_s, anterior wall thickness measured in systole; CO, cardiac output; DBP, diastolic arterial blood pressure; E_a, arterial elastance; ESPVR, slope of end-diastolic PV relationship; HR, heart rate; LVEDD, LV end-diastolic diameter; LVEDP, LV end-diastolic pressure; LVEDV, LV end-diastolic volume; LVESD, LV end-systolic diameter; LVESP, LV end-systolic pressure; LVESV, LV end-systolic volume; PWT_d, posterior wall thickness measured in diastole; PWT_s, posterior wall thickness measured in systole; SBP, systolic arterial blood pressure; SV, stroke volume; VAC, ventriculoarterial coupling. Source: reproduced from Ruppert et al. (121).*

Table 5	**Male**			**Female**		
Parameters	**AB *week 6* (n=10)**	**AB *week 12* (n=10)**	**DB (n=10)**	**AB *week 6* (n=8)**	**AB *week 12* (n=8)**	**DB (n=12)**
ΔBody weight, %	99 ± 1	101 ± 2	94 ± 3	109 ± 4	105 ± 4	104 ± 2
ΔHR, %	104 ± 3	104 ± 2	102 ± 2	102 ± 3	106 ± 2	102 ± 2
ΔSBP, %	151 ± 4	155 ± 4	**118 ± 3*#**	159 ± 7	162 ± 8	**115 ± 4*#**
ΔDBP, %	134 ± 2	140 ± 5	**111 ± 4*#**	142 ± 7	143 ± 6	**107 ± 4*#**
ΔE_a, %	151 ± 12	201 ± 17	**137 ± 12#**	118 ± 14	**167 ± 14***	**114 ± 9#**
ΔLVEDP, %	147 ± 23	209 ± 36	122 ± 19	147 ± 22	**91 ± 10***	101 ± 10
ΔLVESP, %	149 ± 4	157 ± 4	**123 ± 3*#**	144 ± 6	155 ± 6	**111 ± 4*#**
ΔLVEDV, %	108 ± 6	107 ± 5	98 ± 6	112 ± 8	98 ± 3	98 ± 5
ΔLVESV, %	119 ± 7	139 ± 7	**107 ± 7#**	98 ± 12	106 ± 5	98 ± 8
ΔSV, %	99 ± 7	83 ± 7	91 ± 6	124 ± 8	92 ± 5	98 ± 6

Table 5	**Male**			**Female**		
Parameters	**AB *week 6* (n=10)**	**AB *week 12* (n=10)**	**DB (n=10)**	**AB *week 6* (n=8)**	**AB *week 12* (n=8)**	**DB (n=12)**
ΔCO, %	102 ± 6	85 ± 8	92 ± 5	129 ± 11	97 ± 6	100 ± 6
ΔVAC, %	81 ± 13	**176 ± 21***	119 ± 8	62 ± 7	91 ± 11	95 ± 11
ΔAWT_d, %	133 ± 4	123 ± 4	**108 ± 3*#**	129 ± 6	135 ± 7	**110 ± 4#**
ΔAWT_s, %	128 ± 5	**104 ± 4***	**101 ± 4***	117 ± 5	122 ± 4	**106 ± 4#**
ΔPWT_d, %	125 ± 4	116 ± 5	**104 ± 4***	133 ± 8	119 ± 9	**102 ± 4***
ΔPWT_s, %	124 ± 4	**107 ± 3***	**102 ± 4***	130 ± 7	115 ± 4	**104 ± 3***
ΔLVEDD, %	96 ± 3	**108 ± 2***	**99 ± 2***	100 ± 3	101 ± 3	98 ± 3
ΔLVESD, %	92 ± 5	**130 ± 5***	**106 ± 5***	103 ± 7	105 ± 8	101 ± 5

Table 6. Comparing the reverse and anti-remodeling effect of pressure unloading therapy in male vs. female rats

Values expressed as mean ± SE. AWT_d, anterior wall thickness measured in diastole; AWT_s, anterior wall thickness measured in systole; CO, cardiac output; DBP, diastolic arterial blood pressure; E_a, arterial elastance; ESPVR, slope of end-diastolic PV relationship; HR, heart rate; LVEDD, LV end-diastolic diameter; LVEDP, LV end-diastolic pressure; LVEDV, LV end-diastolic volume; LVESD, LV end-systolic diameter; LVESP, LV end-systolic pressure; LVESV, LV end-systolic volume; PWT_d, posterior wall thickness measured in diastole; PWT_s, posterior wall thickness measured in systole; SBP, systolic arterial blood pressure; SV, stroke volume; VAC, ventriculoarterial coupling. Boldface values indicate significant changes. Source: reproduced from Ruppert et al. (121).

Table 6	**Reverse-Remodeling (DB vs. AB *Week 6*)**			**Anti-Remodeling (DB vs. AB *Week 12*)**		
Parameters	**Male (n=10)**	**Female (n=12)**	***P* (reverse remodeling)**	**Male (n=10)**	**Female (n=12)**	***P* (anti-remodeling)**
ΔBody weight, %	−5.0 ± 2.8	−4.6 ± 2.2	0.931	−7.1 ± 2.7	−1.0 ± 2.3	0.100
ΔHW/TL, %	−21.6 ± 1.6	−20.0 ± 2.1	0.561	**−18.8 ± 1.6**	**−24.5 ± 2.0**	**0.041**
ΔHR, %	−1.3 ± 1.7	0.2 ± 2.4	0.548	−1.3 ± 1.7	−3.1 ± 2.3	0.536
ΔMAP, %	−19.3 ± 2.2	−24.5 ± 2.9	0.180	−22.2 ± 2.1	−26.5 ± 2.8	0.242
ΔSBP, %	−22.0 ± 2.1	−27.7 ± 2.8	0.130	−24.3 ± 2.1	−29.2 ± 2.7	0.173
ΔDBP, %	−17.2 ± 2.7	−24.2 ± 3.1	0.226	−20.7 ± 2.6	−25.1 ± 3.0	0.377
ΔE_a, %	−9.5 ± 7.8	−3.8 ± 7.4	0.659	−32.0 ± 6.0	−31.8 ± 5.2	0.902
ΔLVEDP, %	−17.1 ± 12.6	−31.7 ± 7.0	0.301	**−41.6 ± 8.9**	**10.5 ± 11.3**	**0.002**
ΔLVESP, %	−17.7 ± 2.0	−22.5 ± 2.5	0.252	−21.8 ± 6.1	−28.1 ± 2.3	0.069
ΔLVEDV, %	−9.3 ± 5.2	−12.2 ± 4.4	0.809	−8.7 ± 5.2	−0.4 ± 5.0	0.308
ΔLVESV, %	−10.0 ± 6.2	0.4 ± 8.4	0.345	−23.4 ± 5.2	−7.6 ± 7.7	0.122
ΔSV, %	−8.4 ± 6.2	−21.4 ± 4.9	0.113	10.1 ± 7.5	7.0 ± 6.6	0.760
ΔCO, %	−9.4 ± 5.3	−22.6 ± 4.3	0.061	8.2 ± 6.3	3.0 ± 5.6	0.545

Table 6	Reverse-Remodeling (DB vs. AB *Week 6*)			Anti-Remodeling (DB vs. AB *Week 12*)		
Parameters	**Male (n=10)**	**Female (n=12)**	***P* (reverse remodeling)**	**Male (n=10)**	**Female (n=12)**	***P* (anti-remodeling)**
ΔEF, %	0.6 ± 3.7	−4.9 ± 4.3	0.361	**22.7 ± 4.6**	**8.3 ± 4.9**	**0.049**
Δτ, %	−17.4 ± 3.6	−16.2 ± 3.7	0.816	**−29.3 ± 3.1**	**−18.4 ± 3.6**	**0.035**
ΔESPVR, %	−34.3 ± 4.4	−39.6 ± 5.8	0.490	**−3.1 ± 6.5**	**−33.3 ± 6.4**	**0.004**
ΔPRSW, %	−33.7 ± 6.7	−34.3 ± 5.0	0.948	**0.5 ± 10.1**	**−25.4 ± 5.6**	**0.030**
ΔEDPVR, %	12.7 ± 12.5	−1.1 ± 6.3	0.314	−25.7 ± 8.3	−15.6 ± 5.4	0.301
ΔVAC, %	47.0 ± 10	54.4 ± 17.1	0.725	**−32.7 ± 4.6**	**3.9 ± 11.5**	**0.013**
ΔLVmass, %	−20.5 ± 2.7	−27.9 ± 3.4	0.104	−26.5 ± 2.5	−26.2 ± 3.4	0.947
ΔAWT_d, %	−18.9 ± 1.9	−14.3 ± 3.2	0.371	−12.5 ± 2.0	−18.0 ± 3.1	0.371
ΔAWT_s, %	**−20.9 ± 3.0**	**−9.8 ± 3.4**	**0.025**	−3.1 ± 3.7	−13.1 ± 3.3	0.056
ΔPWT_d, %	−16.5 ± 3.2	−23.3 ± 2.7	0.117	−10.2 ± 3.4	−14.0 ± 3.0	0.408
ΔPWT_s, %	−17.5 ± 3.2	−20.2 ± 2.4	0.497	−4.1 ± 3.8	−9.5 ± 2.7	0.250
ΔLVEDD, %	3.2 ± 1.8	−2.0 ± 2.5	0.106	−8.3 ± 1.6	−2.9 ± 2.5	0.083
ΔLVESD, %	**15.7 ± 5.0**	**−2.3 ± 4.6**	**0.015**	**−18.0 ± 3.5**	**−4.0 ± 4.5**	**0.025**
ΔCD, %	−15.7 ± 2.6	−9.5 ± 2.4	0.094	−17.5 ± 2.6	−18.1 ± 2.2	0.848
ΔFibrosis, %	**0.7 ± 7.4**	**−23.9 ± 5.3**	**0.012**	−32.4 ± 5.0	−32.3 ± 4.7	0.989
Δnppa, %	−75.6 ± 6.4	−78.4 ± 4.9	0.739	−76.5 ± 6.2	−75.9 ± 5.4	0.942
Δmyh6/myh7, %	**−40.2 ± 7.1**	**−69.0 ± 3.5**	**0.002**	−35.1 ± 7.8	−41.5 ± 6.5	0.537

4.2.2.1. Reverse Remodeling

Reverse remodeling was assessed by comparing the normalized DB group to the normalized AB week 6 group. The results indicated that pressure unloading significantly decreased MAP, SBP, and DBP, leading to a reduction in LVmass, HW/TL ratio, cardiomyocyte diameter (CD), and the expression of nppa and myh7/myh6 mRNA in both male and female animals (Figs. 8, 9, and 10; Table 5). Notably, interstitial fibrosis exhibited a strong decreasing trend in females ($P = 0.08$) but not in males ($P = 0.998$) (Fig. 8D). Contractility indicators such as PRSW and ESPVR also decreased in both sexes after debanding (Fig. 10, C and D). Additionally, the previously prolonged τ was shortened, although this change reached statistical significance only in the male DB group (Fig. 9D).

When comparing the extent of reverse remodeling between male and female groups, females showed greater regression in interstitial fibrosis, LV myh7/myh6 mRNA expression, and LVESD. Conversely, a greater reduction in anterior wall thickness during systole (AWTs) was observed in males (Table 6). All other parameters exhibited similar changes between the two sexes (Table 6).

4.2.2.2. Anti-Remodeling

The anti-remodeling effects of pressure unloading were evaluated by comparing the normalized DB groups with the normalized AB week 12 groups. This comparison revealed significantly lower MAP, SBP, and DBP values in both male and female DB animals, which correlated with a marked reduction in LVmass, HW/TL ratio, CD, and nppa expression, with the latter showing a P value of 0.07 in females (Table 4). Additionally, the male DB group displayed a higher EF and shorter τ compared to the male AB week 12 group, while τ also tended to decrease in females ($P = 0.08$) (Table 4). Direct comparison between the sexes highlighted a stronger anti-remodeling effect in males regarding LVEDP, EF, τ, VAC, and LVESD (Table 6). On the other hand, females exhibited more pronounced changes in ESPVR, PRSW, and HW/TL (Table 6).

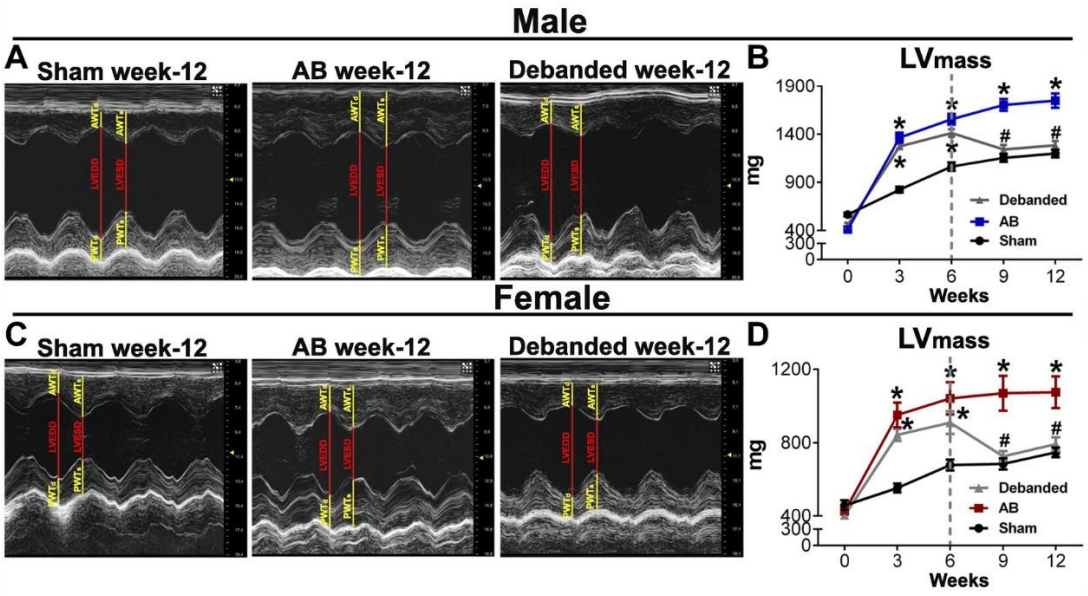

Figure 7. Effect of sex on echocardiography-derived LVmass during the development and regression of pressure overload-induced myocardial hypertrophy

***A** and **C**: representative M-mode echocardiographic images at the midpapillary muscle level are shown in the sham, aortic banded (AB), and DB groups at week 12, demonstrating the development and the regression of LV myocardial hypertrophy in both sexes. **B** and **D**: LVmass increased in both the male and the female AB and DB groups. Removal of the aortic constriction at week 6 resulted in substantial regression of LVmass in both sexes. The experimental groups were compared with each other at every time point using one-way analysis of variance (ANOVA). The number of animals (n) were the following: male sham week 12: n = 9; female sham week 12: n = 9, male AB week 12: n = 10; female AB week 12: n = 8; male DB: n = 11; female DB n = 12. *P < 0.05 vs. sham; #P < 0.05. vs. AB. Source: reproduced from Ruppert et al. (121).*

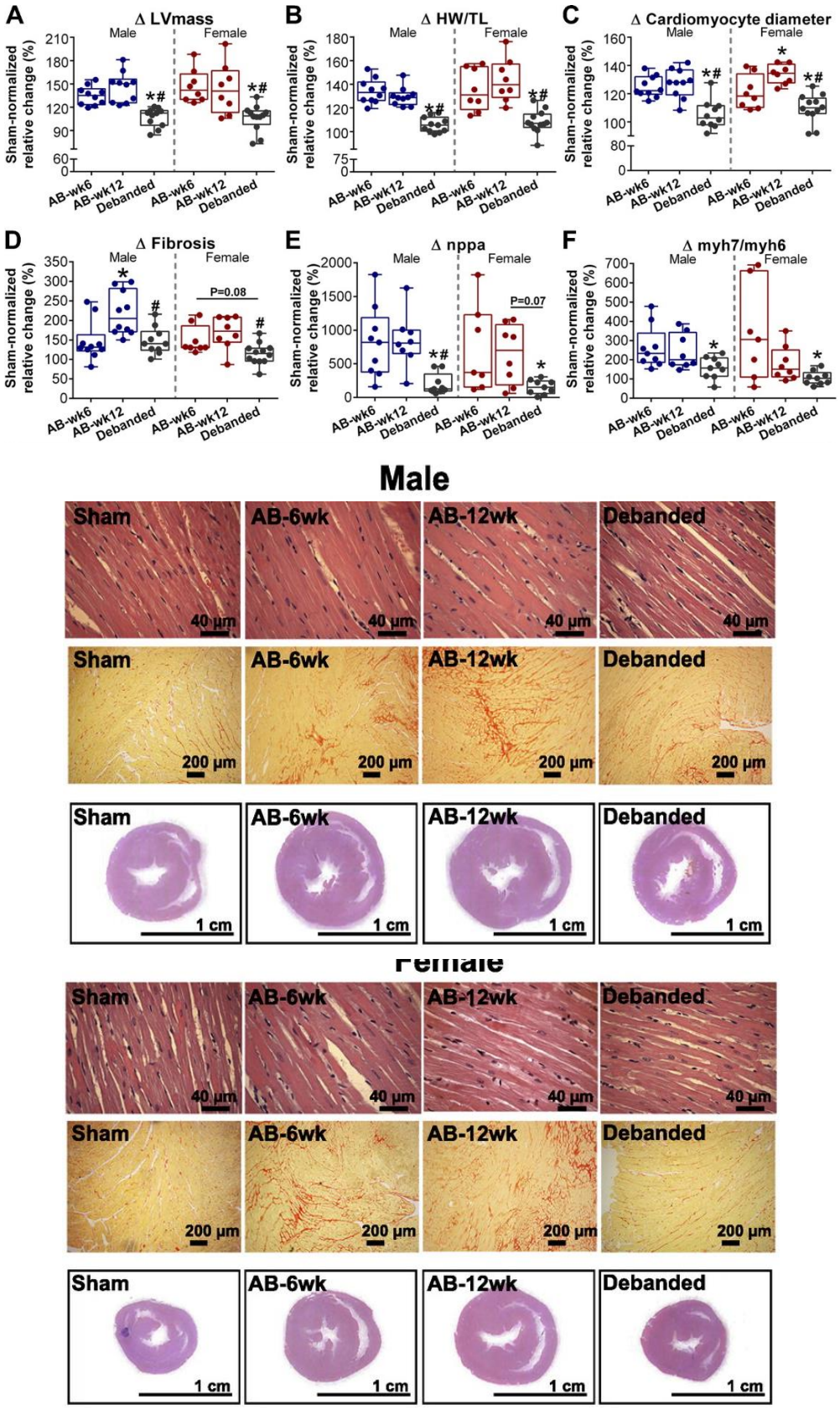
A
Δ LVmass
Male
Female
Sham-normalized relative change (%)
AB-wk6
AB-wk12
Debanded
B
Δ HW/TL
C
Δ Cardiomyocyte diameter
D
Δ Fibrosis
P=0.08
E
Δ nppa
P=0.07
F
Δ myh7/myh6
Male
Sham
AB-6wk
AB-12wk
Debanded
40 μm
200 μm
1 cm
Female

Figure 8. Markers of myocardial hypertrophy, fibrosis, and fetal gene program during pressure unloading-induced reverse and anti-remodeling in male and female rats ***A–C*** *and* ***E****: LVmass, heart weight-to-tibial length ratio (HW/TL), cardiomyocyte diameter (CD), and mRNA levels of atrial type natriuretic peptide (nppa) were decreased in both the male and the female DB groups compared either to the aortic banded (AB) week 6 groups or the AB week 12 groups (in case of nppa only a strong tendency was observed in females).* ***D****: furthermore, interstitial fibrosis was also reduced in the DB groups in both sexes compared with the AB week 12 groups. Nevertheless, only in females, a strong decreasing tendency was also observed when compared with the AB week 6 group (P = 0.08).* ***F****: mRNA levels of β-to α-myosin heavy chain decreased in both DB groups compared with the AB week 6 groups.* ***G****: representative hematoxylin-eosin-stained microphotographs (magnification, ×200; scale bar = 40 μm) of longitudinally orientated cardiomyocytes, Picrosirius red-stained microscopic sections (magnification ×50, scale bar = 200 μm) and cross-sectional whole heart images are shown demonstrating myocardial hypertrophy and intensified fibrosis in the (AB) groups and the regression of these alterations in the DB groups. During statistical analysis, the data sets were previously normalised to the corresponding sham groups (the AB week 6 groups to the sex-matched sham week 6 groups, whereas the AB week 12 and DB groups to the sex-matched sham week 12 groups). These normalised values (expressed as Δ) were compared with each other in males and females with one-way analysis of variance (ANOVA). The number of animals (n) were the following: male AB week 6 group: nppa and myh7/myh6 n = 9, all the other parameters n = 10; female AB week 6 group: nppa and myh7/myh6 n = 7, all the other parameters n = 8; male AB week 12 group: nppa and myh7/myh6 n = 8, all the other parameters n = 10; female AB week 12 group: n = 8 in all measurements, male DB group: LVmass n = 11; nppa and myh7/myh6 n = 9, all the other parameters n = 10; female DB group: nppa and myh7/myh6 n = 9, all the other parameters n = 12. *P < 0.05 vs. AB week 6; #P < 0.05 vs. AB week 12. Source: reproduced from Ruppert et al. (121).*

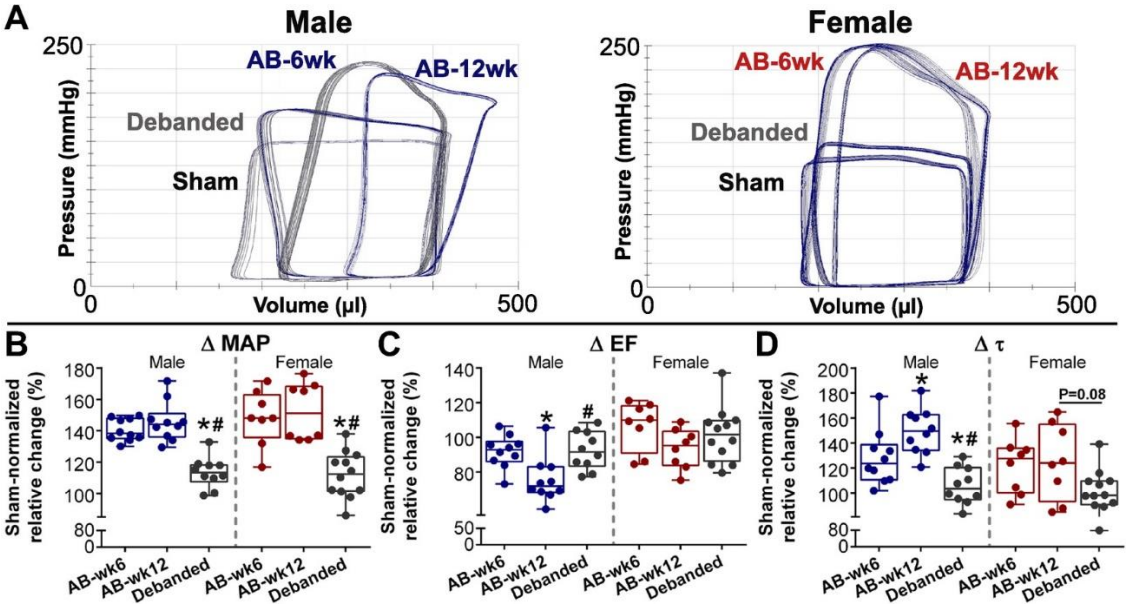

Figure 9. Effect of sex on steady-state hemodynamic parameters

***A**: original recordings of steady-state PV loops are shown in the sham, aortic-banded (AB) week 6 (AB week 6), AB week 12 (AB week 12), and DB male and female groups. **B**: Debanding the aorta resulted in the normalisation of mean arterial pressure (MAP) in both the male and female DB groups compared with either the AB week 6 or the AB week 12 groups. **C**: ejection fraction (EF) showed deterioration in the male but not in the female AB week 12 group compared with the AB week 6 group. Debanding the aortic constriction restored EF in males. **D**: active relaxation time constant τ demonstrated further prolongation in the male AB week 12 group compared with the AB week 6 group. Removing the aortic constriction effectively normalised τ in the male DB group. A strong decreasing trend was also observed in the female DB group compared with the female AB week 12 group. During statistical analysis, the data sets were previously normalised to the corresponding sham groups (the AB week 6 groups to the sex-matched sham week 6 groups, whereas the AB week 12 and DB groups to the sex-matched sham week 12 groups). These normalised values (expressed as Δ) were compared with each other in males and females with one-way analysis of variance (ANOVA). The number of animals (n) was the following: male AB week 6 group: n = 10; female AB week 6 group: n = 8; male AB week 12 group: n = 10; female AB week 12 group: n = 8; male DB group: n = 10; female DB group: n = 12. *P < 0.05 vs. AB week 6; #P < 0.05 vs. AB week 12. Source: reproduced from Ruppert et al. (121).*

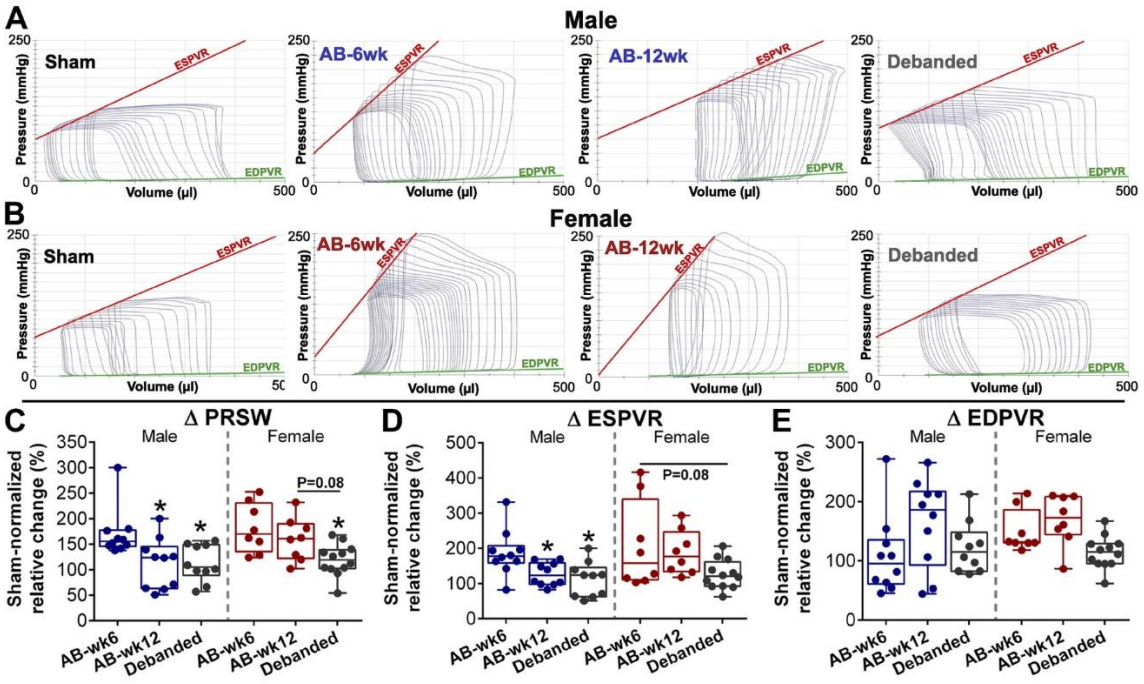

Figure 10. Effect of sex on load-independent contractility and stiffness parameters

A *and* ***B****: original PV (PV) recordings were obtained at different preloads during transient vena cava occlusion in the sham, aortic-banded (AB) week 6 (AB week 6), AB week 12 (AB week 12) and DB male and female groups.* ***C*** *and* ***D****: increases in the slope of the end-systolic PV relationship (ESPVR) and preload recruitable stroke work (PRSW) in the male and female AB week 6 groups were normalised in the DB groups in both sexes. Furthermore, although the contractility markers decreased in the male AB week 12 group compared with the AB week 6 group, ESPVR and PRSW did not change in the female AB week 12 group compared with the AB week 6 group.* ***E****: No statistical difference could be observed in the slope of EDPVR. During statistical analysis, the data sets were previously normalised to the corresponding sham groups. These normalised values (expressed as Δ) were compared with each other in males and females separately with one-way analysis of variance (ANOVA). The number of animals (n) was the following: male AB week 6 group: n = 10; female AB week 6 group: n = 8; male AB week 12 group: n = 10; female AB week 12 group: n = 8; male DB group: n = 10; female DB group: n = 12. *P < 0.05. Source: reproduced from Ruppert et al. (121).*

4.2.2.3. Effect of Sex on Proteomics of Reverse and Anti-Remodeling

Our analysis included 2,348 proteins identified and quantified through LC-MS/MS-based proteomics (for detailed protein expression matrices and analysis tables, refer to the

MSV000089077 entry on the MassIVE repository). To obtain a global overview of the proteomic profiles, we utilised sparse partial least squares discriminant analysis (sPLS-DA) via MixOmics. This analysis revealed a clear distinction between the proteomic profiles of the sham, AB week 6, AB week 12, and DB groups within each sex. The projection of the proteomic data onto the primary axis (C1) accounted for 17% of the variability in the original multidimensional data. In comparison, the secondary axis (C2) captured an additional 6% (Fig. 11A). The top 15 proteins contributing to the separation of the proteomes along the C1 and C2 axes are displayed in order of their importance (Fig. 11B).

To compare individual proteins in greater detail, differential expression analysis was conducted (Fig. 12A and B). The proteomic changes associated with myocardial remodeling due to pressure overload (PO) were found to be of a similar magnitude in both sexes. The number of proteins with significant changes in relative abundance in the AB week 6 groups was comparable between males and females (males: AB week 6 vs. sham: upregulated - 203, downregulated - 227, unchanged - 1,918; females: AB week 6 vs. sham: upregulated - 179, downregulated - 240, unchanged - 1,929; P = 0.3865/NS; Fig. 12, A and B), as well as in the AB week 12 groups (males: AB week 12 vs. sham: upregulated - 220, downregulated - 289, unchanged - 1,839; females: AB week 12 vs. sham: upregulated - 219, downregulated - 256, unchanged - 1,873; P = 0.3148/NS; Fig. 12, A and B). GO enrichment analysis indicated that the key proteomic changes related to PO-induced myocardial remodeling after 6 weeks were characterized by the downregulation of fatty acid metabolism and lipid catabolic processes in both males and females (Fig. 13, A and B).

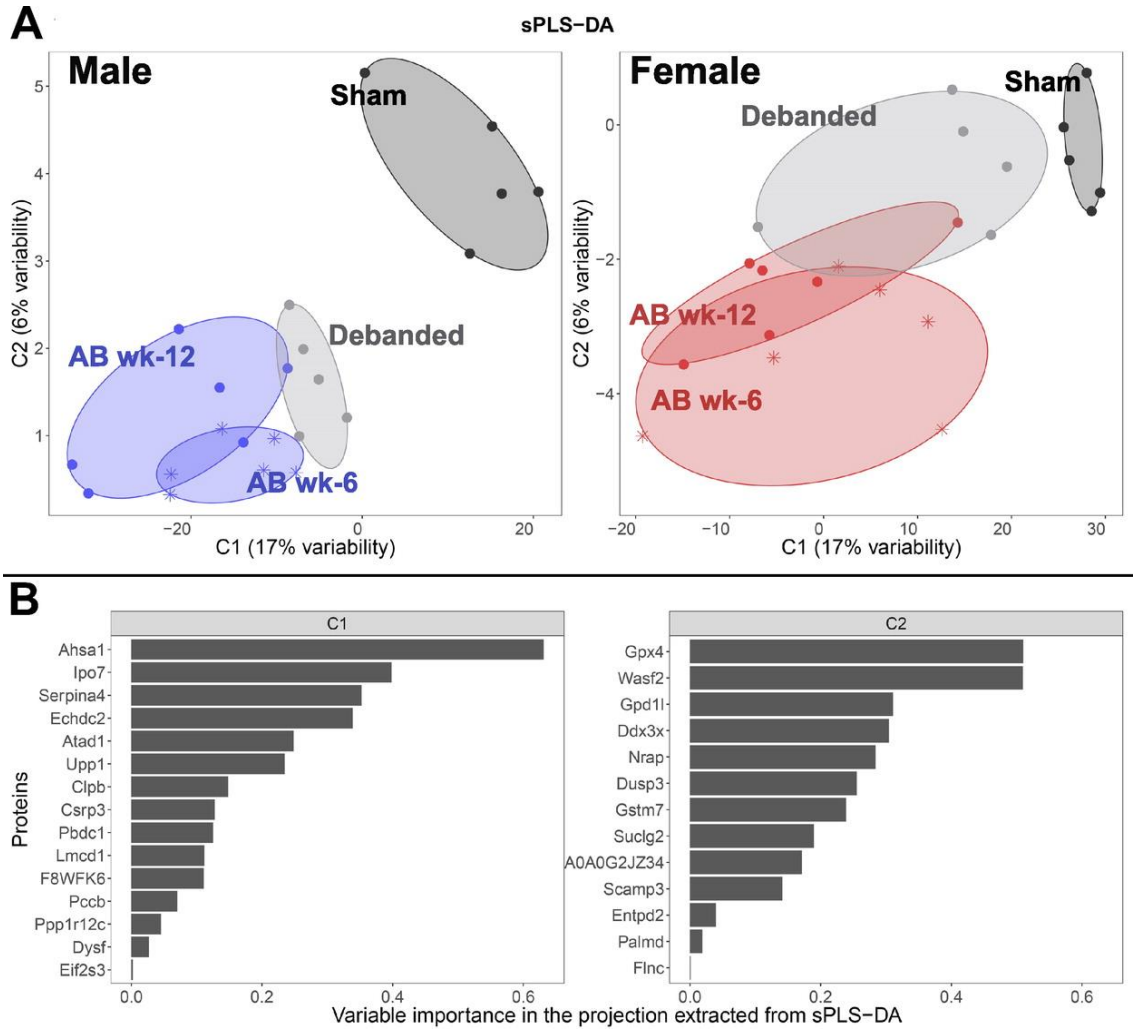

Fig 11. Effect of sex on the proteomic profiles of aortic banded (AB) and DB rats

***A**: A global overview of proteomic profiles was established by sparse partial least squares discriminant analysis. A moderate distinction could be provided among the proteomic profiles of sham, AB week 6, AB week 12, and DB groups of each sex. Projection of the proteomic data set onto the single best axis (C1) has preserved 17% of the variability, whereas the second-best axis (C2) has encompassed 6% of the variability of the original multidimensional data. **B**: 15-15 proteins with the most significant contribution to the separation of proteomes of the individuals of our experimental groups along the C1 and C2 axes are visualised in order of their importance. The number of animals (n) were the following: male sham group: n = 5; female sham group: n = 5; male AB week 6 group: n = 6; female AB week 6 group: n = 6; male AB week 12 group: n = 6; female AB week 12 group: n = 6, male DB group: n = 5; female DB group: n = 5. Source: reproduced from Ruppert et al. (121).*

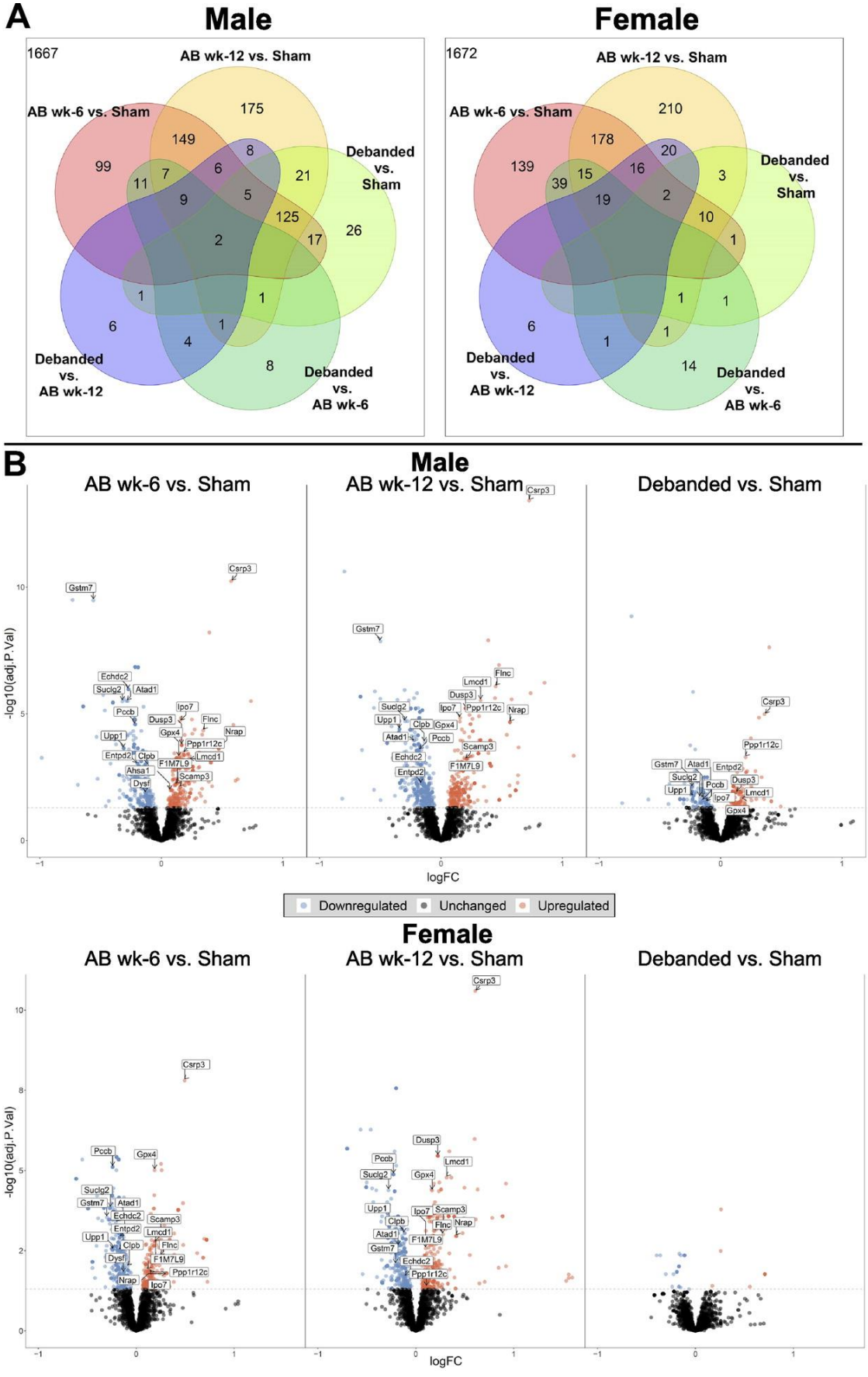
A
Male
1667
AB wk-12 vs. Sham
AB wk-6 vs. Sham
Debanded vs. Sham
Debanded vs. AB wk-12
Debanded vs. AB wk-6
175
149
8
99
7
6
21
11
9
5
125
26
2
17
1
1
6
1
4
8
Female
1672
AB wk-12 vs. Sham
AB wk-6 vs. Sham
Debanded vs. Sham
Debanded vs. AB wk-12
Debanded vs. AB wk-6
210
178
20
139
15
16
3
39
19
2
10
1
1
1
6
1
1
14
B
Male
AB wk-6 vs. Sham
AB wk-12 vs. Sham
Debanded vs. Sham
-log10(adj.P.Val)
logFC
Downregulated
Unchanged
Upregulated
Female
AB wk-6 vs. Sham
AB wk-12 vs. Sham
Debanded vs. Sham
-log10(adj.P.Val)
logFC

Fig 12. Venn diagrams and volcano plots of differential expression analysis

***A**: Venn diagrams of all group comparisons in males and females showing the number of proteins with significantly altered relative expression in each contrast. **B**: volcano plots of the differential expression analysis. The male and female aortic banded (AB) week 6 and AB week 12 groups showed comparable extent of alterations in protein expression when compared with the corresponding sham groups. In contrast, only the male, but not the female, DB group exhibited a substantial difference in protein expression compared with the sex-matched control group. Proteins with high variable importance in the sPLS-DA were labelled. Differential expression analysis was executed with Linear Models for Microarray Data (limma). A protein with an FDR-adjusted $P < 0.05$ was considered significant. Log2-transformed fold changes are represented as logFC. The number of animals (n) were the following: male sham group: n = 5; female sham group: n = 5; male AB week 6 group: n = 6; female AB week 6 group: n = 6; male AB week 12 group: n = 6; female AB week 12 group: n = 6, male DB group: n = 5; female DB group: n = 5. Source: reproduced from Ruppert et al. (121).*

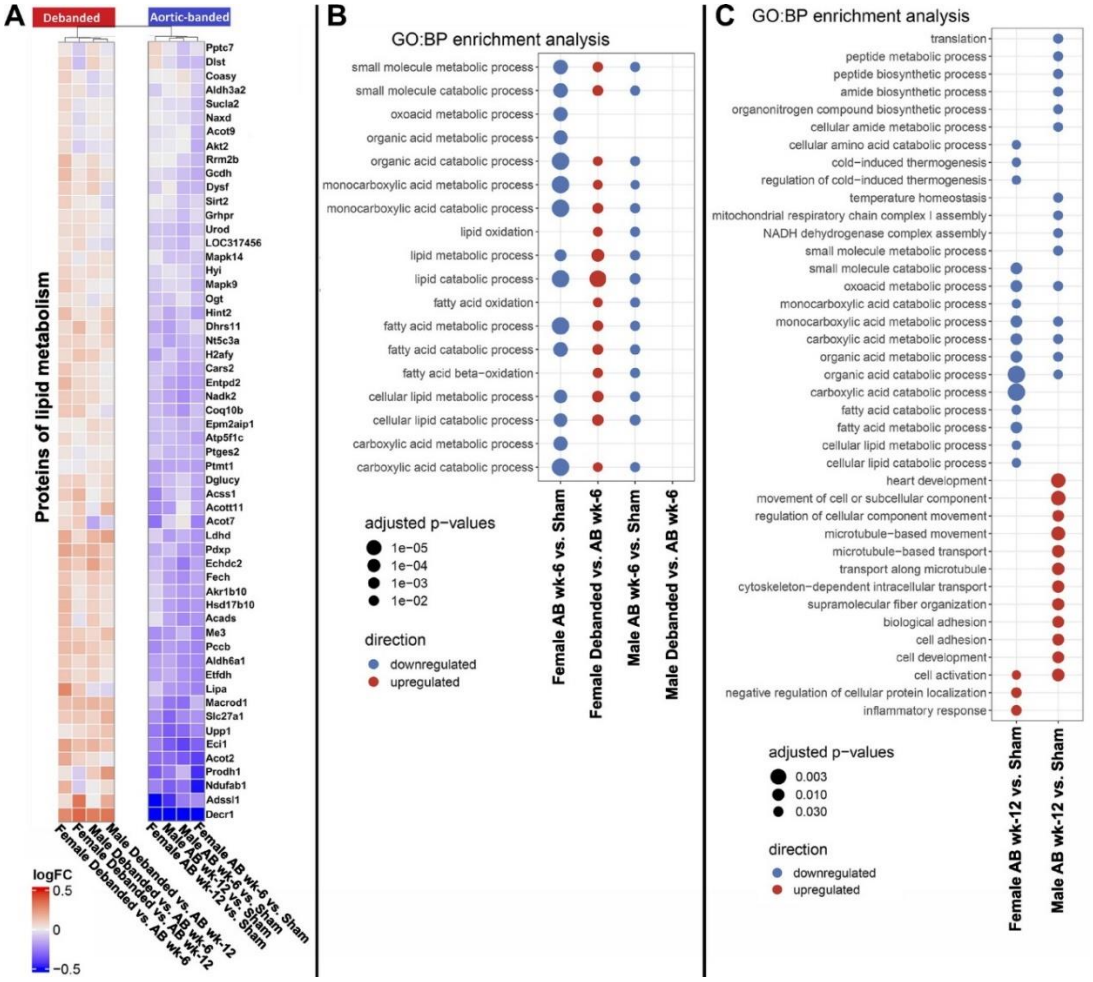

Figure 13. Gene ontology biological process enrichment analysis

***A**: heatmap of proteins related to lipid metabolism that were significantly altered in our analysis. Hierarchical clustering automatically distinguishes aortic banding (AB) and debanding-related changes in expression of lipid metabolism-related proteins. **B**: markedly enriched gene ontology: biological process (GO: BP) terms show sex-dependence of myocardial reverse remodeling. Upregulation and thus normalisation of expression of proteins involved in lipid metabolism can only be observed in DB females, but not in males. **C**: significantly enriched GO: BP terms after 12 wk of pressure overload (PO) showcasing sex-dependent differences. In the male AB rats, upregulation of proteins related to the cytoskeleton and downregulation of peptide biosynthesis and translation, whereas in female AB animals, upregulation of inflammatory processes was identified to be the most characteristic changes. GO:BP overrepresentation analysis was executed with cluster Profiler based on Fisher's exact test. Multiple testing correction was carried out using Benjamini-Hochberg's method. Source: reproduced from Ruppert et al. (121).*

To assess reverse remodeling, the extent of residual proteomic differences that failed to resolve after cessation of PO was investigated in the comparison of DB and sham goups. Following 6 wk of pressure unloading, reverse remodeling has run a full course in females, whereas in males, PO induced proteomic alterations still persisted (Fig. 12, A and B) (male: DB vs. sham: upregulated - 95, downregulated - 103, not significantly changed - 2,150; female: DB vs. sham: upregulated - 5, downregulated - 13, not significantly changed - 2,330; $P < 0.001$). Furthermore, by comparing the GO:BP enrichment of DB rats with their respective AB week 6 groups (reverse remodeling), we observed a recovery from PO-induced alterations in lipid metabolism following pressure unloading exclusively in females. This recovery was marked by significant upregulation of terms including cellular lipid catabolic process, monocarboxylic acid catabolic process, lipid catabolic process, and fatty acid β-oxidation. In contrast, expression of lipid catabolizing proteins in male DB animals did not demonstrate a consistent reversal (Fig. 13, A and B).

The preventive effect of pressure unloading (anti-remodeling) was examined through the detection of proteomic alterations in the week 12 groups (Fig. 13, A and C). Although lipid metabolism-related terms remained prevalent among the significantly downregulated GO:BP categories in both sexes, by week 12, sex-specific differences in the up- and downregulation of particular biological processes became evident. Females showed an upregulation of proteins involved in the inflammatory response (Fig. 13C). In males, terms related to cytoskeleton-dependent intracellular transport, microtubule-based movement, and supramolecular fiber organization indicated extensive cytoskeletal remodeling accompanied by increased expression of proteins involved in cell adhesion. Additionally, males exhibited specific downregulation of proteins associated with peptide biosynthesis and translation (Fig. 13C). A comprehensive table of all GO term-associated proteins and numerous volcano plots, annotated by enriched GO terms, are available as supplementary files in the MassIVE repository.

4.3. Cardiac functional-proteomic reanalysis of the AB-DB Study

After reanalysis of the original mass spectrometry raw files from the AB-Debanding Study using FragPipe, we integrated the most promising parameters from PV analysis, echocardiography, and our updated proteomics data to select functional or morphological parameters that are most reflective of molecular alterations induced by PO and pressure unloading (Fig. 14.).

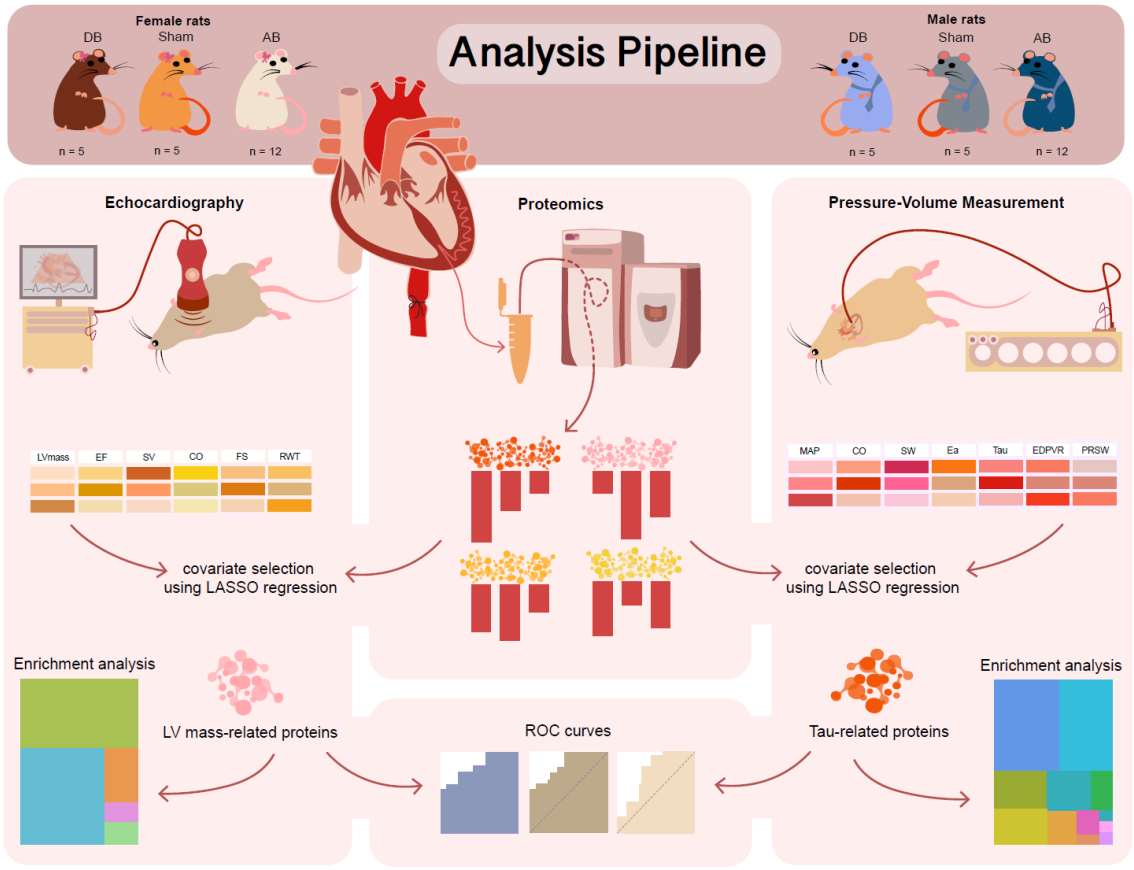

Figure 14. Illustration of data processing steps, including data collection and feature selection

AB, aortic banded; DB, debanded; EF, ejection fraction; SV, stroke volume; CO, cardiac output; FS, fractional shortening; RWT, relative wall thickness; MAP, mean arterial pressure; SW, stroke work; Ea, arterial elastance; EDPVR, end-diastolic pressure–volume relationship; PRSW, preload-recruitable stroke work. Source: Barta et al. ESC Heart Failure in press.

4.3.1. Selecting parameters of PV analysis and echocardiography most reflective of myocardial proteomic alterations

Covariate selection using LASSO regression, with either PV parameters or echocardiographic parameters as predictors for protein abundances, we found one parameter per modality that clearly outperformed the others. The highest number of proteins with a non-zero coefficient and significant limma P value were obtained for τ (the time constant of active LV relaxation) as determined by PV analysis and for LVmass as measured using echocardiography during myocardial remodeling and reverse remodeling (Figure 15). Thus, the following studies are focused on these two key ventricular parameters to uncover their associated proteomic alterations during myocardial remodeling.

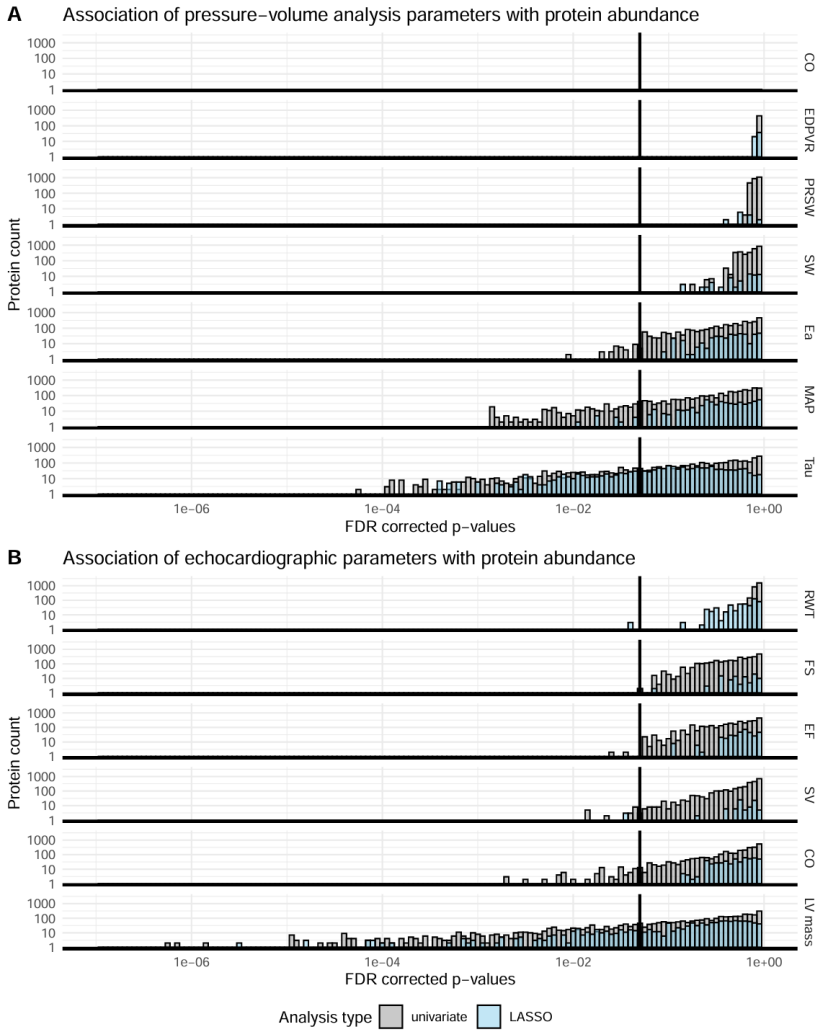

Figure 15. Number of proteins associated with sensitive parameters of PV analysis and echocardiography

Association was determined through multivariate analysis of all proteins with feature selection by LASSO regression. For LASSO, we performed a subsequent limma analysis and defined parameters with a P value < 0.05 as significantly associated with PV or echocardiographic parameters. Panel A illustrates that τ emerges as the PV parameter associated with the largest number of proteins, and Panel B highlights LV mass as the most prevalent echocardiographic parameter. SV: stroke volume; CO: cardiac output; SW: stroke work; dP/dtmax: maximal rate of rise in LV pressure; EF: ejection fraction; PRSW: preload recruitable stroke work; Ea: arterial elastance; MAP: mean arterial pressure; FS: fractional shortening; RWT: relative wall thickness; EDPVR: slope of the end diastolic pressure-volume relationship. Source: Barta et al. ESC Heart Failure in press.

4.3.2. τ surpasses LVmass in both diversity and quantity of protein associations

Gene Ontology enrichment analysis identified significant biological processes, molecular functions, and cellular components associated with both τ and LVmass-linked proteins. Notably, τ, being associated with abundance changes in 842 proteins, displayed a more comprehensive enrichment profile than LVmass, which was associated with 568 proteins. In terms of cellular components, τ shows a stronger association with the protein expression of structural elements of the sarcomere ('supramolecular complex', 'myofibril', 'contractile fibre', 'I band') and the spliceosomal complex. Enrichment of molecular functions results in various gene ontology terms related to DNA binding, regulation of transcription as associated with alterations in τ and LVmass during myocardial remodeling and reverse remodeling (Figure 16).

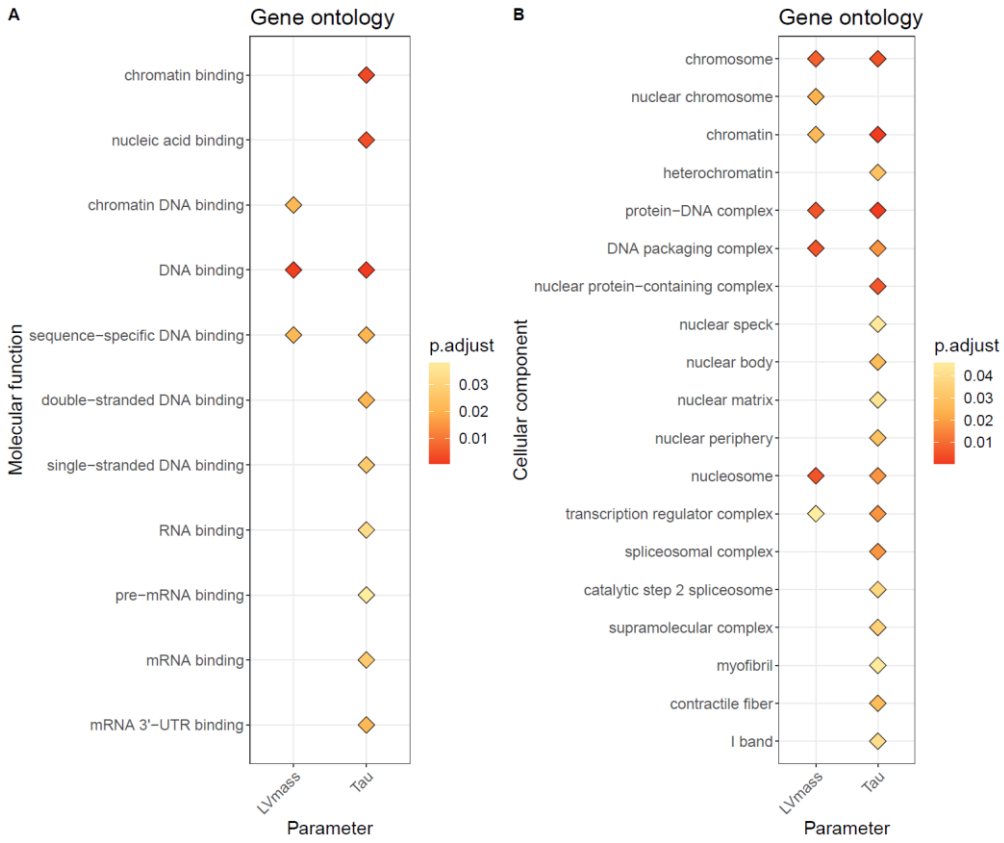

Figure 16 Gene Ontology enrichment analysis for τ and LVmass-related proteins. Plots identifying the molecular functions and cellular compartments of proteins associated with each parameter. The continuous colour scale illustrates the respective FDR-adjusted P-values. Source: Barta et al. ESC Heart Failure in press.

Proteins related to τ are connected to diverse biological processes. Notably, of the 842 τ -related proteins, 47 are connected to cardiac muscle cell development (Figure 17). Further, we identified that τ-related proteins are involved in gene expression regulation and mRNA splicing within the spliceosome machinery. Additionally, τ-related proteins are connected to functions like single-stranded DNA binding, RNA binding, and transcriptional coregulation and coactivation.

Conversely, LVmass was linked to a more confined set of 568 proteins. Those indicate different aspects of myocardial adaptation, with enriched functions of these proteins including DNA-binding transcription factor binding and protein heterodimerization activity (Figure 18). Despite fewer proteins being associated with LVmass than with τ, Gene Ontology terms, such as chromatin binding, nucleic acid binding, DNA binding, and transcription factor binding, were shared among τ and LVmass.

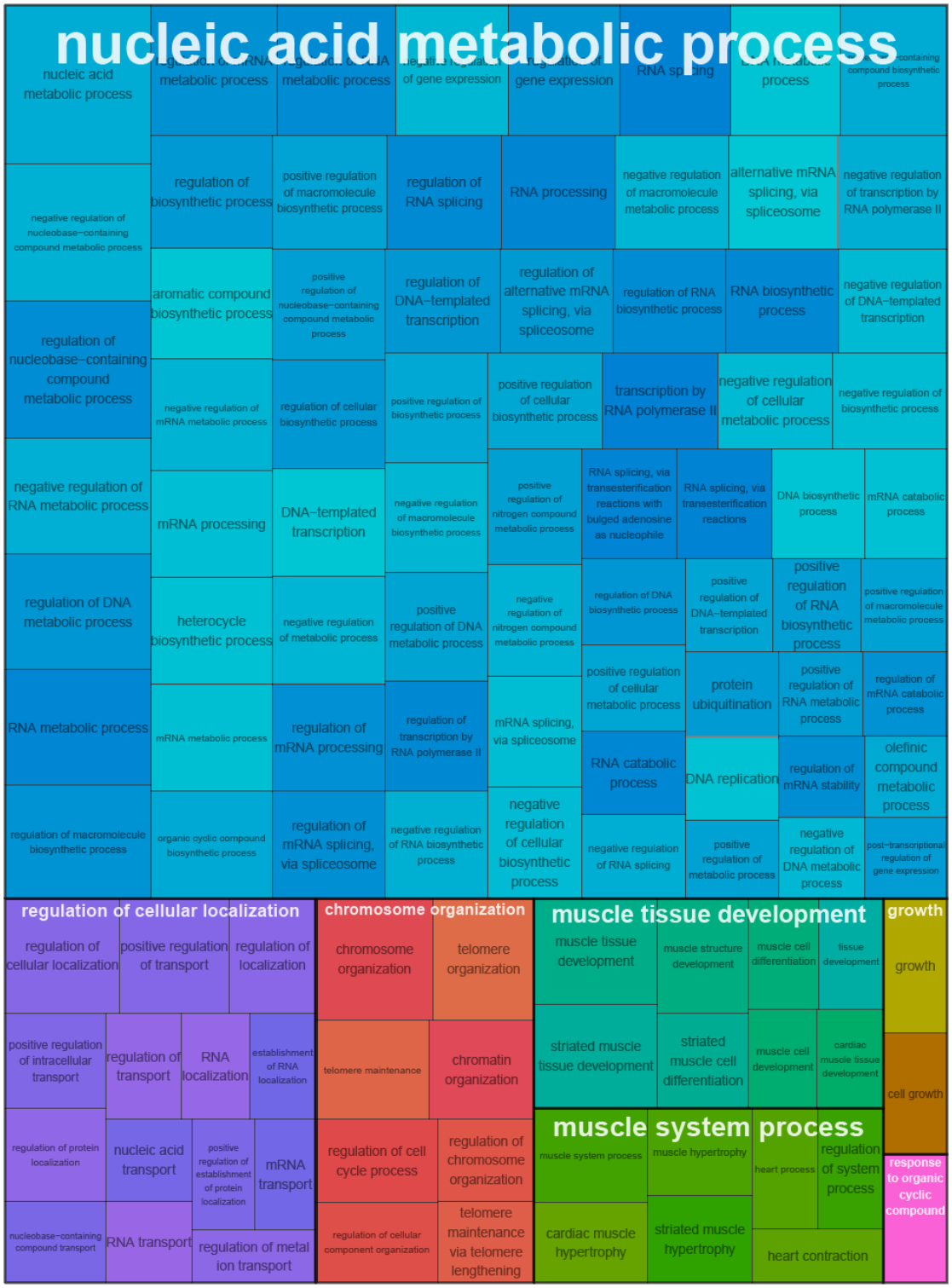

Figure 17. Enrichment of biological process for τ-related proteins

Gene ontology biological process terms significantly enriched in proteins associeted to τ. To provide a better overview, terms were automatically grouped based on semantic similarity. Groups were titled according to the broadest term in the catergory. Source: Barta et al. ESC Heart Failure in press.

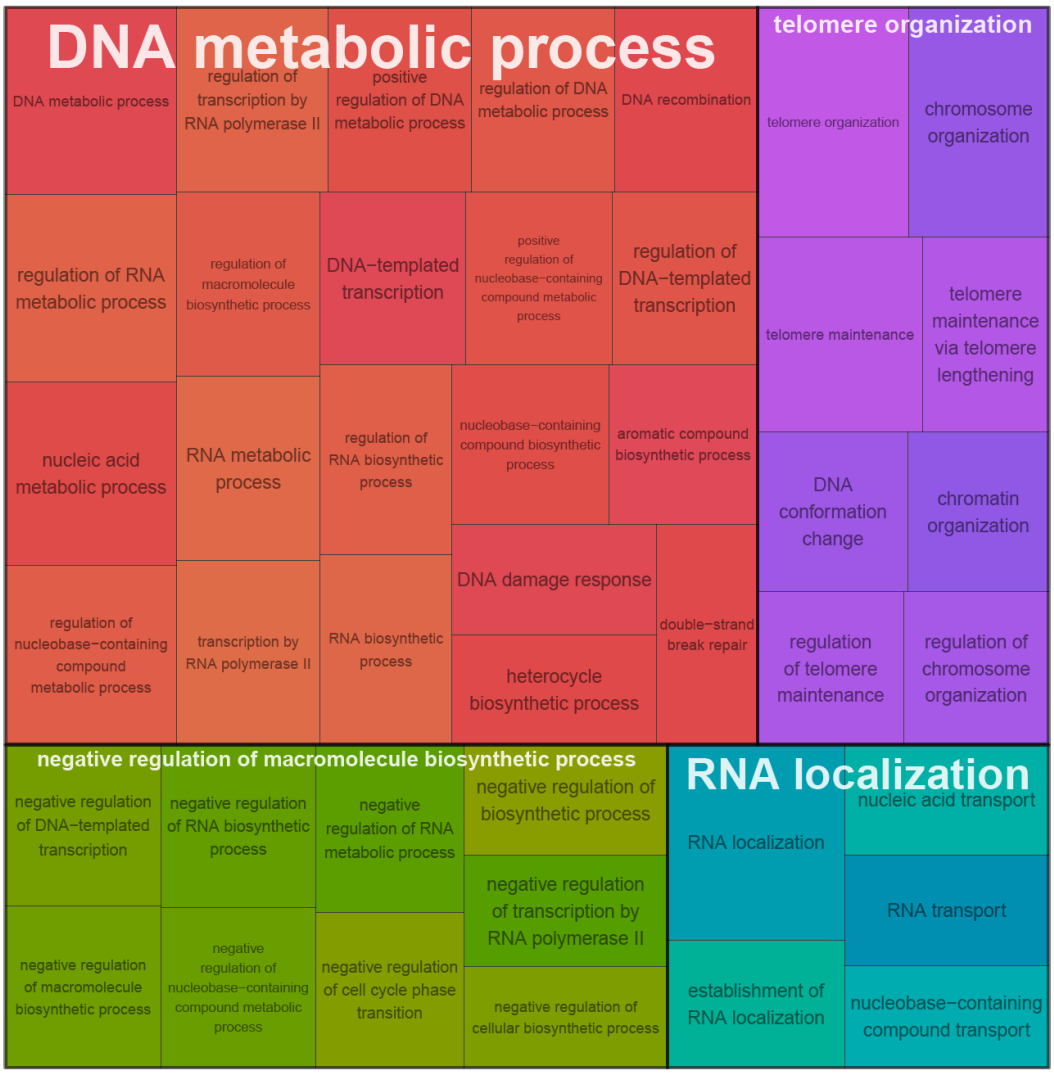

Figure 18. Enrichment of biological processes for LVmass-related proteins

Gene ontology biological process terms were significantly enriched in proteins associated with LVmass. To provide a clearer overview, terms were automatically grouped by semantic similarity. Groups were titled according to the broadest term in the category. Source: Barta et al. ESC Heart Failure in press.

4.3.3. Several τ-related proteins can be used to detect active myocardial remodeling with high accuracy

To investigate the potential of our proteins of interest being used as biomarkers for myocardial remodeling, Co and DB animals were combined into a 'non-banded' group, based on the high functional and proteomic similarity of these conditions substantiated by our previous findings in the same cohort (18). Non-banded animals, thus, represent inactive remodeling, while AB groups active myocardial remodeling. Receiver operating characteristic (ROC) curves of (Figure 19) the proteins associated with τ and/or LVmass revealed a subset of proteins that exhibited an Area under the curve (AUC) higher than 0.85, effectively differentiating the active remodeling of aortic banded (AB) rats from non-banded conditions. Of these, 19 τ -related proteins were identified, compared to only 9 proteins associated with LVmass. Proteins identified as being related exclusively to τ included *ANXA5, GSTK1, COQ9, TMOD4, PCCA, PDLIM5, FBLIM1, EIF4G1, SORBS2, TST, PSME1, DBT, and NRAP*.

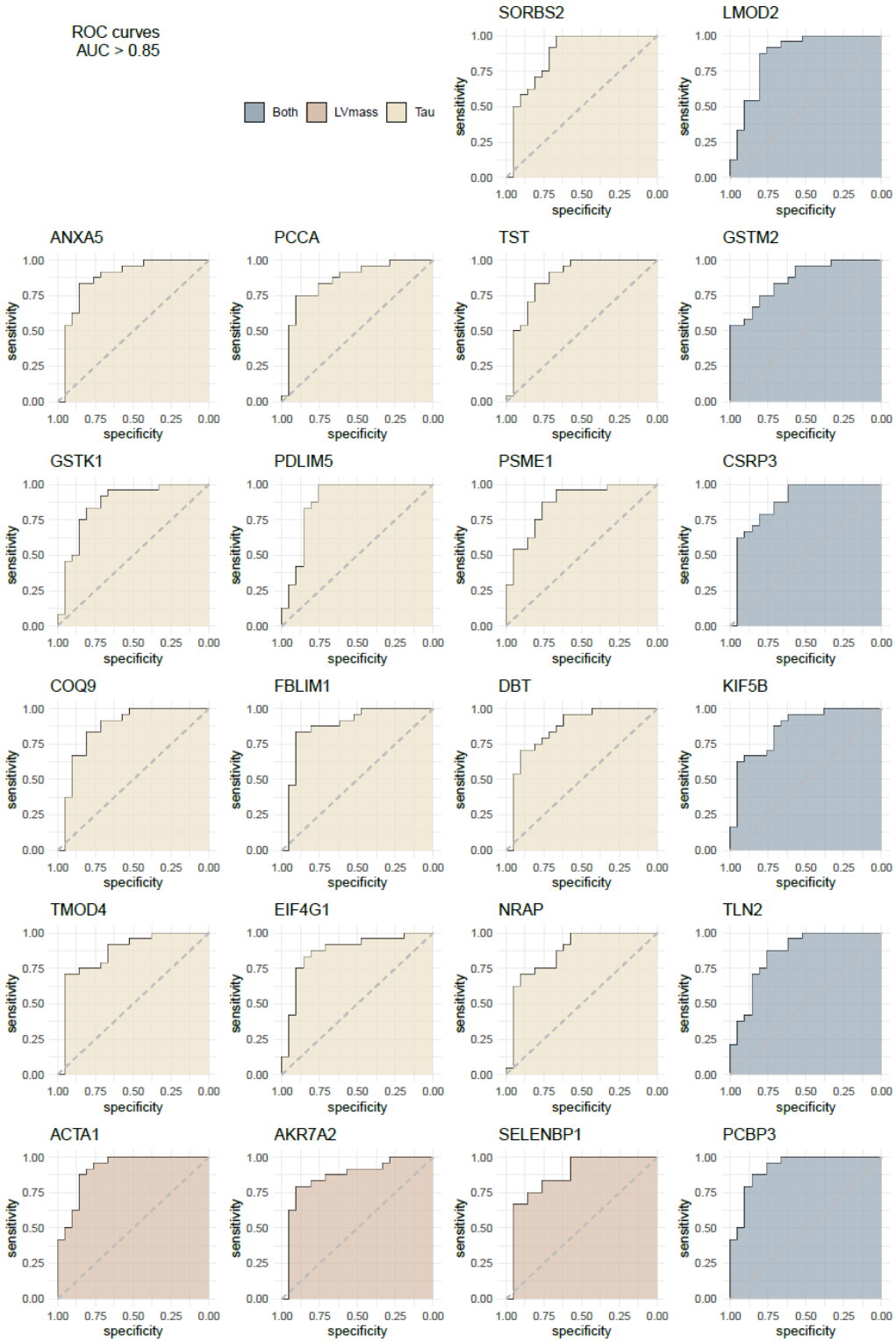

Figure 19. ROC curves of proteins associated with τ with an AUC of more than 0.85

ROC curves based on the calculation of sensitivity and specificity across different thresholds, differentiating active myocardial remodeling (AB) from non-banded (CO, DB) rat proteomes. Source: Barta et al. ESC Heart Failure in press.

4.3.4. Molecular Complex Detection analysis reveals a network of closely interconnected proteins

To investigate the potential interplay among τ-associated proteins in myocardial remodeling and reverse remodeling, protein-protein interaction networks were acquired from the STRING database (Figure 20). Based on the subset of τ-associated proteins a network of 839 closely interconnected nodes with 6142 edges was detected using the MCODE plugin (27) of Cytoscape (28).

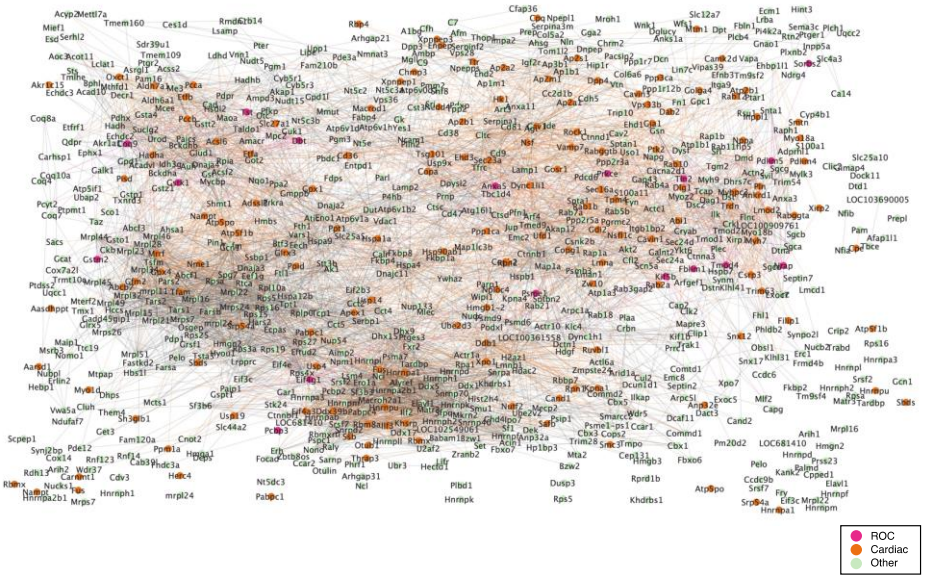

Figure 20. Protein-protein interaction network

Nodes correspond to τ-associated proteins, while the edges represent potential protein-protein interactions, generated using Cytoscape/MCODE on STRING results. Orange-colored proteins are related to cardiac GO terms containing the following expressions: 'heart', 'muscle', 'contraction', 'I band'. Pink-colored proteins have been identified by the high AUC of ROC curves. Source: Barta et al. ESC Heart Failure in press.

Several of the τ-related proteins, which demonstrated an AUC > 0.85, were confirmed as hub genes by the MCODE analysis (Figure 20). Proteins related to cardiac GO terms containing the following expressions: 'heart', 'muscle', 'contraction', 'I band', and 'cardiac' were also identified and highlighted in the network plot. Furthermore, MCODE analysis identified three main protein clusters, or subnetworks (MCODE scores: 9.138, 5.419, and 3.231). These subnetworks highlight functionally closely related or interacting proteins within the network of τ-associated proteins. To shed light on the dynamic relationship among the members of the subnetworks, pairwise correlations were calculated for each condition (Co, AB, DB; Fig. 21).

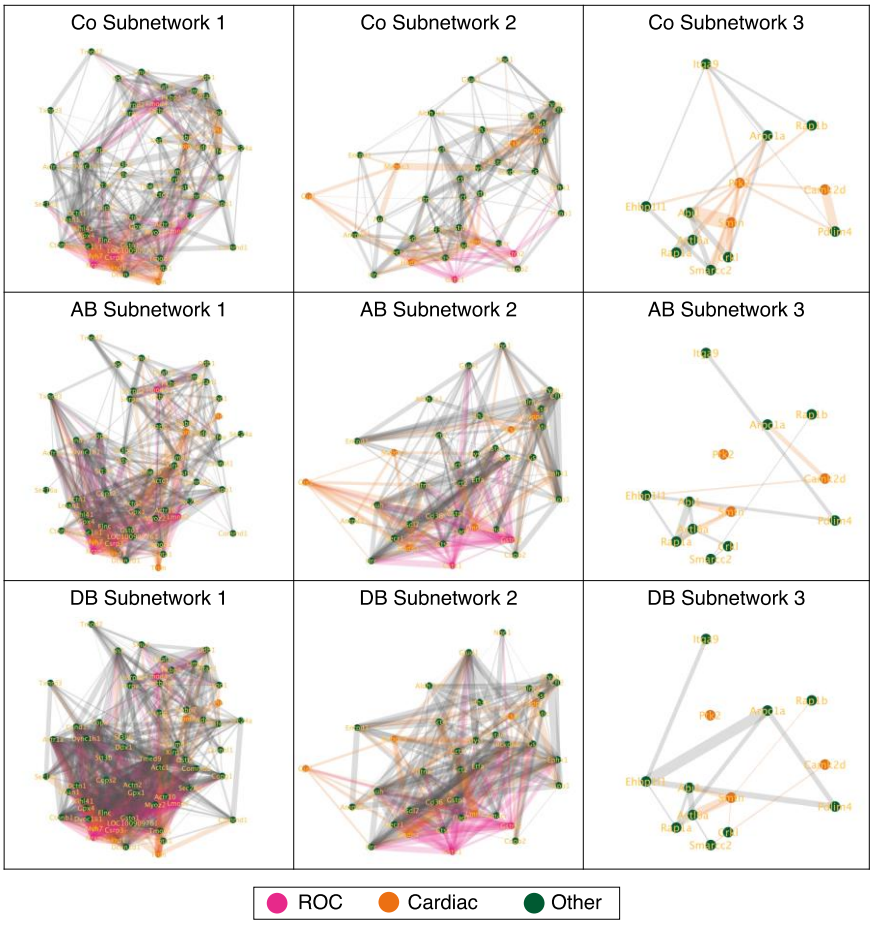

Figure 21. Network plots of proteins of closely interlinked subnetworks extracted from the main network identified by MCODE

MCODE is based on potential protein-protein interactions of the STRING database (Subnetwork 1, MCODE Score 9.138; Subnetwork 2, MCODE Score 5.419; Subnetwork 3, MCODE Score 3.231). The edges represent the observed correlation coefficients among the proteins under the different conditions (Co, AB, DB), with the proteins depicted as nodes. The width of the edge (edge weight) increases with a higher correlation coefficient. Orange-colored proteins are related to cardiac GO terms containing the following expressions: 'heart', 'muscle', 'contraction', 'I band', and 'cardiac'. Pink-coloured proteins had an AUC greater than 0.85 based on sensitivity and specificity calculations across various thresholds that differentiated banded from non-banded rats. (Subnetwork 1, MCODE Score 9.138; Subnetwork 2, MCODE Score 5.419; Subnetwork 3, MCODE Score 3.231). Source: Barta et al. ESC Heart Failure in press.

Finally, transcription factor analysis was performed using the ChEA3 algorithm to find the most likely culprits that may drive the changes in expression of τ-associated proteins (Figure 9). The ten transcription factors with the highest significance were: MAX, REST, MYOD1, MYC, MYOG, ATF3, GATA1, MAFF, USF1, and IRF1.

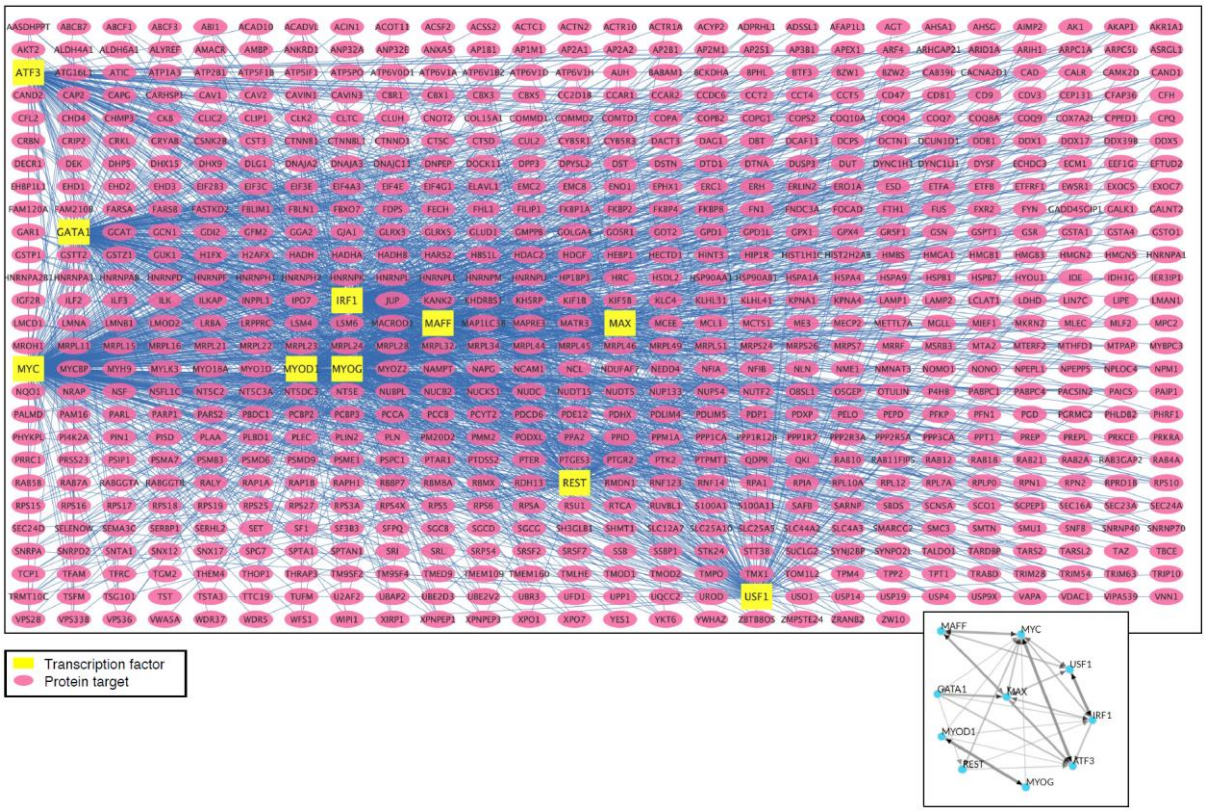

Figure 22. *Plot of the transcription factor analysis*

The ten most likely drivers (yellow) of τ associated proteomic remodeling as identified by transcription factor analysis (ChEA3), and their target proteins (pink). Source: Barta et al. ESC Heart Failure in press.

5. Discussion

Our overarching objective was to compare how the LV of male and female rats adapts across three settings: acute, diffuse ischemia; chronic pressure-overload hypertrophy; and reverse-remodeling after pressure relief. For every model, we combined load-independent PV indices with high-depth, TMT-proteomics, thereby surpassing the proteomic depth and reliability of functional assessments of preceding rat myocardial inquiries (146). This shared workflow lets us align ischemia-related findings next to pressure overload and unloading projects to highlight common, sex-specific, and model-unique themes.

5.1. Sex-neutral tissue injury in global ischemia with a shared inflammatory signature

Unlike coronary ligation, high-dose ISO engulfs the whole myocardium—particularly the subendocardium—in O_2 debt. Both sexes developed comparable heart-rate surges and scattered necrotic “islands”. Consequently, this model can be best translated to bedside cases of global ischemia. Digital slide analysis confirmed a similar loss of viable fibres, and heart-weight-to-tibia-length ratios rose in males and females alike, consistent with early oedema and inflammation (Fig. 1). Contrary to the majority of previous literature data (as reviewed by Regitz-Zagrosek and Kararigas (11)) we found equal infarct sizes in the surviving males and females. Similar outcomes were reported by Shioura et al. (147) Questioning the paradigm of the extent of myocardial damage being the sole determinant of functional outcomes. Of the seven most strongly and uniformly regulated proteins (Fig. 3B, PLS-DA), five (COQ8A, MRRF, APOOL, ATP5ME, KNG2) pointed to mitochondrial stress and inflammatory signalling, while two (JPH2, CAVIN2) reflected disruption of the T-tubule–sarcolemmal scaffold essential for excitation–contraction coupling (148), These sex-independent signatures parallel the early mitochondrial and cytoskeletal disturbances we observed during pressure-overload hypertrophy, underscoring a core, model-agnostic stress programme.

5.2. Female hearts preserve contractility via rapid structural repair

Existing literature on Langendorff perfused hearts after ISO treatment indicates better systolic adaptation in females (149, 150). Indeed, at 48 h male rats showed a clear drop in preload-recruitable stroke work and ejection fraction, accompanied by lower arterial pressures; females did not. Proteomic mapping helps explain this divergence. While both

sexes down-regulated a broad set of proteins, females up-regulated **56% more than males, and this** surplus clustered around contractile and cytoskeletal components. Up-surges in Junctophilin-2, α-actinin, and actin-filament organisers point to enhanced replacement of damaged sarcomeric units, mirroring the accelerated sarcomere turnover we recently documented during unloading-induced reverse remodeling. Females also preferentially induced chaperones ORP-150 (151), HSP90AA1 (152), HSP90AB1 (153), CALR (154), PDIA3 (155) and BIP (156), all recognised guards against ischemic injury. Males, by contrast, suppressed a larger fraction of mitochondrial enzymes—particularly tricarboxylic-acid-cycle dehydrogenases (ACO2, OGDH, IDH3A, IDH2, FH) and fatty-acid-oxidation flavoproteins (ECI1, ETFRF1, ETFA, ETFB, ETFDH, CISD1, CPT2, ACOT2) —explaining their lower mechano-energetic efficiency. Notably, males down-regulated β-enolase, whereas females boosted α-enolase, an isoform previously linked to better post-ischemic pump performance (157).

5.3. Transient myocardial stiffening predominates in females

Although earlier Langendorff work suggested superior female relaxation (149, 150), in vivo measurements by Shioura et al (147), and by the current team of investigators showed higher end-diastolic pressure, a steeper EDPVR, and prolonged T only in female rats. Stroke volume and cardiac output consequently fell in females but not in males. Proteomics again offered clues: females exhibited a richer induction of extracellular-matrix, wound-healing, and inflammatory proteins (16). Acute oedema likely dominates stiffness at this early time-point (158). Yet, the early rise of structural remodelers such as COL18A1 and integrin-α5 foreshadows the collagen deposition we later recorded during PO-induced hypertrophy. Nevertheless, this may be beneficial overall, as inhibition of inflammatory processes in the first days after MI was found to result in worse long-term outcomes by impeding cardiac remodeling and tissue repair (159). Inhibition of COL18A1 was found to deteriorate myocardial remodeling after infarction (160), and deletion of ITGA5 was found to inhibit tissue fibrosis in multiple organs (161), both of which were uniquely upregulated in females. Of particular note were matricellular proteins: we identified SPARC, SPP1, and CTSB as sex-specifically upregulated in females, while CST3 was upregulated only in males. Matricellular proteins highlighted diverging strategies: females up-regulated SPARC, SPP1 (osteopontin), and cathepsin B—each associated with timely scar maturation. (162-164) —whereas males uniquely

increased cystatin C, an endogenous cathepsin inhibitor (165), which might contribute to the more passive remodeling strategy of males. This restraint aligns with the slower remodeling trajectory we previously documented by us in male pressure-overload hearts and by Cavasin et al. after ischemia (166).

5.4. 2-Hydroxyestrone and 4-Hydroxyestrone emerge as influential hormones

The most studied estrogen for cardioprotection is E2, but it is far from the only sex hormone that could exert potentially beneficial or detrimental effects (167). The majority of metabolites of both E1 and E2 are known to bind to estrogen receptor subtypes (168) and may contribute to sex-related differences (54, 55, 169, 170). Circulating E2 and E1 are constantly hydroxylated by cytochrome-P450 isoforms to yield 2-hydroxy- (2-OHE1/E2) and 4-hydroxy- (4-OHE1/E2) catechol-estrogens. These metabolites retain appreciable affinity for both ER-α and ER-β, translocate with the receptors into mitochondria, and can also signal through redox-sensitive pathways independent of classical ER binding. The "2-hydroxy" route is generally regarded as vasculoprotective, whereas excessive 4-hydroxylation has been linked to oxidative stress in other organs (60). Unsupervised clustering of F-Isch rats split the cohort into animals with mild versus severe left-ventricular dysfunction despite comparable infarct burden. PLS-DA highlighted five steroid molecules—PROG, ALDO, 2-OHE1, 4-OHE1 and 4-MeE2—as the top biochemical discriminators. Of these, only 2-OHE1 showed robust, monotonic correlations with load-independent indices of contractility (PRSW), relaxation (dP/dt_{min}, T) and cardiac oedema (HW/TL), suggesting that a favourable 2-hydroxy/4-hydroxy balance contributes to the superior functional outcome. PLS modelling allowed us to establish associations among post-ischaemic protein expression values and the blood steroid hormone content. We then probed each hormone-associated protein cluster for Gene Ontology enrichment. The analysis resolved three functionally distinct modules. First, proteins that tracked with circulating E2, together with its 2-hydroxy metabolite (2-OHE1), converged on mitochondrial energy pathways—electron-transport complexes, tricarboxylic-acid-cycle enzymes, and β-oxidation components. Their concerted up-regulation suggests that the E2/2-OHE1 axis sustains ATP output while keeping reactive-O_2 species in check during early recovery. Second, 2-OHE1 on its own showed an

additional, more selective linkage to fatty-acid import and oxidation. This pattern implies that 2-OHE1 preserves fuel flexibility when glycolytic throughput is limited by ischaemic injury. Finally, proteins most tightly associated with 4-hydroxyestrone (4-OHE1) were almost exclusively structural—actin-binding and supramolecular-fibre regulators—pointing to a role for this metabolite in rapid cytoskeletal repair and reinforcement of the contractile apparatus.

5.5. Sex-specific reverse and anti-remodeling after pressure unloading

We then turned our attention to how biological sex shapes the myocardial "reset" that follows relief of chronic pressure overload—an aspect that clinical data have thus far left ambiguous due to unavoidable confounders (age, coronary artery disease, valve gradient, etc.). (94, 95, 99, 171). First, because of the cardioprotective effect of estrogen, CAD shows a typical sex-dependent distribution between the two sexes, with male predominance (94, 95, 99, 171). Furthermore, female patients undergoing SAVR/TAVR are frequently older than their male counterparts (94, 95, 172, 173). A greater aortic valve gradient has also been reported in women with AS compared with men (97). Working in a controlled rat model of AB/DB eliminates these variables and lets us zero in on structural (174, 175), functional (88, 89), and molecular end-points; all the while recapitulating alterations that occur after SAVR/TAVR (176).

5.6. Similar decrease in ventricular mass following pressure unloading

Removal of the constriction triggered a sudden fall in left-ventricular mass in both sexes, with ~80 % of the regression completed within the first three weeks—mirroring the rapid hypertrophy "melting" reported after SAVR/TAVR (88, 89, 94, 99, 177, 178). Petrov et al. found that just 3 days after SAVR, women had smaller LVEDD and absolute LV mass, suggesting that early "regression" primarily reflected cavity shrinkage rather than actual mass loss (94). By 3 months post-TAVR, Stangl et al. saw hypertrophy regression equal in both sexes (99). A later MRI study showed greater absolute LV-mass decline in men 6 months after SAVR/TAVR, but this sex gap vanished once changes were normalised to each patient's baseline mass (95). In our study, echocardiographic wall thickness, post-mortem heart-weight-to-tibia-length and histological cardiomyocyte diameter all shrank to a comparable absolute extent (Fig. 7, A–C and Tables 5 and 6). When normalised to each animal's pre-debanding burden, however, females showed a slightly larger fractional

drop in HW/TL, consistent with their more exuberant late-stage hypertrophic growth during banding (122). Thus, at the macroscopic level, pressure unloading behaves largely sex-neutral.

5.7. Fetal-gene program indicates greater plasticity in females

Pathological LVH switches on the fetal gene program (179) consisting of a set of genes that are silent in the adult ventricle under physiological circumstances (180, 181), with the female heart expressing higher levels of both (182). Nevertheless, the difference between female and male rats was much higher in the case of α-MHC (+736%) than in β-MHC (+469%), leading to a relative decrease in the myh7/my6 ratio in females (49). Consistent with these results, our analysis showed that female sex was associated with lower myh7/myh6 (β/α-MHC) expression in sham and AB animals (Tables 2 and 3). Debanding suppressed these transcripts in both sexes, but the β-/α-MHC ratio remained lower in females, echoing the pattern observed in sham hearts and suggesting a more rapid transcriptional reset on the female side (Table 5). The observation aligns with our ischaemia dataset, where females also reinstated contractile-protein expression more efficiently than males.

5.8. Collagen turnover is more modest in males after pressure unloading

Dobson et al. (95) Suggested that in the clinical setting of SAVR after AS only females experienced a reduction in replacement fibrosis based on late-gadolinium enchancement. In our study, interstitial collagen content fell after pressure relief in every DB group, yet the decrement was significantly larger in females. DB males derived most of their benefit from halting the further collagen accretion that would have continued between weeks 6 and 12 of banding, whereas DB females actively resorbed pre-existing matrix. (Table 6). Although the preformed fibrosis was found to be more plastic in females, prevention of further accumulation (anti-remodeling) occurred to a comparable level between the two sexes. Recently, sexual differences in cardiac fibroblast activation and subsequently in myofibroblast transformation during chronic β-adrenergic excitation have been observed (183). This echoes the accentuated extracellular-matrix remodeling we documented in female hearts 48 h after diffuse ischaemia, suggesting a recurring female trait of quick matrix turnover.

5.9. Haemodynamic recovery: apparent male superiority driven by worse baseline

In sham hearts, females showed higher LV end-systolic pressure, arterial elastance and ESPVR (Table 2). Six weeks after banding, both sexes still displayed boosted contractility, preserved ventriculo-arterial coupling and lengthened relaxation (184). By week 12, however, only males lost this contractile reserve, resulting in impaired VAC, lower systolic output and worse diastolic function, whereas females fared better. (Table 3). In addition, diastolic dysfunction became more pronounced in males at week 12 compared with females (122). Regarding the extent of reverse remodelling, no differences were detected in the normalisation of contractility augmentation or the improvement of active relaxation between the DB groups (Figs. 9 and 10 and Table 6). In good agreement with our findings, a comparable degree of EF recovery in men and women was reported by prior clinical studies at the early postoperative phase (94), as well as during a midterm follow-up period (95). Notably, no significant differences in baseline LV function were noted neither in the cited clinical studies nor in our experiment. In contrast, in a recent echocardiographic analysis, male patients with AS were found to have substantially lower preoperative longitudinal strain values, which were associated with a greater functional improvement after TAVR (98). Our current data also indicate that the anti-remodeling effect of debanding was noted to be higher on the functional level (regarding EF, VAC, LVEDP, and τ) in males compared with females (Table 6). In short, males display greater vulnerability during chronic PO, yet can stage an impressive rebound once the load is lifted. In contrast, females resist early decline, thus exhibit only a modest bounce-back.

5.10. Females approach the control proteome more closely

The sPLS-DA (Fig. 11) and unsupervised hierarchical clustering (Fig. 13A) separated banded from DB proteomes along axes dominated by hypertrophy-linked proteins [LMCD1 (185), AHSA1 (186), FLNC (187), CSRP3 (188), GPX4 (189), DUSP3 (190), and DYSF (191)] and metabolic enzymes [ENTPD2 (192), SUCLG2 (193), and DPGD1L (194)]. Mutations in the FLNC gene were implicated in numerous types of cardiomyopathies, possibly because of the disturbance of Z-disk-sarcolemma interaction during muscle contraction. DYSF and CSRP3 are key players in the response to mechanical stress, with the former participating in the resealing of disrupted sarcolemma

(195), whereas the latter mediate downstream signal transduction. LMCD1 has been shown to promote cardiac hypertrophy through the calcineurin pathway (185). Compensatory elevation of GPX4 expression has been linked to increased oxidative stress in instances of cardiac stress (189). DUSPs serve as a negative feedback loop against overactivation of MAPK signaling, for example, because of elevated afterload, with DUSP3 specifically dephosphorylating ERK1/2 in vivo (195). Six weeks of overload produced similar numbers of differentially abundant proteins in both sexes, chiefly a down-shift in lipid-oxidation machinery (Fig. 12). Prior studies have come to the conclusion that the development of PO-evoked pathological LVH is accompanied by decreased expression of lipid metabolizing and oxidizing enzymes, leading to compromised myocardial energetics (196, 197) and a shift towards glycolysis (198). Substantiating our findings, Tian et al. (199) has recently pointed out that metabolic remodeling in the failing pressure overloaded heart is sex dependent. By week 12, sex divergence surfaced: males up-regulated cytoskeletal components and curtailed protein-synthesis pathways, whereas females displayed a stronger inflammatory signature (Fig. 13)—echoing the early-ischaemia study (129). Recently, excess microtubule network density was found to be associated with decreased cardiac contractility (200), these changes might signify the deterioration of systolic function on the subcellular level in male AB animals. Pressure unloading rewound these changes in both sexes, but females achieved a nearer-to-sham proteomic landscape, especially reinstating fatty-acid–catabolic enzymes (Fig. 12AB and 13AB).

5.11. Current options for therapy control in myocardial reverse remodeling

Adverse remodeling can be slowed or reversed, through pharmacotherapy (201-204), mechanical unloading, CRT, valve replacement, and revascularisation (205-209). Heart failure therapies can improve LV ejection fraction, reduce LV size, lower LV end-diastolic PV relationships, and increase global longitudinal strain (106, 107, 112, 210-212). Currently, two-dimensional echocardiography is the gold standard for assessing morphological and functional alterations (213, 214), and cardiac magnetic resonance imaging and single-photon emission computerized tomography (SPECT) characterize the myocardial changes associated with reverse remodeling (214-218). Thus, monitoring success still hinges on imaging (2-D echo, CMR, SPECT) whose predictive value is

inconsistent and whose “reverse-remodeling” cut-offs vary. A molecular surrogate that shifts earlier than gross anatomy would therefore sharpen therapeutic timing.

5.12. τ shows the strongest association with proteomic alterations

Re-mining the banding/de-banding dataset and applying the PV analysis, echocardiography, and proteomics pipeline allowed us to screen variables with an unbiased LASSO approach, to reveal which functional parameter mirrors the broadest spectrum of proteomic change (219). Of all PV and echo variables, τ linked to the greatest number of differentially expressed proteins. Hypertrophy (LVmass) closely tracked structural regression, but τ emerged as the functional metric most tightly coupled to molecular re-programming during both load-induced remodeling and its reversal. τ, the time constant of active LV relaxation, is derived from measurements in PV analysis, and is a key parameter in the assessment of diastolic dysfunction of the heart (220, 221). The set of proteins most tightly correlated with τ mapped to three familiar biological “hot spots”: energy supply, cytoskeletal renewal, and transcriptional control. Oxidative-phosphorylation enzymes and lipid-handling factors that had resurfaced in female hearts after pressure unloading re-appeared here, as did actin-myosin repair proteins previously linked to 4-hydroxy-estrone–driven recovery in the ischaemia study. In parallel, chromatin and RNA-processing proteins—the very signatures of the early transcriptional burst we saw after diffuse ischaemia—clustered with τ as well. Thus a parameter measured during diastole integrates metabolic, structural and nuclear adaptations that span the full remodeling spectrum.

5.13. Sensitivity and specificity calculation identifies proteomic signatures of ongoing cardiac remodeling

The ROC curves identified a set of 22 proteins, predominantly associated with τ, exhibiting an Area Under the Curve (AUC) > 0.85. 13 proteins linked to τ but not to LVmass sensitively and specifically detect active or ongoing myocardial remodeling (Figure 19). These proteins offer insights into molecular signatures associated with cardiac remodeling; GSTK1 was identified in hypertrophic cardiomyopathy remodeling processes (222). COQ9 plays a role in the synthesis of coenzyme Q, vital for mitochondrial function, has also been associated with accelerated oxidative stress in cardiomyocytes (223). TMOD4 is linked to actin dynamics, influencing cardiac

contractility and myocardial hypertrophy (224). PDLIM5 is involved in heart development and may partake in the regulation of cardiomyocyte expansion (225). EIF4G1 plays a role in regulating muscle mass (226). SORBS2 is involved in mechanotransduction, contributing to cardiac response to mechanical stress, dilated cardiomyopathy and maladaptive responses to pressure overload (227, 228). NRAP contributes to cardiac muscle structure and assembly (229).

5.14. Interaction networks and subnetworks reveal cardiac importance of τ

Protein-protein interaction networks offer several benefits in the scope of our study. First, the visualization of the identified τ-related proteins (Figure 20) and their potential interactions as connections enables the identification of many individual cardiac nodes, and those directly linked to them. Second, the strength of correlations can be visualized as edge weights to assess convergent and divergent alterations of the proteome in the different conditions, demonstrating integration of cardiac and non-cardiac nodes into the respective networks (142). The interlinked τ-related nodes form the basis for further MCODE analysis, revealing three subnetworks with high potential for protein-to-protein interaction (Subnetwork 1, 2 and 3, Figure 21), confirming condition-specific protein signatures associated with AB, DB, and Co conditions. The potential importance of τ as a parameter of active relaxation is underlined by the respective subnetworks' individual proteomic components. Subnetwork 1 prominently features actin and myosin chain components, and proteins of the oxidative stress response (e.g., glutathione peroxidase). Subnetwork 2 is rich in proteins involved in the maintenance of muscle cell structure, from the nucleus to the extracellular matrix (Cryab, Dag1, Dtna, Dysf, and Lmna) and in metabolic proteins (Acsl6, Aldh7a1, Ampd3, Atic, Etfa, Glud1, Gsn, Gsr, and Nqo1). Finally, cytoskeletal organization, gene regulation, and signaling are the main functions of proteins in subnetwork 3 (Abi1, Actl6a, Arpc1a, Camk2d, Crkl, Ehbp1l1, Hist2h4, Itga9, Pdlim4, Ptk2, Rap1a, Rap1b, Smarcc2, Smtn).

5.15. Drivers of τ-associated myocardial remodeling

Ultimately, transcription factor analysis uncovered genes that are presumably driving the observed τ-associated proteomic alterations (Figure 22). ranscription factors integrate mechanical and biochemical stress signals into coordinated remodeling programs, so factors best known for roles in apoptosis or immunity often acquire cardiac, context-

dependent functions. ATF3 illustrates this principle well: although classically induced by oxidative and ER stress, it rises sharply after pressure overload and limits maladaptive hypertrophy and inflammation; ATF3-deficient mice show exaggerated fibrosis, while its re-expression during unloading facilitates regression of ECM and hypertrophic markers (230, 231). Similarly, MYC-MAX (and likely USF1) regulate ribosomal biogenesis, glycolysis, and mitochondrial function (232-234). MYC activation initially supports growth but becomes maladaptive with chronic stress (235-237). During unloading, MYC-driven programs wane and oxidative phosphorylation pathways recover (238, 239) a pattern reflected in our data: MYC/MAX-associated glycolytic/translation proteins decreased as mitochondrial and fatty-acid-oxidation proteins increased. Reverse remodeling also depends on fibroblast–immune interactions (240). Although IRF1 and MAFF are classically immune regulators, emerging evidence suggests they operate in fibroblasts under stress and may influence ECM turnover (241-248). Likewise, GATA1—better known in hematopoiesis—has been linked to endothelial remodelling and may contribute indirectly to anti-fibrotic signalling (249-251). REST contributes to electrical stability and calcium handling (252, 253), and the transient appearance of developmental TFs such as MYOD1 and MYOG in injury settings may reflect partial reactivation of cytoskeletal renewal programs (254, 255).

5.16. Relevance and impact of proteomic observations

Identifying τ as a key parameter of active relaxation on a proteomic level holds crucial clinical implications for effective assessment of myocardial remodeling states. By reframing parameters of active relaxation as proxies for energy re-fueling, cytoskeletal repair and transcriptional reset, we provide a functional-molecular bridge that precedes anatomical change. Whether applied to timing valve surgery, titrating mechanical unloaders or guiding metabolism-targeted drugs, a τ-centred protein signature could add precision to therapy control—capturing the sex- and load-dependent dynamics woven through our three linked projects.

6. Limitations

Several limitations must be acknowledged regarding the methodologies and interpretations presented in this thesis.

In the first study employing an ISO-induced ischemia model, our findings are constrained by the use of young rats, and thus may not be directly applicable to older populations or clinical settings involving chronic ischemic heart diseases. Additionally, only animals that survived the two-day ischemic protocol were analyzed, potentially introducing survival bias into our data interpretation. The acute pharmacological induction of global myocardial ischemia differs significantly from the more complex, chronic ischemic conditions encountered in human patients, thereby limiting direct translational applicability. Moreover, blood samples for steroid hormone profiling were collected post-pressure–volume (P–V) measurements to avoid interference with hemodynamic assessment. However, circulating steroid hormone levels may not accurately reflect local myocardial hormone concentrations, considering that steroid hormones can be synthesized and metabolized within cardiac tissues independently. Further studies employing local myocardial hormone measurements or hormone supplementation strategies, particularly in gonadectomized rodent models, are necessary to fully elucidate the role of these hormones in ischemic cardiac remodeling.

The second study, which evaluated myocardial remodeling following AB (AB) and its reversal by debanding, also presents important limitations. The use of a standardized needle size for aortic constriction in both sexes, consistent with prior studies, may have unintentionally imposed a relatively greater pressure overload on male animals due to their larger body mass. Nevertheless, comparable hemodynamic (SBP, DBP, MAP, Ea) and molecular (ANP) indicators of pressure overload between sexes suggest similar initial conditions, somewhat mitigating this concern. Another limitation arises from the supra-renal location of aortic constriction, which might have caused renal hypoperfusion and subsequent activation of the renin-angiotensin-aldosterone system (RAAS). Given the documented impact of sex hormones on RAAS regulation, sex-specific differences in RAAS activation may have influenced the observed remodeling and reverse remodeling outcomes. Additionally, animals in the debanding group underwent two surgical procedures (initial banding followed by debanding), whereas the corresponding sham group experienced only one laparotomy, potentially influencing physiological stress

responses differently across groups. Furthermore, our intermediate follow-up period of six weeks post-debanding may not capture longer-term differences in reverse remodeling or mortality outcomes between sexes. Hence, extended follow-up studies are necessary to determine whether observed sex-specific remodeling patterns persist or evolve over time.

The final proteomic reanalysis study utilized invasive P–V measurements to comprehensively characterize LV mechanics, particularly active relaxation assessed by τ. Although this approach provides detailed insights into cardiac function, its invasive nature restricts routine clinical implementation, limiting generalizability to human patient populations. Tissue Doppler imaging and diastolic strain rate (E/SRe) measurements are known to be good tools to estimate LV active relaxation (256-261), and myocardial reverse remodeling typically improves diastolic function. Non-invasive quantitative measurement of τ can support the prognosis of diastolic function (262) and guide therapy for cardiac interventions. While echocardiographic methods offer safer, more accessible, and widely applicable alternatives for routine assessment of LV active relaxation, our study prioritized detailed mechanistic insights over broader clinical applicability. Nonetheless, the use of echocardiography as a standard assessment method should be considered for future clinical translational research.

Portions of this text were refined with the assistance of AI tools. ChatGPT 4 and 5 was used solely to rephrase or reformulate sentences, correct grammatical errors, and improve overall readability; the substantive content remains unchanged.

7. Summary

This thesis knits together three complementary experiments to create a unified picture of how the mammalian heart adapts when it is first injured by diffuse ischaemia or chronic pressure overload (AB), and undergoing pressure unloading (DB). By pairing beat-to-beat pressure–volume haemodynamics with deep tandem-mass-tag proteomics and targeted steroid profiling, we were able to trace a straight line from mechanical performance to the molecular landscape that enables—or sabotages—recovery.

In the ISO model of global ischaemia, males and females incurred comparable histological damage, yet their trajectories immediately diverged. Female rats retained contractile reserve: PV loops showed preserved preload-recruitable stroke work and ejection fraction, whereas males lost both. Proteomics hinted at the reason. Female hearts mobilised an emergency toolkit of cytoskeletal rebuilders and stress chaperones—ACTN2, TPM1, ORP-150, HSP90, CALR—that stabilised excitation–contraction coupling. Male hearts, in contrast, down-regulated key enzymes of the tricarboxylic-acid cycle and fatty-acid β-oxidation, a metabolic collapse mirrored by falling cardiac efficiency. This early female advantage came at a diastolic price: end-diastolic pressure and the time-constant of relaxation (τ) rose only in females, in step with an inflammatory proteome that is likely essential for long-term scar maturation. Sex hormones offered an explanatory thread. Among dozens of measured steroids, the oestrone metabolites 2-hydroxy- and 4-hydroxy-E1 stratified female rats into mild versus severe dysfunction, the first associating with mitochondrial fuel enzymes, the second with actin-assembly modules, pointing to metabolite-specific control over recovery pathways.

AB recapitulated pressure-overload induced hypertrophy, and debanding mimicked surgical pressure relief. Both sexes generated similar wall thickening, yet males lost their early boost in contractility by week twelve while diastolic relaxation worsened; females maintained function. When the band was removed, each sex improved, but along different lines. Females displayed the cleaner structural reversal—greater regression of interstitial collagen, normalisation of the fetal myh7/myh6 gene ratio, and near-complete restoration of lipid-oxidation proteins. Males, paradoxically, showed the larger functional rebound in ejection fraction, ventriculo-arterial coupling and τ; however, that rebound merely recouped a steeper prior decline rather than revealing a superior intrinsic capacity for repair. At the proteomic level, in early AB the expression of lipid- and fatty-acid–

oxidation enzymes decreased in both sexes, but after DB this normalized only in females. In late-stage AB, males showed a decline in cytoskeletal remodeling and peptide biosynthesis, whereas females exhibited heightened inflammatory activity alongside reduced fatty-acid metabolism. A focused re-analysis of the AB dataset closed the loop between mechanics and molecules. Least-absolute-shrinkage regression singled out τ—the index of active relaxation—as the haemodynamic variable most tightly interwoven with proteomic change. Twenty-two τ-linked proteins, including GSTK1, COQ9 and PDLIM5, separated loading states with high sensitivity and specificity. Network partitioning revealed three densely connected modules: contractile–antioxidant, nucleo-cytoskeletal–metabolic, and signalling–chromatin. Upstream-regulator analysis pointed to MYC/MAX, MYOD/MYOG, ATF3 and MAFF as transcription factors guide the molecular changes during myocardial remodeling. Taken together, the data argue that biological sex colours every layer of cardiac adaptation. Females buffer early systolic loss yet accept an early diastolic decline; myocardial function of males tends to decline earlier but can stage an impressive comeback once afterload is lifted. Metabolic plasticity—preserved in females, unreliable in males—emerges as a pivotal determinant of outcome. Oestrogen metabolites, not merely oestradiol, operate as functional gatekeepers that steer cytoskeletal repair and oxidative metabolism. Most practically, τ behaves as a molecular barometer: because it mirrors deep proteomic shifts, non-invasive surrogates of active relaxation could serve as early read-outs of remodeling and its reversal.

8. References

1. Federation WH. World Heart Report 2023: Confronting the World's Number One Killer. Geneva; 2023.

2. Mensah GA, Fuster V, Murray CJL, Roth GA, Global Burden of Cardiovascular D, Risks C. Global Burden of Cardiovascular Diseases and Risks, 1990-2022. J Am Coll Cardiol. 2023;82(25):2350–473.

3. Luengo-Fernandez R, Walli-Attaei M, Gray A, Torbica A, Maggioni AP, Huculeci R, Bairami F, Aboyans V, Timmis AD, Vardas P, Leal J. Economic burden of cardiovascular diseases in the European Union: a population-based cost study. Eur Heart J. 2023;44(45):4752–67.

4. Martin SS, Aday AW, Almarzooq ZI, Anderson CAM, Arora P, Avery CL, Baker-Smith CM, Barone Gibbs B, Beaton AZ, Boehme AK, Commodore-Mensah Y, Currie ME, Elkind MSV, Evenson KR, Generoso G, Heard DG, Hiremath S, Johansen MC, Kalani R, Kazi DS, Ko D, Liu J, Magnani JW, Michos ED, Mussolino ME, Navaneethan SD, Parikh NI, Perman SM, Poudel R, Rezk-Hanna M, Roth GA, Shah NS, St-Onge MP, Thacker EL, Tsao CW, Urbut SM, Van Spall HGC, Voeks JH, Wang NY, Wong ND, Wong SS, Yaffe K, Palaniappan LP, American Heart Association Council on E, Prevention Statistics C, Stroke Statistics S. 2024 Heart Disease and Stroke Statistics: A Report of US and Global Data From the American Heart Association. Circulation. 2024;149(8):e347–e913.

5. Lopez AD, Adair T. Is the long-term decline in cardiovascular-disease mortality in high-income countries over? Evidence from national vital statistics. Int J Epidemiol. 2019;48(6):1815–23.

6. Regitz-Zagrosek V, Gebhard C. Gender medicine: effects of sex and gender on cardiovascular disease manifestation and outcomes. Nat Rev Cardiol. 2023;20(4):236–47.

7. Shpargel KB, Sengoku T, Yokoyama S, Magnuson T. UTX and UTY demonstrate histone demethylase-independent function in mouse embryonic development. PLoS Genet. 2012;8(9):e1002964.

8. Conlon FL, Arnold AP. Sex chromosome mechanisms in cardiac development and disease. Nat Cardiovasc Res. 2023;2(4):340–50.

9. Shi W, Sheng X, Dorr KM, Hutton JE, Emerson JI, Davies HA, Andrade TD, Wasson LK, Greco TM, Hashimoto Y, Federspiel JD, Robbe ZL, Chen X, Arnold AP, Cristea IM, Conlon FL. Cardiac proteomics reveals sex chromosome-dependent differences between males and females that arise prior to gonad formation. Dev Cell. 2021;56(21):3019–34 e7.

10. Luo T, Kim JK. The Role of Estrogen and Estrogen Receptors on Cardiomyocytes: An Overview. Can J Cardiol. 2016;32(8):1017–25.

11. Regitz-Zagrosek V, Kararigas G. Mechanistic Pathways of Sex Differences in Cardiovascular Disease. Physiol Rev. 2017;97(1):1–37.

12. McSweeney JC, Cody M, O'Sullivan P, Elberson K, Moser DK, Garvin BJ. Women's early warning symptoms of acute myocardial infarction. Circulation. 2003;108(21):2619–23.

13. Cenko E, Yoon J, Kedev S, Stankovic G, Vasiljevic Z, Krljanac G, Kalpak O, Ricci B, Milicic D, Manfrini O, van der Schaar M, Badimon L, Bugiardini R. Sex Differences in Outcomes After STEMI: Effect Modification by Treatment Strategy and Age. JAMA Intern Med. 2018;178(5):632–9.

14. Samad Z, Boyle S, Ersboll M, Vora AN, Zhang Y, Becker RC, Williams R, Kuhn C, Ortel TL, Rogers JG, O'Connor CM, Velazquez EJ, Jiang W, Investigators R. Sex differences in platelet reactivity and cardiovascular and psychological response to mental stress in patients with stable ischemic heart disease: insights from the REMIT study. J Am Coll Cardiol. 2014;64(16):1669–78.

15. Kwan AC, Wei J, Ouyang D, Ebinger JE, Merz CNB, Berman D, Cheng S. Sex differences in contributors to coronary microvascular dysfunction. Front Cardiovasc Med. 2023;10:1085914.

16. Jain M, Liao R, Podesser BK, Ngoy S, Apstein CS, Eberli FR. Influence of gender on the response to hemodynamic overload after myocardial infarction. Am J Physiol Heart Circ Physiol. 2002;283(6):H2544–50.

17. Treibel TA, Kozor R, Fontana M, Torlasco C, Reant P, Badiani S, Espinoza M, Yap J, Diez J, Hughes AD, Lloyd G, Moon JC. Sex Dimorphism in the Myocardial Response to Aortic Stenosis. JACC Cardiovasc Imaging. 2018;11(7):962–73.

18. Douglas PS, Katz SE, Weinberg EO, Chen MH, Bishop SP, Lorell BH. Hypertrophic remodeling: gender differences in the early response to left ventricular pressure overload. J Am Coll Cardiol. 1998;32(4):1118–25.

19. Beale AL, Meyer P, Marwick TH, Lam CSP, Kaye DM. Sex Differences in Cardiovascular Pathophysiology: Why Women Are Overrepresented in Heart Failure With Preserved Ejection Fraction. Circulation. 2018;138(2):198–205.

20. Aurigemma GP, Silver KH, McLaughlin M, Mauser J, Gaasch WH. Impact of chamber geometry and gender on left ventricular systolic function in patients > 60 years of age with aortic stenosis. Am J Cardiol. 1994;74(8):794–8.

21. Carroll JD, Carroll EP, Feldman T, Ward DM, Lang RM, McGaughey D, Karp RB. Sex-associated differences in left ventricular function in aortic stenosis of the elderly. Circulation. 1992;86(4):1099–107.

22. Villari B, Campbell SE, Schneider J, Vassalli G, Chiariello M, Hess OM. Sex-dependent differences in left ventricular function and structure in chronic pressure overload. Eur Heart J. 1995;16(10):1410–9.

23. Douglas PS, Otto CM, Mickel MC, Labovitz A, Reid CL, Davis KB. Gender differences in left ventricle geometry and function in patients undergoing balloon dilatation of the aortic valve for isolated aortic stenosis. NHLBI Balloon Valvuloplasty Registry. Br Heart J. 1995;73(6):548–54.

24. Kararigas G, Dworatzek E, Petrov G, Summer H, Schulze TM, Baczko I, Knosalla C, Golz S, Hetzer R, Regitz-Zagrosek V. Sex-dependent regulation of fibrosis and inflammation in human left ventricular remodelling under pressure overload. Eur J Heart Fail. 2014;16(11):1160–7.

25. Singh A, Musa TA, Treibel TA, Vassiliou VS, Captur G, Chin C, Dobson LE, Pica S, Loudon M, Malley T, Rigolli M, Foley JRJ, Bijsterveld P, Law GR, Dweck MR, Myerson SG, Prasad SK, Moon JC, Greenwood JP, McCann GP. Sex differences in left ventricular remodelling, myocardial fibrosis and mortality after aortic valve replacement. Heart. 2019;105(23):1818–24.

26. Cao Y, Vergnes L, Wang YC, Pan C, Chella Krishnan K, Moore TM, Rosa-Garrido M, Kimball TH, Zhou Z, Charugundla S, Rau CD, Seldin MM, Wang J, Wang Y, Vondriska TM, Reue K, Lusis AJ. Sex differences in heart mitochondria regulate diastolic dysfunction. Nat Commun. 2022;13(1):3850.

27. Clayton JA, Collins FS. Policy: NIH to balance sex in cell and animal studies. Nature. 2014;509(7500):282–3.

28. Pfeffer MA, Braunwald E. Ventricular remodeling after myocardial infarction. Experimental observations and clinical implications. Circulation. 1990;81(4):1161–72.

29. Frangogiannis NG. The inflammatory response in myocardial injury, repair, and remodelling. Nat Rev Cardiol. 2014;11(5):255–65.

30. van Hout GP, Arslan F, Pasterkamp G, Hoefer IE. Targeting danger-associated molecular patterns after myocardial infarction. Expert Opin Ther Targets. 2016;20(2):223–39.

31. Prabhu SD, Frangogiannis NG. The Biological Basis for Cardiac Repair After Myocardial Infarction: From Inflammation to Fibrosis. Circ Res. 2016;119(1):91–112.

32. Burchfield JS, Xie M, Hill JA. Pathological ventricular remodeling: mechanisms: part 1 of 2. Circulation. 2013;128(4):388–400.

33. Lyon RC, Zanella F, Omens JH, Sheikh F. Mechanotransduction in cardiac hypertrophy and failure. Circ Res. 2015;116(8):1462–76.

34. Wu X, Eder P, Chang B, Molkentin JD. TRPC channels are necessary mediators of pathologic cardiac hypertrophy. Proc Natl Acad Sci U S A. 2010;107(15):7000–5.

35. Yu ZY, Gong H, Kesteven S, Guo Y, Wu J, Li JV, Cheng D, Zhou Z, Iismaa SE, Kaidonis X, Graham RM, Cox CD, Feneley MP, Martinac B. Piezo1 is the cardiac mechanosensor that initiates the cardiomyocyte hypertrophic response to pressure overload in adult mice. Nat Cardiovasc Res. 2022;1(6):577–91.

36. Lopez JE, Myagmar BE, Swigart PM, Montgomery MD, Haynam S, Bigos M, Rodrigo MC, Simpson PC. beta-myosin heavy chain is induced by pressure overload in a minor subpopulation of smaller mouse cardiac myocytes. Circ Res. 2011;109(6):629–38.

37. Kong Y, Tannous P, Lu G, Berenji K, Rothermel BA, Olson EN, Hill JA. Suppression of class I and II histone deacetylases blunts pressure-overload cardiac hypertrophy. Circulation. 2006;113(22):2579–88.

38. Wilkins BJ, Dai YS, Bueno OF, Parsons SA, Xu J, Plank DM, Jones F, Kimball TR, Molkentin JD. Calcineurin/NFAT coupling participates in pathological, but not physiological, cardiac hypertrophy. Circ Res. 2004;94(1):110–8.

39. Rosca MG, Tandler B, Hoppel CL. Mitochondria in cardiac hypertrophy and heart failure. J Mol Cell Cardiol. 2013;55:31–41.

40. Bradshaw AD, Baicu CF, Rentz TJ, Van Laer AO, Boggs J, Lacy JM, Zile MR. Pressure overload-induced alterations in fibrillar collagen content and myocardial diastolic function: role of secreted protein acidic and rich in cysteine (SPARC) in post-synthetic procollagen processing. Circulation. 2009;119(2):269–80.

41. Shiojima I, Sato K, Izumiya Y, Schiekofer S, Ito M, Liao R, Colucci WS, Walsh K. Disruption of coordinated cardiac hypertrophy and angiogenesis contributes to the transition to heart failure. J Clin Invest. 2005;115(8):2108–18.

42. Sousa Nunes F, Amaral Marques C, Isabel Pinho A, Sousa-Pinto B, Beco A, Ricardo Silva J, Saraiva F, Macedo F, Leite-Moreira A, Sousa C. Reverse left ventricular remodeling after aortic valve replacement for aortic stenosis: a systematic review and meta-analysis. Front Cardiovasc Med. 2024;11:1407566.

43. Medvedofsky D, Koifman E, Miyoshi T, Rogers T, Wang Z, Goldstein SA, Ben-Dor I, Satler LF, Torguson R, Waksman R, Asch FM. Usefulness of Longitudinal Strain to Assess Remodeling of Right and Left Cardiac Chambers Following Transcatheter Aortic Valve Implantation. Am J Cardiol. 2019;124(2):253–61.

44. Ravassa S, Lopez B, Ferreira JP, Girerd N, Bozec E, Pellicori P, Mariottoni B, Cosmi F, Hazebroek M, Verdonschot JAJ, Cuthbert J, Petutschnigg J, Moreno MU, Heymans S, Staessen JA, Pieske B, Edelmann F, Clark AL, Cleland JGF, Zannad F, Diez J, Gonzalez A, Committees HT, Investigators. Biomarker-based assessment of collagen cross-linking identifies patients at risk of heart failure more likely to benefit from spironolactone effects on left atrial remodelling. Insights from the HOMAGE clinical trial. Eur J Heart Fail. 2022;24(2):321–31.

45. Martinsson A, Torngren C, Nielsen SJ, Pan E, Hansson EC, Taha A, Jeppsson A. Renin-angiotensin system inhibition after surgical aortic valve replacement for aortic stenosis. Heart. 2024;110(3):202–8.

46. Schiattarella GG, Hill JA. Inhibition of hypertrophy is a good therapeutic strategy in ventricular pressure overload. Circulation. 2015;131(16):1435–47.

47. Sacharczuk W, Dankowski R, Ozegowski S, Rojna M, Szyszka A. Evaluation of early left-sided cardiac reverse remodeling under combined therapy of sacubitril-

valsartan and spironolactone compared with angiotensin-converting enzyme inhibitors and spironolactone. Front Cardiovasc Med. 2023;10:1103688.

48. Kubanek M, Binova J, Piherova L, Krebsova A, Kotrc M, Hartmannova H, Hodanova K, Musalkova D, Stranecky V, Palecek T, Chaloupka A, Grochova I, Krejci J, Petrkova J, Melenovsky V, Kmoch S, Kautzner J. Genotype is associated with left ventricular reverse remodelling and early events in recent-onset dilated cardiomyopathy. ESC Heart Fail. 2024;11(6):4127–38.

49. Biondi-Zoccai GG, Abate A, Bussani R, Camilot D, Giorgio FD, Marino MP, Silvestri F, Baldi F, Biasucci LM, Baldi A. Reduced post-infarction myocardial apoptosis in women: a clue to their different clinical course? Heart. 2005;91(1):99–101.

50. Fang L, Gao XM, Moore XL, Kiriazis H, Su Y, Ming Z, Lim YL, Dart AM, Du XJ. Differences in inflammation, MMP activation and collagen damage account for gender difference in murine cardiac rupture following myocardial infarction. J Mol Cell Cardiol. 2007;43(5):535–44.

51. Koricanac G, Tepavcevic S, Romic S, Zivkovic M, Stojiljkovic M, Milosavljevic T, Stankovic A, Petkovic M, Kamceva T, Zakula Z. Estradiol enhances effects of fructose rich diet on cardiac fatty acid transporter CD36 and triglycerides accumulation. Eur J Pharmacol. 2012;694(1-3):127–34.

52. Rattanasopa C, Phungphong S, Wattanapermpool J, Bupha-Intr T. Significant role of estrogen in maintaining cardiac mitochondrial functions. J Steroid Biochem Mol Biol. 2015;147:1–9.

53. Zhai P, Eurell TE, Cotthaus R, Jeffery EH, Bahr JM, Gross DR. Effect of estrogen on global myocardial ischemia-reperfusion injury in female rats. Am J Physiol Heart Circ Physiol. 2000;279(6):H2766–75.

54. Booth EA, Marchesi M, Kilbourne EJ, Lucchesi BR. 17Beta-estradiol as a receptor-mediated cardioprotective agent. J Pharmacol Exp Ther. 2003;307(1):395–401.

55. Booth EA, Marchesi M, Knittel AK, Kilbourne EJ, Lucchesi BR. The pathway-selective estrogen receptor ligand WAY-169916 reduces infarct size after myocardial ischemia and reperfusion by an estrogen receptor dependent mechanism. J Cardiovasc Pharmacol. 2007;49(6):401–7.

56. Deschamps AM, Murphy E. Activation of a novel estrogen receptor, GPER, is cardioprotective in male and female rats. Am J Physiol Heart Circ Physiol. 2009;297(5):H1806–13.
57. Carbajal-Garcia A, Reyes-Garcia J, Montano LM. Androgen Effects on the Adrenergic System of the Vascular, Airway, and Cardiac Myocytes and Their Relevance in Pathological Processes. Int J Endocrinol. 2020;2020:8849641.
58. Wang Y, Ma W, Lu S, Yan L, Hu F, Wang Z, Cheng B. Androgen receptor regulates cardiac fibrosis in mice with experimental autoimmune myocarditis by increasing microRNA-125b expression. Biochem Biophys Res Commun. 2018;506(1):130–6.
59. Marsh JD, Lehmann MH, Ritchie RH, Gwathmey JK, Green GE, Schiebinger RJ. Androgen receptors mediate hypertrophy in cardiac myocytes. Circulation. 1998;98(3):256–61.
60. Lira-Silva E, Del Valle Mondragon L, Perez-Torres I, Posadas-Sanchez R, Roldan Gomez FJ, Posadas-Romero C, Vargas-Barron J, Pavon N. Possible implication of estrogenic compounds on heart disease in menopausal women. Biomed Pharmacother. 2023;162:114649.
61. Dubey RK, Gillespie DG, Jackson EK, Keller PJ. 17Beta-estradiol, its metabolites, and progesterone inhibit cardiac fibroblast growth. Hypertension. 1998;31(1 Pt 2):522–8.
62. Lijnen P, Petrov V. Induction of cardiac fibrosis by aldosterone. J Mol Cell Cardiol. 2000;32(6):865–79.
63. Constantinescu G, Gruber S, Fuld S, Peitzsch M, Schulze M, Remde H, Kurzinger L, Yang J, Yen T, Williams TA, Muller L, Reincke M, Lenders JWM, Beuschlein F, Pamporaki C, Eisenhofer GF. Steroidomics-Based Screening for Primary Aldosteronism: Impact of antihypertensive Drugs. Hypertension. 2024;81(10):2060–71.
64. Zhang Z, Wu S, Stenoien DL, Pasa-Tolic L. High-throughput proteomics. Annu Rev Anal Chem (Palo Alto Calif). 2014;7:427–54.
65. Garmany R, Dasari S, Bos JM, Kim ET, Gluscevic M, Martinez KA, Tester DJ, Dos Remedios C, Maleszewski JJ, Dearani JA, Ommen SR, Geske JB, Giudicessi JR, Ackerman MJ. A multi-omics atlas of sex-specific differences in obstructive hypertrophic cardiomyopathy. J Mol Cell Cardiol. 2024;196:26–34.

66. Shuken SR. An Introduction to Mass Spectrometry-Based Proteomics. J Proteome Res. 2023;22(7):2151–71.
67. Toby TK, Fornelli L, Kelleher NL. Progress in Top-Down Proteomics and the Analysis of Proteoforms. Annu Rev Anal Chem (Palo Alto Calif). 2016;9(1):499–519.
68. Catherman AD, Skinner OS, Kelleher NL. Top Down proteomics: facts and perspectives. Biochem Biophys Res Commun. 2014;445(4):683–93.
69. Doerr A. Mass spectrometry-based targeted proteomics. Nat Methods. 2013;10(1):23.
70. Zhang Y, Fonslow BR, Shan B, Baek MC, Yates JR, 3rd. Protein analysis by shotgun/bottom-up proteomics. Chem Rev. 2013;113(4):2343–94.
71. Chen D, McCool EN, Yang Z, Shen X, Lubeckyj RA, Xu T, Wang Q, Sun L. Recent advances (2019-2021) of capillary electrophoresis-mass spectrometry for multilevel proteomics. Mass Spectrom Rev. 2023;42(2):617–42.
72. Neagu AN, Jayathirtha M, Baxter E, Donnelly M, Petre BA, Darie CC. Applications of Tandem Mass Spectrometry (MS/MS) in Protein Analysis for Biomedical Research. Molecules. 2022;27(8).
73. Keerthikumar S, Mathivanan S. Proteotypic Peptides and Their Applications. Methods Mol Biol. 2017;1549:101–7.
74. Bian Y, Zheng R, Bayer FP, Wong C, Chang YC, Meng C, Zolg DP, Reinecke M, Zecha J, Wiechmann S, Heinzlmeir S, Scherr J, Hemmer B, Baynham M, Gingras AC, Boychenko O, Kuster B. Robust, reproducible and quantitative analysis of thousands of proteomes by micro-flow LC-MS/MS. Nat Commun. 2020;11(1):157.
75. Li J, Cai Z, Bomgarden RD, Pike I, Kuhn K, Rogers JC, Roberts TM, Gygi SP, Paulo JA. TMTpro-18plex: The Expanded and Complete Set of TMTpro Reagents for Sample Multiplexing. J Proteome Res. 2021;20(5):2964–72.
76. da Veiga Leprevost F, Haynes SE, Avtonomov DM, Chang HY, Shanmugam AK, Mellacheruvu D, Kong AT, Nesvizhskii AI. Philosopher: a versatile toolkit for shotgun proteomics data analysis. Nat Methods. 2020;17(9):869–70.
77. Hollander JM, Baseler WA, Dabkowski ER. Proteomic remodeling of mitochondria in heart failure. Congest Heart Fail. 2011;17(6):262–8.
78. Neff LS, Bradshaw AD. Cross your heart? Collagen cross-links in cardiac health and disease. Cell Signal. 2021;79:109889.

79. Lindsey ML, Kassiri Z, Virag JAI, de Castro Bras LE, Scherrer-Crosbie M. Guidelines for measuring cardiac physiology in mice. Am J Physiol Heart Circ Physiol. 2018;314(4):H733–H52.

80. Liu N, Olson EN. CRISPR Modeling and Correction of Cardiovascular Disease. Circ Res. 2022;130(12):1827–50.

81. Lobo Filho HG, Ferreira NL, Sousa RB, Carvalho ER, Lobo PL, Lobo Filho JG. Experimental model of myocardial infarction induced by isoproterenol in rats. Rev Bras Cir Cardiovasc. 2011;26(3):469–76.

82. Woolf N, Davies MJ, Shaw MJ, Trickey RJ. Exeriences with isoprenaline induced myocardial necrosis in the rat. J Pathol. 1976;120(2):65–73.

83. Clements P, Brady S, York M, Berridge B, Mikaelian I, Nicklaus R, Gandhi M, Roman I, Stamp C, Davies D, McGill P, Williams T, Pettit S, Walker D, Group IHCTW, Turton J. Time course characterization of serum cardiac troponins, heart fatty acid-binding protein, and morphologic findings with isoproterenol-induced myocardial injury in the rat. Toxicol Pathol. 2010;38(5):703–14.

84. Koga M, Karim MR, Kuramochi M, Izawa T, Kuwamura M, Yamate J. Appearance of Heterogeneous Macrophages During Development of Isoproterenol-Induced Rat Myocardial Fibrosis. Toxicol Pathol. 2021;49(5):1048–61.

85. York M, Scudamore C, Brady S, Chen C, Wilson S, Curtis M, Evans G, Griffiths W, Whayman M, Williams T, Turton J. Characterization of troponin responses in isoproterenol-induced cardiac injury in the Hanover Wistar rat. Toxicol Pathol. 2007;35(4):606–17.

86. Zhang J, Knapton A, Lipshultz SE, Weaver JL, Herman EH. Isoproterenol-induced cardiotoxicity in sprague-dawley rats: correlation of reversible and irreversible myocardial injury with release of cardiac troponin T and roles of iNOS in myocardial injury. Toxicol Pathol. 2008;36(2):277–8.

87. Ku HC, Lee SY, Wu YA, Yang KC, Su MJ. A Model of Cardiac Remodeling Through Constriction of the Abdominal Aorta in Rats. J Vis Exp. 2016(118).

88. Ruppert M, Korkmaz-Icoz S, Li S, Nemeth BT, Hegedus P, Brlecic P, Matyas C, Zorn M, Merkely B, Karck M, Radovits T, Szabo G. Myocardial reverse remodeling after pressure unloading is associated with maintained cardiac mechanoenergetics in a rat

model of left ventricular hypertrophy. Am J Physiol Heart Circ Physiol. 2016;311(3):H592–603.

89. Ruppert M, Korkmaz-Icoz S, Li S, Merkely B, Karck M, Radovits T, Szabo G. Reverse electrical remodeling following pressure unloading in a rat model of hypertension-induced left ventricular myocardial hypertrophy. Hypertens Res. 2017;40(7):637–45.

90. Pacher P, Nagayama T, Mukhopadhyay P, Batkai S, Kass DA. Measurement of cardiac function using pressure-volume conductance catheter technique in mice and rats. Nat Protoc. 2008;3(9):1422–34.

91. Wearing OH, Chesler NC, Colebank MJ, Hacker TA, Lorenz JN, Simpson JA, West CR. Guidelines for assessing ventricular pressure-volume relationships in rodents. Am J Physiol Heart Circ Physiol. 2025;328(1):H120–H40.

92. Donner DG, Kiriazis H, Du XJ, Marwick TH, McMullen JR. Improving the quality of preclinical research echocardiography: observations, training, and guidelines for measurement. Am J Physiol Heart Circ Physiol. 2018;315(1):H58–H70.

93. Chen SC, Leu HB, Chang HH, Chen IM, Chen PL, Lin SM, Chen YH. Women had favourable reverse left ventricle remodelling after TAVR. Eur J Clin Invest. 2020;50(1):e13183.

94. Petrov G, Regitz-Zagrosek V, Lehmkuhl E, Krabatsch T, Dunkel A, Dandel M, Dworatzek E, Mahmoodzadeh S, Schubert C, Becher E, Hampl H, Hetzer R. Regression of myocardial hypertrophy after aortic valve replacement: faster in women? Circulation. 2010;122(11 Suppl):S23–8.

95. Dobson LE, Fairbairn TA, Musa TA, Uddin A, Mundie CA, Swoboda PP, Ripley DP, McDiarmid AK, Erhayiem B, Garg P, Malkin CJ, Blackman DJ, Sharples LD, Plein S, Greenwood JP. Sex-related differences in left ventricular remodeling in severe aortic stenosis and reverse remodeling after aortic valve replacement: A cardiovascular magnetic resonance study. Am Heart J. 2016;175:101–11.

96. Vicente JA, Blasco IL, Perez PP, Sanchez BS, Nadal MR, Arroyo JR, Carretero MG, Ligorit Adel R. Impact of moderate coronary atherosclerosis on long-term left ventricular remodeling after aortic valve replacemen. Cardiol J. 2011;18(3):277–81.

97. Fuchs C, Mascherbauer J, Rosenhek R, Pernicka E, Klaar U, Scholten C, Heger M, Wollenek G, Czerny M, Maurer G, Baumgartner H. Gender differences in clinical presentation and surgical outcome of aortic stenosis. Heart. 2010;96(7):539–45.

98. Bochenek T, Kusz B, Mizia M, Lelek M, Turski M, Wita K, Ochala A, Mizia-Stec K. Echocardiographic evaluation of myocardial strain in patients after transcatheter aortic valve implantation. Postepy Kardiol Interwencyjnej. 2015;11(2):95–9.

99. Stangl V, Baldenhofer G, Knebel F, Zhang K, Sanad W, Spethmann S, Grubitzsch H, Sander M, Wernecke KD, Baumann G, Stangl K, Laule M. Impact of gender on three-month outcome and left ventricular remodeling after transfemoral transcatheter aortic valve implantation. Am J Cardiol. 2012;110(6):884–90.

100. Rienks M, Papageorgiou AP, Frangogiannis NG, Heymans S. Myocardial extracellular matrix: an ever-changing and diverse entity. Circ Res. 2014;114(5):872–88.

101. Kirchhof P, Klimas J, Fabritz L, Zwiener M, Jones LR, Schafers M, Hermann S, Boknik P, Schmitz W, Breithardt G, Kirchhefer U, Neumann J. Stress and high heart rate provoke ventricular tachycardia in mice expressing triadin. J Mol Cell Cardiol. 2007;42(5):962–71.

102. Milani-Nejad N, Janssen PM. Small and large animal models in cardiac contraction research: advantages and disadvantages. Pharmacol Ther. 2014;141(3):235–49.

103. Goldman JM, Murr AS, Cooper RL. The rodent estrous cycle: characterization of vaginal cytology and its utility in toxicological studies. Birth Defects Res B Dev Reprod Toxicol. 2007;80(2):84–97.

104. Constantinides C, Murphy K. Molecular and Integrative Physiological Effects of Isoflurane Anesthesia: The Paradigm of Cardiovascular Studies in Rodents using Magnetic Resonance Imaging. Front Cardiovasc Med. 2016;3:23.

105. Barnabei MS, Palpant NJ, Metzger JM. Influence of genetic background on ex vivo and in vivo cardiac function in several commonly used inbred mouse strains. Physiol Genomics. 2010;42A(2):103–13.

106. Merlo M, Pyxaras SA, Pinamonti B, Barbati G, Di Lenarda A, Sinagra G. Prevalence and prognostic significance of left ventricular reverse remodeling in dilated cardiomyopathy receiving tailored medical treatment. J Am Coll Cardiol. 2011;57(13):1468–76.

107. Solomon SD, Skali H, Anavekar NS, Bourgoun M, Barvik S, Ghali JK, Warnica JW, Khrakovskaya M, Arnold JM, Schwartz Y, Velazquez EJ, Califf RM, McMurray JV, Pfeffer MA. Changes in ventricular size and function in patients treated with valsartan, captopril, or both after myocardial infarction. Circulation. 2005;111(25):3411–9.

108. Pitzalis MV, Iacoviello M, Romito R, Massari F, Rizzon B, Luzzi G, Guida P, Andriani A, Mastropasqua F, Rizzon P. Cardiac resynchronization therapy tailored by echocardiographic evaluation of ventricular asynchrony. J Am Coll Cardiol. 2002;40(9):1615–22.

109. Verma S, Mazer CD, Yan AT, Mason T, Garg V, Teoh H, Zuo F, Quan A, Farkouh ME, Fitchett DH, Goodman SG, Goldenberg RM, Al-Omran M, Gilbert RE, Bhatt DL, Leiter LA, Juni P, Zinman B, Connelly KA. Effect of Empagliflozin on Left Ventricular Mass in Patients With Type 2 Diabetes Mellitus and Coronary Artery Disease: The EMPA-HEART CardioLink-6 Randomized Clinical Trial. Circulation. 2019;140(21):1693–702.

110. Wilcox JE, Fonarow GC, Yancy CW, Albert NM, Curtis AB, Heywood JT, Inge PJ, McBride ML, Mehra MR, O'Connor CM, Reynolds D, Walsh MN, Gheorghiade M. Factors associated with improvement in ejection fraction in clinical practice among patients with heart failure: findings from IMPROVE HF. Am Heart J. 2012;163(1):49–56 e2.

111. Bhatt AS, Ambrosy AP, Velazquez EJ. Adverse Remodeling and Reverse Remodeling After Myocardial Infarction. Curr Cardiol Rep. 2017;19(8):71.

112. Aimo A, Gaggin HK, Barison A, Emdin M, Januzzi JL, Jr. Imaging, Biomarker, and Clinical Predictors of Cardiac Remodeling in Heart Failure With Reduced Ejection Fraction. JACC Heart Fail. 2019;7(9):782–94.

113. Ranalli MG, Salvati N, Petrella L, Pantalone F. M-quantile regression shrinkage and selection via the Lasso and Elastic Net to assess the effect of meteorology and traffic on air quality. Biom J. 2023;65(8):e2100355.

114. Linden A. Measuring diagnostic and predictive accuracy in disease management: an introduction to receiver operating characteristic (ROC) analysis. J Eval Clin Pract. 2006;12(2):132–9.

115. Szklarczyk D, Nastou K, Koutrouli M, Kirsch R, Mehryary F, Hachilif R, Hu D, Peluso ME, Huang Q, Fang T, Doncheva NT, Pyysalo S, Bork P, Jensen LJ, von Mering

C. The STRING database in 2025: protein networks with directionality of regulation. Nucleic Acids Res. 2025;53(D1):D730–D7.

116. Bader GD, Hogue CW. An automated method for finding molecular complexes in large protein interaction networks. BMC Bioinformatics. 2003;4:2.

117. Keenan AB, Torre D, Lachmann A, Leong AK, Wojciechowicz ML, Utti V, Jagodnik KM, Kropiwnicki E, Wang Z, Ma'ayan A. ChEA3: transcription factor enrichment analysis by orthogonal omics integration. Nucleic Acids Res. 2019;47(W1):W212–W24.

118. Bayne K. Revised Guide for the Care and Use of Laboratory Animals available. American Physiological Society. Physiologist. 1996;39(4):199, 208–11.

119. Kilkenny C, Browne WJ, Cuthill IC, Emerson M, Altman DG. Improving bioscience research reporting: the ARRIVE guidelines for reporting animal research. PLoS Biol. 2010;8(6):e1000412.

120. Korkmaz S, Radovits T, Barnucz E, Hirschberg K, Neugebauer P, Loganathan S, Veres G, Pali S, Seidel B, Zollner S, Karck M, Szabo G. Pharmacological activation of soluble guanylate cyclase protects the heart against ischemic injury. Circulation. 2009;120(8):677–86.

121. Ruppert M, Barta BA, Korkmaz-Icoz S, Loganathan S, Olah A, Sayour AA, Benke K, Nagy D, Balint T, Karck M, Schilling O, Merkely B, Radovits T, Szabo G. Sex similarities and differences in the reverse and anti-remodeling effect of pressure unloading therapy in a rat model of aortic banding and debanding. Am J Physiol Heart Circ Physiol. 2022;323(1):H204–H22.

122. Ruppert M, Korkmaz-Icoz S, Loganathan S, Jiang W, Lehmann L, Olah A, Sayour AA, Barta BA, Merkely B, Karck M, Radovits T, Szabo G. Pressure-volume analysis reveals characteristic sex-related differences in cardiac function in a rat model of aortic banding-induced myocardial hypertrophy. Am J Physiol Heart Circ Physiol. 2018;315(3):H502–H11.

123. Korkmaz-Icoz S, Lehner A, Li S, Vater A, Radovits T, Brune M, Ruppert M, Sun X, Brlecic P, Zorn M, Karck M, Szabo G. Left ventricular pressure-volume measurements and myocardial gene expression profile in type 2 diabetic Goto-Kakizaki rats. Am J Physiol Heart Circ Physiol. 2016;311(4):H958–H71.

124. Yamamoto K. The time constant of left ventricular relaxation: extrication from load dependence and overestimation of functional abnormality. Circ Heart Fail. 2010;3(2):178–80.

125. Kass DA, Beyar R, Lankford E, Heard M, Maughan WL, Sagawa K. Influence of contractile state on curvilinearity of in situ end-systolic pressure-volume relations. Circulation. 1989;79(1):167–78.

126. Sunagawa K, Maughan WL, Burkhoff D, Sagawa K. Left ventricular interaction with arterial load studied in isolated canine ventricle. Am J Physiol. 1983;245(5 Pt 1):H773–80.

127. Bankhead P, Loughrey MB, Fernandez JA, Dombrowski Y, McArt DG, Dunne PD, McQuaid S, Gray RT, Murray LJ, Coleman HG, James JA, Salto-Tellez M, Hamilton PW. QuPath: Open source software for digital pathology image analysis. Sci Rep. 2017;7(1):16878.

128. van Putten M, de Winter C, van Roon-Mom W, van Ommen GJ, t Hoen PA, Aartsma-Rus A. A 3 months mild functional test regime does not affect disease parameters in young mdx mice. Neuromuscul Disord. 2010;20(4):273–80.

129. Barta BA, Ruppert M, Frohlich KE, Cosenza-Contreras M, Olah A, Sayour AA, Kovacs K, Karvaly GB, Biniossek M, Merkely B, Schilling O, Radovits T. Sex-related differences of early cardiac functional and proteomic alterations in a rat model of myocardial ischemia. J Transl Med. 2021;19(1):507.

130. Ruppert M, Korkmaz-Icoz S, Loganathan S, Jiang W, Olah A, Sayour AA, Barta BA, Karime C, Merkely B, Karck M, Radovits T, Szabo G. Incomplete structural reverse remodeling from late-stage left ventricular hypertrophy impedes the recovery of diastolic but not systolic dysfunction in rats. J Hypertens. 2019;37(6):1200–12.

131. Baumert HM, Metzger E, Fahrner M, George J, Thomas RK, Schilling O, Schule R. Depletion of histone methyltransferase KMT9 inhibits lung cancer cell proliferation by inducing non-apoptotic cell death. Cancer Cell Int. 2020;20:52.

132. Cox J, Mann M. MaxQuant enables high peptide identification rates, individualized p.p.b.-range mass accuracies and proteome-wide protein quantification. Nat Biotechnol. 2008;26(12):1367–72.

133. Huang T, Choi M, Tzouros M, Golling S, Pandya NJ, Banfai B, Dunkley T, Vitek O. MSstatsTMT: Statistical Detection of Differentially Abundant Proteins in Experiments

with Isobaric Labeling and Multiple Mixtures. Mol Cell Proteomics. 2020;19(10):1706–23.

134. Hughes CS, Moggridge S, Muller T, Sorensen PH, Morin GB, Krijgsveld J. Single-pot, solid-phase-enhanced sample preparation for proteomics experiments. Nat Protoc. 2019;14(1):68–85.

135. Stekhoven DJ, Buhlmann P. MissForest--non-parametric missing value imputation for mixed-type data. Bioinformatics. 2012;28(1):112–8.

136. Leek JT, Johnson WE, Parker HS, Jaffe AE, Storey JD. The sva package for removing batch effects and other unwanted variation in high-throughput experiments. Bioinformatics. 2012;28(6):882–3.

137. Kong AT, Leprevost FV, Avtonomov DM, Mellacheruvu D, Nesvizhskii AI. MSFragger: ultrafast and comprehensive peptide identification in mass spectrometry-based proteomics. Nat Methods. 2017;14(5):513–20.

138. Yu G, Wang LG, Han Y, He QY. clusterProfiler: an R package for comparing biological themes among gene clusters. OMICS. 2012;16(5):284–7.

139. Phipson B, Lee S, Majewski IJ, Alexander WS, Smyth GK. Robust Hyperparameter Estimation Protects against Hypervariable Genes and Improves Power to Detect Differential Expression. Ann Appl Stat. 2016;10(2):946–63.

140. Rohart F, Gautier B, Singh A, Le Cao KA. mixOmics: An R package for 'omics feature selection and multiple data integration. PLoS Comput Biol. 2017;13(11):e1005752.

141. Friedman J, Hastie T, Tibshirani R. Regularization Paths for Generalized Linear Models via Coordinate Descent. J Stat Softw. 2010;33(1):1–22.

142. von Mering C, Jensen LJ, Snel B, Hooper SD, Krupp M, Foglierini M, Jouffre N, Huynen MA, Bork P. STRING: known and predicted protein-protein associations, integrated and transferred across organisms. Nucleic Acids Res. 2005;33(Database issue):D433–7.

143. Szklarczyk D, Kirsch R, Koutrouli M, Nastou K, Mehryary F, Hachilif R, Gable AL, Fang T, Doncheva NT, Pyysalo S, Bork P, Jensen LJ, von Mering C. The STRING database in 2023: protein-protein association networks and functional enrichment analyses for any sequenced genome of interest. Nucleic Acids Res. 2023;51(D1):D638–D46.

144. Shannon P, Markiel A, Ozier O, Baliga NS, Wang JT, Ramage D, Amin N, Schwikowski B, Ideker T. Cytoscape: a software environment for integrated models of biomolecular interaction networks. Genome Res. 2003;13(11):2498–504.

145. Luo Y, Hitz BC, Gabdank I, Hilton JA, Kagda MS, Lam B, Myers Z, Sud P, Jou J, Lin K, Baymuradov UK, Graham K, Litton C, Miyasato SR, Strattan JS, Jolanki O, Lee JW, Tanaka FY, Adenekan P, O'Neill E, Cherry JM. New developments on the Encyclopedia of DNA Elements (ENCODE) data portal. Nucleic Acids Res. 2020;48(D1):D882–D9.

146. Lim SH, Lee J, Han MJ. Comprehensive analysis of the cardiac proteome in a rat model of myocardial ischemia-reperfusion using a TMT-based quantitative proteomic strategy. Proteome Sci. 2020;18:2.

147. Shioura KM, Geenen DL, Goldspink PH. Sex-related changes in cardiac function following myocardial infarction in mice. Am J Physiol Regul Integr Comp Physiol. 2008;295(2):R528–34.

148. Chan BYH, Roczkowsky A, Cho WJ, Poirier M, Lee TYT, Mahmud Z, Schulz R. Junctophilin-2 is a target of matrix metalloproteinase-2 in myocardial ischemia-reperfusion injury. Basic Res Cardiol. 2019;114(6):42.

149. Gabel SA, Walker VR, London RE, Steenbergen C, Korach KS, Murphy E. Estrogen receptor beta mediates gender differences in ischemia/reperfusion injury. J Mol Cell Cardiol. 2005;38(2):289–97.

150. Wang M, Tsai BM, Reiger KM, Brown JW, Meldrum DR. 17-beta-Estradiol decreases p38 MAPK-mediated myocardial inflammation and dysfunction following acute ischemia. J Mol Cell Cardiol. 2006;40(2):205–12.

151. Aleshin AN, Sawa Y, Kitagawa-Sakakida S, Bando Y, Ono M, Memon IA, Tohyama M, Ogawa S, Matsuda H. 150-kDa oxygen-regulated protein attenuates myocardial ischemia-reperfusion injury in rat heart. J Mol Cell Cardiol. 2005;38(3):517–25.

152. Zhu WS, Guo W, Zhu JN, Tang CM, Fu YH, Lin QX, Tan N, Shan ZX. Hsp90aa1: a novel target gene of miR-1 in cardiac ischemia/reperfusion injury. Sci Rep. 2016;6:24498.

153. Haase M, Fitze G. HSP90AB1: Helping the good and the bad. Gene. 2016;575(2 Pt 1):171–86.

154. Wang JL, Li YZ, Tao TQ, Wang XR, Wang Y, Song DD, Liu XH. Postconditioning with Calreticulin Attenuates Myocardial Ischemia/Reperfusion Injury and Improves Autophagic Flux. Shock. 2020;53(3):363–72.

155. Yoo DY, Cho SB, Jung HY, Kim W, Lee KY, Kim JW, Moon SM, Won MH, Choi JH, Yoon YS, Kim DW, Choi SY, Hwang IK. Protein disulfide-isomerase A3 significantly reduces ischemia-induced damage by reducing oxidative and endoplasmic reticulum stress. Neurochem Int. 2019;122:19–30.

156. Bodalia A, Li H, Jackson MF. Loss of endoplasmic reticulum Ca2+ homeostasis: contribution to neuronal cell death during cerebral ischemia. Acta Pharmacol Sin. 2013;34(1):49–59.

157. Diaz-Ramos A, Roig-Borrellas A, Garcia-Melero A, Lopez-Alemany R. alpha-Enolase, a multifunctional protein: its role on pathophysiological situations. J Biomed Biotechnol. 2012;2012:156795.

158. Jugdutt BI. Ventricular remodeling after infarction and the extracellular collagen matrix: when is enough enough? Circulation. 2003;108(11):1395–403.

159. Maleki Dizaji N, Garjani A, Mousavi S, Mohammadi M, Vaez H. Time-dependent influence of infliximab on hemodynamic responses and cardiac injuries of isoproterenol-induced myocardial infarction in rats. Eur J Pharmacol. 2021;903:174122.

160. Isobe K, Kuba K, Maejima Y, Suzuki J, Kubota S, Isobe M. Inhibition of endostatin/collagen XVIII deteriorates left ventricular remodeling and heart failure in rat myocardial infarction model. Circ J. 2010;74(1):109–19.

161. Henderson NC, Arnold TD, Katamura Y, Giacomini MM, Rodriguez JD, McCarty JH, Pellicoro A, Raschperger E, Betsholtz C, Ruminski PG, Griggs DW, Prinsen MJ, Maher JJ, Iredale JP, Lacy-Hulbert A, Adams RH, Sheppard D. Targeting of alphav integrin identifies a core molecular pathway that regulates fibrosis in several organs. Nat Med. 2013;19(12):1617–24.

162. McCurdy SM, Dai Q, Zhang J, Zamilpa R, Ramirez TA, Dayah T, Nguyen N, Jin YF, Bradshaw AD, Lindsey ML. SPARC mediates early extracellular matrix remodeling following myocardial infarction. Am J Physiol Heart Circ Physiol. 2011;301(2):H497–505.

163. Wu RX, Laser M, Han H, Varadarajulu J, Schuh K, Hallhuber M, Hu K, Ertl G, Hauck CR, Ritter O. Fibroblast migration after myocardial infarction is regulated by transient SPARC expression. J Mol Med (Berl). 2006;84(3):241–52.

164. Wu QQ, Xu M, Yuan Y, Li FF, Yang Z, Liu Y, Zhou MQ, Bian ZY, Deng W, Gao L, Li H, Tang QZ. Cathepsin B deficiency attenuates cardiac remodeling in response to pressure overload via TNF-alpha/ASK1/JNK pathway. Am J Physiol Heart Circ Physiol. 2015;308(9):H1143–54.

165. Xie L, Terrand J, Xu B, Tsaprailis G, Boyer J, Chen QM. Cystatin C increases in cardiac injury: a role in extracellular matrix protein modulation. Cardiovasc Res. 2010;87(4):628–35.

166. Cavasin MA, Tao Z, Menon S, Yang XP. Gender differences in cardiac function during early remodeling after acute myocardial infarction in mice. Life Sci. 2004;75(18):2181–92.

167. Nikolic I, Liu D, Bell JA, Collins J, Steenbergen C, Murphy E. Treatment with an estrogen receptor-beta-selective agonist is cardioprotective. J Mol Cell Cardiol. 2007;42(4):769–80.

168. Zhu BT, Han GZ, Shim JY, Wen Y, Jiang XR. Quantitative structure-activity relationship of various endogenous estrogen metabolites for human estrogen receptor alpha and beta subtypes: Insights into the structural determinants favoring a differential subtype binding. Endocrinology. 2006;147(9):4132–50.

169. Patten RD, Pourati I, Aronovitz MJ, Baur J, Celestin F, Chen X, Michael A, Haq S, Nuedling S, Grohe C, Force T, Mendelsohn ME, Karas RH. 17beta-estradiol reduces cardiomyocyte apoptosis in vivo and in vitro via activation of phospho-inositide-3 kinase/Akt signaling. Circ Res. 2004;95(7):692–9.

170. Cavasin MA, Tao ZY, Yu AL, Yang XP. Testosterone enhances early cardiac remodeling after myocardial infarction, causing rupture and degrading cardiac function. Am J Physiol Heart Circ Physiol. 2006;290(5):H2043–50.

171. Petrov G, Dworatzek E, Schulze TM, Dandel M, Kararigas G, Mahmoodzadeh S, Knosalla C, Hetzer R, Regitz-Zagrosek V. Maladaptive remodeling is associated with impaired survival in women but not in men after aortic valve replacement. JACC Cardiovasc Imaging. 2014;7(11):1073–80.

172. Forrest JK, Adams DH, Popma JJ, Reardon MJ, Deeb GM, Yakubov SJ, Hermiller JB, Jr., Huang J, Skelding KA, Lansky A. Transcatheter Aortic Valve Replacement in Women Versus Men (from the US CoreValve Trials). Am J Cardiol. 2016;118(3):396–402.

173. Yousif N, Obeid S, Binder R, Denegri A, Shahin M, Templin C, Luscher TF. Impact of gender on outcomes after transcatheter aortic valve implantation. J Geriatr Cardiol. 2018;15(6):394–400.

174. Chen J, Chemaly ER, Liang LF, LaRocca TJ, Yaniz-Galende E, Hajjar RJ. A new model of congestive heart failure in rats. Am J Physiol Heart Circ Physiol. 2011;301(3):H994–1003.

175. Gao XM, Kiriazis H, Moore XL, Feng XH, Sheppard K, Dart A, Du XJ. Regression of pressure overload-induced left ventricular hypertrophy in mice. Am J Physiol Heart Circ Physiol. 2005;288(6):H2702–7.

176. Andersen NM, Stansfield WE, Tang RH, Rojas M, Patterson C, Selzman CH. Recovery from decompensated heart failure is associated with a distinct, phase-dependent gene expression profile. J Surg Res. 2012;178(1):72–80.

177. Yang DK, Choi BY, Lee YH, Kim YG, Cho MC, Hong SE, Kim DH, Hajjar RJ, Park WJ. Gene profiling during regression of pressure overload-induced cardiac hypertrophy. Physiol Genomics. 2007;30(1):1–7.

178. Christakis GT, Joyner CD, Morgan CD, Fremes SE, Buth KJ, Sever JY, Rao V, Panagiotopoulos KP, Murphy PM, Goldman BS. Left ventricular mass regression early after aortic valve replacement. Ann Thorac Surg. 1996;62(4):1084–9.

179. Frey N, Olson EN. Cardiac hypertrophy: the good, the bad, and the ugly. Annu Rev Physiol. 2003;65:45–79.

180. Weinberg EO, Thienelt CD, Katz SE, Bartunek J, Tajima M, Rohrbach S, Douglas PS, Lorell BH. Gender differences in molecular remodeling in pressure overload hypertrophy. J Am Coll Cardiol. 1999;34(1):264–73.

181. Witt H, Schubert C, Jaekel J, Fliegner D, Penkalla A, Tiemann K, Stypmann J, Roepcke S, Brokat S, Mahmoodzadeh S, Brozova E, Davidson MM, Ruiz Noppinger P, Grohe C, Regitz-Zagrosek V. Sex-specific pathways in early cardiac response to pressure overload in mice. J Mol Med (Berl). 2008;86(9):1013–24.

182. Rosenkranz-Weiss P, Tomek RJ, Mathew J, Eghbali M. Gender-specific differences in expression of mRNAs for functional and structural proteins in rat ventricular myocardium. J Mol Cell Cardiol. 1994;26(2):261–70.
183. Peter AK, Walker CJ, Ceccato T, Trexler CL, Ozeroff CD, Lugo KR, Perry AR, Anseth KS, Leinwand LA. Cardiac Fibroblasts Mediate a Sexually Dimorphic Fibrotic Response to beta-Adrenergic Stimulation. J Am Heart Assoc. 2021;10(11):e018876.
184. Hayward CS, Kalnins WV, Kelly RP. Gender-related differences in left ventricular chamber function. Cardiovasc Res. 2001;49(2):340–50.
185. Frank D, Frauen R, Hanselmann C, Kuhn C, Will R, Gantenberg J, Fuzesi L, Katus HA, Frey N. Lmcd1/Dyxin, a novel Z-disc associated LIM protein, mediates cardiac hypertrophy in vitro and in vivo. J Mol Cell Cardiol. 2010;49(4):673–82.
186. Cui H, Schlesinger J, Schoenhals S, Tonjes M, Dunkel I, Meierhofer D, Cano E, Schulz K, Berger MF, Haack T, Abdelilah-Seyfried S, Bulyk ML, Sauer S, Sperling SR. Phosphorylation of the chromatin remodeling factor DPF3a induces cardiac hypertrophy through releasing HEY repressors from DNA. Nucleic Acids Res. 2016;44(6):2538–53.
187. Cui H, Wang J, Zhang C, Wu G, Zhu C, Tang B, Zou Y, Huang X, Hui R, Song L, Wang S. Mutation profile of FLNC gene and its prognostic relevance in patients with hypertrophic cardiomyopathy. Mol Genet Genomic Med. 2018;6(6):1104–13.
188. Geier C, Gehmlich K, Ehler E, Hassfeld S, Perrot A, Hayess K, Cardim N, Wenzel K, Erdmann B, Krackhardt F, Posch MG, Osterziel KJ, Bublak A, Nagele H, Scheffold T, Dietz R, Chien KR, Spuler S, Furst DO, Nurnberg P, Ozcelik C. Beyond the sarcomere: CSRP3 mutations cause hypertrophic cardiomyopathy. Hum Mol Genet. 2008;17(18):2753–65.
189. Hoffmann FW, Hashimoto AS, Lee BC, Rose AH, Shohet RV, Hoffmann PR. Specific antioxidant selenoproteins are induced in the heart during hypertrophy. Arch Biochem Biophys. 2011;512(1):38–44.
190. Mutlak M, Kehat I. Dual specific phosphatases (DUSPs) in cardiac hypertrophy and failure. Cell Signal. 2021;84:110033.
191. Wenzel K, Geier C, Qadri F, Hubner N, Schulz H, Erdmann B, Gross V, Bauer D, Dechend R, Dietz R, Osterziel KJ, Spuler S, Ozcelik C. Dysfunction of dysferlin-deficient hearts. J Mol Med (Berl). 2007;85(11):1203–14.

192. Toczek M, Zielonka D, Zukowska P, Marcinkowski JT, Slominska E, Isalan M, Smolenski RT, Mielcarek M. An impaired metabolism of nucleotides underpins a novel mechanism of cardiac remodeling leading to Huntington's disease related cardiomyopathy. Biochim Biophys Acta. 2016;1862(11):2147–57.

193. Haas J, Frese KS, Sedaghat-Hamedani F, Kayvanpour E, Tappu R, Nietsch R, Tugrul OF, Wisdom M, Dietrich C, Amr A, Weis T, Niederdrank T, Murphy MP, Krieg T, Dorr M, Volker U, Fielitz J, Frey N, Felix SB, Keller A, Katus HA, Meder B. Energy Metabolites as Biomarkers in Ischemic and Dilated Cardiomyopathy. Int J Mol Sci. 2021;22(4).

194. Shen E, Diao X, Wang X, Chen R, Hu B. MicroRNAs involved in the mitogen-activated protein kinase cascades pathway during glucose-induced cardiomyocyte hypertrophy. Am J Pathol. 2011;179(2):639–50.

195. Todd JL, Tanner KG, Denu JM. Extracellular regulated kinases (ERK) 1 and ERK2 are authentic substrates for the dual-specificity protein-tyrosine phosphatase VHR. A novel role in down-regulating the ERK pathway. J Biol Chem. 1999;274(19):13271–80.

196. Gallego-Delgado J, Lazaro A, Osende JI, Barderas MG, Duran MC, Vivanco F, Egido J. Comparison of the protein profile of established and regressed hypertension-induced left ventricular hypertrophy. J Proteome Res. 2006;5(2):404–13.

197. Junhong W, Jing Y, Jizheng M, Shushu Z, Xiangjian C, Hengfang W, Di Y, Jinan Z. Proteomic analysis of left ventricular diastolic dysfunction hearts in renovascular hypertensive rats. Int J Cardiol. 2008;127(2):198–207.

198. Tran DH, Wang ZV. Glucose Metabolism in Cardiac Hypertrophy and Heart Failure. J Am Heart Assoc. 2019;8(12):e012673.

199. Ritterhoff J, McMillen TS, Villet O, Young S, Kolwicz SC, Jr., Senn T, Caudal A, Tian R. Increasing fatty acid oxidation elicits a sex-dependent response in failing mouse hearts. J Mol Cell Cardiol. 2021;158:1–10.

200. Cooper Gt. Cytoskeletal networks and the regulation of cardiac contractility: microtubules, hypertrophy, and cardiac dysfunction. Am J Physiol Heart Circ Physiol. 2006;291(3):H1003–14.

201. Hochman JS, Bulkley BH. Expansion of acute myocardial infarction: an experimental study. Circulation. 1982;65(7):1446–50.

202. McMurray JJ, Packer M, Desai AS, Gong J, Lefkowitz MP, Rizkala AR, Rouleau JL, Shi VC, Solomon SD, Swedberg K, Zile MR, Investigators P-H, Committees. Angiotensin-neprilysin inhibition versus enalapril in heart failure. N Engl J Med. 2014;371(11):993–1004.

203. Pitt B, Remme W, Zannad F, Neaton J, Martinez F, Roniker B, Bittman R, Hurley S, Kleiman J, Gatlin M, Eplerenone Post-Acute Myocardial Infarction Heart Failure E, Survival Study I. Eplerenone, a selective aldosterone blocker, in patients with left ventricular dysfunction after myocardial infarction. N Engl J Med. 2003;348(14):1309–21.

204. Tardif JC, O'Meara E, Komajda M, Bohm M, Borer JS, Ford I, Tavazzi L, Swedberg K, Investigators S. Effects of selective heart rate reduction with ivabradine on left ventricular remodelling and function: results from the SHIFT echocardiography substudy. Eur Heart J. 2011;32(20):2507–15.

205. Dor V. The Endoventricular Circular Patch Plasty ("Dor Procedure") in Ischemic Akinetic Dilated Ventricles. Heart Failure Reviews. 2001;6(3):187–93.

206. Enriquez-Sarano M, Akins CW, Vahanian A. Mitral regurgitation. Lancet. 2009;373(9672):1382–94.

207. Kim GH, Uriel N, Burkhoff D. Reverse remodelling and myocardial recovery in heart failure. Nat Rev Cardiol. 2018;15(2):83–96.

208. Linde C, Abraham WT, Gold MR, St John Sutton M, Ghio S, Daubert C, Group RS. Randomized trial of cardiac resynchronization in mildly symptomatic heart failure patients and in asymptomatic patients with left ventricular dysfunction and previous heart failure symptoms. J Am Coll Cardiol. 2008;52(23):1834–43.

209. Shao X, Yang Y, Wang Y, Qian Y, Wang J. The amount of viable myocardium predicts left ventricular functional improvement and volume reduction in patients with coronary artery disease after coronary artery bypass grafting. Int J Clin Exp Med. 2017;10(9):13491–9.

210. McKay RG, Pfeffer MA, Pasternak RC, Markis JE, Come PC, Nakao S, Alderman JD, Ferguson JJ, Safian RD, Grossman W. Left ventricular remodeling after myocardial infarction: a corollary to infarct expansion. Circulation. 1986;74(4):693–702.

211. Pfeffer MA, Pfeffer JM. Ventricular enlargement and reduced survival after myocardial infarction. Circulation. 1987;75(5 Pt 2):IV93–7.

212. Smiseth OA, Torp H, Opdahl A, Haugaa KH, Urheim S. Myocardial strain imaging: how useful is it in clinical decision making? European Heart Journal. 2015;37(15):1196–207.

213. Anand IS, Florea VG, Solomon SD, Konstam MA, Udelson JE. Noninvasive assessment of left ventricular remodeling: concepts, techniques, and implications for clinical trials. J Card Fail. 2002;8(6 Suppl):S452–64.

214. White HD, Norris RM, Brown MA, Brandt PW, Whitlock R, Wild CJ. Left ventricular end-systolic volume as the major determinant of survival after recovery from myocardial infarction. Circulation. 1987;76(1):44–51.

215. Antman EM, Anbe DT, Armstrong PW, Bates ER, Green LA, Hand M, Hochman JS, Krumholz HM, Kushner FG, Lamas GA, Mullany CJ, Ornato JP, Pearle DL, Sloan MA, Smith SC, Jr., American College of C, American Heart A, Canadian Cardiovascular S. ACC/AHA guidelines for the management of patients with ST-elevation myocardial infarction--executive summary. A report of the American College of Cardiology/American Heart Association Task Force on Practice Guidelines (Writing Committee to revise the 1999 guidelines for the management of patients with acute myocardial infarction). J Am Coll Cardiol. 2004;44(3):671–719.

216. Bing R, Dweck MR. Myocardial fibrosis: why image, how to image and clinical implications. Heart. 2019;105(23):1832–40.

217. Migrino RQ, Young JB, Ellis SG, White HD, Lundergan C, Miller DP, Granger CB, Ross AM, Califf RM, Topol EJ. End-systolic volume index at 90 to 180 minutes into reperfusion therapy for acute myocardial infarction is a strong predictor of early and late mortality. The Global Utilization of Streptokinase and t-PA for Occluded Coronary Arteries (GUSTO)-I Angiographic Investigators. Circulation. 1997;96(1):116–21.

218. Ypenburg C, Schalij MJ, Bleeker GB, Steendijk P, Boersma E, Dibbets-Schneider P, Stokkel MP, van der Wall EE, Bax JJ. Impact of viability and scar tissue on response to cardiac resynchronization therapy in ischaemic heart failure patients. European heart journal. 2007;28(1):33–41.

219. Tibshirani R. Regression shrinkage and selection via the lasso. Journal of the Royal Statistical Society Series B: Statistical Methodology. 1996;58(1):267–88.

220. Chen C, Rodriguez L, Levine RA, Weyman AE, Thomas JD. Noninvasive measurement of the time constant of left ventricular relaxation using the continuous-wave Doppler velocity profile of mitral regurgitation. Circulation. 1992;86(1):272–8.
221. Bastos MB, Burkhoff D, Maly J, Daemen J, Den Uil CA, Ameloot K, Lenzen M, Mahfoud F, Zijlstra F, Schreuder JJ. Invasive left ventricle pressure–volume analysis: overview and practical clinical implications. European heart journal. 2020;41(12):1286–97.
222. Sasagawa S, Nishimura Y, Okabe S, Murakami S, Ashikawa Y, Yuge M, Kawaguchi K, Kawase R, Okamoto R, Ito M. Downregulation of GSTK1 is a common mechanism underlying hypertrophic cardiomyopathy. Frontiers in pharmacology. 2016;7:162.
223. Dludla PV, Silvestri S, Orlando P, Mazibuko-Mbeje SE, Johnson R, Marcheggiani F, Cirilli I, Muller CJ, Louw J, Chellan N. Palmitate-induced toxicity is associated with impaired mitochondrial respiration and accelerated oxidative stress in cultured cardiomyocytes: The critical role of coenzyme Q9/10. Toxicology in Vitro. 2020;68:104948.
224. Luo A, Jia Y, Hao R, Zhou X, Bao C, Yang L, Gu C, Tang H, Chu A-A. Proteomic and phosphoproteomic analysis of right ventricular hypertrophy in the Pulmonary Hypertension rat model. Journal of Proteome Research. 2023;23(1):264–76.
225. Yamazaki T, Wälchli S, Fujita T, Ryser S, Hoshijima M, Schlegel W, Kuroda Si, Maturana AD. Splice variants of enigma homolog, differentially expressed during heart development, promote or prevent hypertrophy. Cardiovascular research. 2010;86(3):374–82.
226. Liang R, Shen X, Wang F, Wang X, DesJarlais A, Syed A, Saba R, Tan Z, Yu F, Ji X. H19X-encoded miR-322 (424)/miR-503 regulates muscle mass by targeting translation initiation factors. Journal of cachexia, sarcopenia and muscle. 2021;12(6):2174–86.
227. Filomena MC, Yamamoto DL, Carullo P, Medvedev R, Ghisleni A, Piroddi N, Scellini B, Crispino R, D'Autilia F, Zhang J. Myopalladin knockout mice develop cardiac dilation and show a maladaptive response to mechanical pressure overload. Elife. 2021;10:e58313.

228. McLendon JM, Zhang X, Matasic DS, Kumar M, Koval OM, Grumbach IM, Sadayappan S, London B, Boudreau RL. Knockout of sorbin and SH3 domain containing 2 (Sorbs2) in cardiomyocytes leads to dilated cardiomyopathy in mice. Journal of the American Heart Association. 2022;11(13):e025687.
229. Raabe J. Role of the nebulin related anchoring protein–NRAP in the development of heart disease: Staats-und Universitätsbibliothek Hamburg Carl von Ossietzky; 2023.
230. Zhou H, Shen D-F, Bian Z-Y, Zong J, Deng W, Zhang Y, Guo Y-Y, Li H, Tang Q-Z. Activating Transcription Factor 3 Deficiency Promotes Cardiac Hypertrophy, Dysfunction, and Fibrosis Induced by Pressure Overload. PLOS ONE. 2011;6(10):e26744.
231. Davis J. Putting the Brakes on Hypertensive Remodeling: An ATF3 Mechanism of Myofibroblast Restraint. Circulation. 2017;135(21):2058–61.
232. Popay TM, Wang J, Adams CM, Howard GC, Codreanu SG, Sherrod SD, McLean JA, Thomas LR, Lorey SL, Machida YJ, Weissmiller AM, Eischen CM, Liu Q, Tansey WP. MYC regulates ribosome biogenesis and mitochondrial gene expression programs through its interaction with host cell factor–1. eLife. 2021;10:e60191.
233. Ahuja P, Zhao P, Angelis E, Ruan H, Korge P, Olson A, Wang Y, Jin ES, Jeffrey FM, Portman M, Maclellan WR. Myc controls transcriptional regulation of cardiac metabolism and mitochondrial biogenesis in response to pathological stress in mice. J Clin Invest. 2010;120(5):1494–505.
234. Carroll PA, Freie BW, Mathsyaraja H, Eisenman RN. The MYC transcription factor network: balancing metabolism, proliferation and oncogenesis. Front Med. 2018;12(4):412–25.
235. Zhang W, Elimban V, Nijjar MS, Gupta SK, Dhalla NS. Role of mitogen-activated protein kinase in cardiac hypertrophy and heart failure. Exp Clin Cardiol. 2003;8(4):173–83.
236. Ahuja P, Zhao P, Angelis E, Ruan H, Korge P, Olson A, Wang Y, Jin ES, Jeffrey FM, Portman M, MacLellan WR. Myc controls transcriptional regulation of cardiac metabolism and mitochondrial biogenesis in response to pathological stress in mice. The Journal of Clinical Investigation. 2010;120(5):1494–505.

237. Zhu J, Blenis J, Yuan J. Activation of PI3K/Akt and MAPK pathways regulates Myc-mediated transcription by phosphorylating and promoting the degradation of Mad1. Proc Natl Acad Sci U S A. 2008;105(18):6584–9.
238. Lopaschuk GD, Karwi QG, Tian R, Wende AR, Abel ED. Cardiac Energy Metabolism in Heart Failure. Circulation Research. 2021;128(10):1487–513.
239. Nomura S, Satoh M, Fujita T, Higo T, Sumida T, Ko T, Yamaguchi T, Tobita T, Naito AT, Ito M, Fujita K, Harada M, Toko H, Kobayashi Y, Ito K, Takimoto E, Akazawa H, Morita H, Aburatani H, Komuro I. Cardiomyocyte gene programs encoding morphological and functional signatures in cardiac hypertrophy and failure. Nature Communications. 2018;9(1):4435.
240. Sikking Maurits A, Stroeks Sophie LVM, Marelli-Berg F, Heymans Stephane RB, Ludewig B, Verdonschot Job AJ. Immunomodulation of Myocardial Fibrosis. JACC: Basic to Translational Science. 2023;8(11):1477–88.
241. von Scheidt M, Zhao Y, de Aguiar Vallim TQ, Che N, Wierer M, Seldin MM, Franzén O, Kurt Z, Pang S, Bongiovanni D, Yamamoto M, Edwards PA, Ruusalepp A, Kovacic JC, Mann M, Björkegren JLM, Lusis AJ, Yang X, Schunkert H. Transcription Factor MAFF (MAF Basic Leucine Zipper Transcription Factor F) Regulates an Atherosclerosis Relevant Network Connecting Inflammation and Cholesterol Metabolism. Circulation. 2021;143(18):1809–23.
242. Jiang D-S, Li L, Huang L, Gong J, Xia H, Liu X, Wan N, Wei X, Zhu X, Chen Y, Chen X, Zhang X-D, Li H. Interferon Regulatory Factor 1 Is Required for Cardiac Remodeling in Response to Pressure Overload. Hypertension. 2014;64(1):77–86.
243. Jiang D-S, Li L, Huang L, Gong J, Xia H, Liu X, Wan N, Wei X, Zhu X, Chen Y, Zhang X-d, Li H. Interferon Regulatory Factor 1 Is Required for Cardiac Remodeling in Response to Pressure Overload. Hypertension. 2014;64.
244. Yan L, Wang J, Cai X, Liou Y-C, Shen H-M, Hao J, Huang C, Luo G, He W. Macrophage plasticity: signaling pathways, tissue repair, and regeneration. MedComm. 2024;5(8):e658.
245. Katsuoka F, Motohashi H, Ishii T, Aburatani H, Engel JD, Yamamoto M. Genetic evidence that small maf proteins are essential for the activation of antioxidant response element-dependent genes. Mol Cell Biol. 2005;25(18):8044–51.

246. Averill-Bates D. Reactive oxygen species and cell signaling. Review. Biochimica et Biophysica Acta (BBA) - Molecular Cell Research. 2024;1871(2):119573.
247. Wang X, Zhang Y, Wan X, Guo C, Cui J, Sun J, Li L. Responsive Expression of MafF to β-Amyloid-Induced Oxidative Stress. Dis Markers. 2020;2020:8861358.
248. Moran JA, Dahl EL, Mulcahy RT. Differential induction of mafF, mafG and mafK expression by electrophile-response-element activators. Biochem J. 2002;361(Pt 2):371–7.
249. Pikkarainen S, Tokola H, Kerkelä R, Ruskoaho H. GATA transcription factors in the developing and adult heart. Cardiovasc Res. 2004;63(2):196–207.
250. Fan C, Ouyang P, Timur AA, He P, You SA, Hu Y, Ke T, Driscoll DJ, Chen Q, Wang QK. Novel roles of GATA1 in regulation of angiogenic factor AGGF1 and endothelial cell function. J Biol Chem. 2009;284(35):23331–43.
251. Zaytouni T, Efimenko EE, Tevosian SG. 4 - GATA Transcription Factors in the Developing Reproductive System. In: Friedmann T, Dunlap JC, Goodwin SF, editors. Advances in Genetics. 76: Academic Press; 2011. p. 93–134.
252. Inazumi H, Kuwahara K. NRSF/REST-Mediated Epigenomic Regulation in the Heart: Transcriptional Control of Natriuretic Peptides and Beyond. Biology (Basel). 2022;11(8).
253. Jin L, Liu Y, Wu Y, Huang Y, Zhang D. REST Is Not Resting: REST/NRSF in Health and Disease. Biomolecules. 2023;13(10):1477.
254. Vo L, Schmidtke MW, Da Rosa-Junior NT, Ren M, Schlame M, Greenberg ML. Cardiolipin metabolism regulates expression of muscle transcription factor MyoD1 and muscle development. J Biol Chem. 2023;299(3):102978.
255. Yohe ME, Gryder BE, Shern JF, Song YK, Chou HC, Sindiri S, Mendoza A, Patidar R, Zhang X, Guha R, Butcher D, Isanogle KA, Robinson CM, Luo X, Chen JQ, Walton A, Awasthi P, Edmondson EF, Difilippantonio S, Wei JS, Zhao K, Ferrer M, Thomas CJ, Khan J. MEK inhibition induces MYOG and remodels super-enhancers in RAS-driven rhabdomyosarcoma. Sci Transl Med. 2018;10(448).
256. Dahl JS, Barros-Gomes S, Videbæk L, Poulsen MK, Issa IF, Carter-Storch R, Christensen NL, Kumme A, Pellikka PA, Møller JE. Early diastolic strain rate in relation to systolic and diastolic function and prognosis in aortic stenosis. JACC: Cardiovascular Imaging. 2016;9(5):519–28.

257. Dokainish H. Left ventricular diastolic function and dysfunction: Central role of echocardiography. Global Cardiology Science and Practice. 2015;2015(1):3.

258. Myreng Y, Smiseth OA. Assessment of left ventricular relaxation by Doppler echocardiography. Comparison of isovolumic relaxation time and transmitral flow velocities with time constant of isovolumic relaxation. Circulation. 1990;81(1):260–6.

259. Yu WC, Chiou KR, Lin YP, Lee WH, Huang WB, Chen CH. Non-invasive determination of left ventricular relaxation time constant by Transthoracic Doppler echocardiography. Journal of the Chinese Medical Association: JCMA. 2004;67(7):317–22.

260. Nagueh SF, Appleton CP, Gillebert TC, Marino PN, Oh JK, Smiseth OA, Waggoner AD, Flachskampf FA, Pellikka PA, Evangelisa A. Recommendations for the evaluation of left ventricular diastolic function by echocardiography. European journal of echocardiography. 2009;10(2):165–93.

261. Nagueh SF, Smiseth OA, Appleton CP, Byrd BF, Dokainish H, Edvardsen T, Flachskampf FA, Gillebert TC, Klein AL, Lancellotti P. Recommendations for the evaluation of left ventricular diastolic function by echocardiography: an update from the American Society of Echocardiography and the European Association of Cardiovascular Imaging. European Journal of Echocardiography. 2016;17(12):1321–60.

262. Plitt GD, Spring JT, Moulton MJ, Agrawal DK. Mechanisms, diagnosis, and treatment of heart failure with preserved ejection fraction and diastolic dysfunction. Expert Rev Cardiovasc Ther. 2018;16(8):579–89.

9. Bibliography of the candidates publications

Scientific publications involved in the current dissertation

Barta Bálint András, Ruppert Mihály, Frohlich Klemens Erwin, Cosenza-Contreras Miguel, Oláh Attila, Sayour Alex Ali, Kovács Krisztián, Karvaly Gellért Balázs, Biniossek Martin, Merkely Béla, Schilling Oliver, Radovits Tamás
Sex-related differences of early cardiac functional and proteomic alterations in a rat model of myocardial ischemia
JOURNAL OF TRANSLATIONAL MEDICINE 19: 1 Paper: 507, 15 p. (2021)
IF: 8,448

Ruppert Mihály*, Barta Bálint András*, Korkmaz-Icöz Sevil, Loganathan Sivakkanan, Oláh Attila, Sayour Alex Ali, Benke Kálmán, Nagy Dávid, Bálint Tímea, Karck Matthias, Schilling Oliver, Merkely Béla, Radovits Tamás, Szabó Gábor
Sex similarities and differences in the reverse and anti-remodeling effect of pressure unloading therapy in a rat model of aortic banding and debanding
AMERICAN JOURNAL OF PHYSIOLOGY: HEART AND CIRCULATORY PHYSIOLOGY 323: 1 pp. H204-H222. (2022)
*Shared first authors
IF: 4,8

Myocardial Active Relaxation Mirrors the Myocardial Proteome in Remodelling and Reverse Remodelling by Bálint András Barta, Sylvia Spiesshofer, Mihály Ruppert, Niko Pinter, Eva Brombacher, Clemens Kreutz, Sevil Korkmaz-Icoz, Attila Olah, Alex Ali Sayour, Gábor Szabo, Béla Merkely, Tamás Radovits, Oliver Schilling
Manuscript submitted to ESC Heart Failure

Scientific publications not involved in the current dissertation

Bálint Tímea, Ruppert Mihály, Ágg Bence, Nagy Dávid, Pálóczi Krisztina, Szenthe Kálmán, Bánáti Ferenc, Sayour Alex Ali, Oláh Attila, Barta Bálint András, Javier Barallobre-Barreiro, Ferdinandy Péter, Merkely Béla, Radovits Tamás
Atrial fibrillation is not associated with altered left atrial microRNA expression profile in patients with advanced heart failure
HEART RHYTHM 2025, 11 p. (2025)
IF: 5,8

Nagy Dávid, Onódi Zsófia, Kocsis Márton, Tóth Artúr, Bálint Tímea, Oláh Attila, Sayour Alex Ali, Barta Bálint András, Merkely Béla, Ferdinandy Péter, Radovits Tamás, Varga Zoltán V, Ruppert Mihály
Multiorgan characterization of inflammasome component expression in a rat model of advanced heart failure
ESC HEART FAILURE 12: 5 pp. 3601–3613. (2025)
IF: 3,7

Oláh Attila, Bódi Beáta, Barta Bálint András, Bottlik Olívia, Sayour Alex Ali, Ruppert Mihály, Kolodziejska Karolina Katarzyna, Kovács Andrea, Varga Zoltán V, Ferdinandy Péter, Schilling Oliver, Papp Zoltán, Merkely Béla, Radovits Tamás
Long-term exercise training is associated with unique cardiac troponin I phosphorylation pattern and benign myocardial hypertrophy in the right ventricle in an experimental model of exercise-induced myocardial remodelling
JOURNAL OF MOLECULAR AND CELLULAR CARDIOLOGY 207 pp. 81–91. (2025)
IF: 4,7

Nagy Dávid, Radovits Tamás, Bálint Tímea, Horváth Zoltán, Kocsis-Balogh Petra, Tóth Ákos Gergely, Oláh Attila, Sayour Alex Ali, Barta Bálint András, Merkely Béla, Ruppert Mihály
The anti-fibrotic effects of novel heart failure pharmacotherapies in advanced heart failure patients
BRITISH JOURNAL OF PHARMACOLOGY 2025, 15 p. (2025)
IF: 7,7

Sayour Alex Ali, Oláh Attila, Ruppert Mihály, Barta Bálint András, Merkely Béla, Radovits Tamás
Effect of pharmacological selectivity of SGLT2 inhibitors on cardiovascular outcomes in patients with type 2 diabetes: a meta-analysis
SCIENTIFIC REPORTS 14: 1 Paper: 2188, 9 p. (2024)
IF: 3,9

Székely A, Pállinger É, Töreki E, Ifju M, Barta BA, Szécsi B, Losoncz E, Dohy Z, Barabás IJ, Kosztin A, Buzás EI, Radovits T, Merkely B
Recipient Pericardial Apolipoprotein Levels Might Be an Indicator of Worse Outcomes after Orthotopic Heart Transplantation
INTERNATIONAL JOURNAL OF MOLECULAR SCIENCES 25: 3 Paper: 1752, 16 p. (2024)
IF: 4,9

Barta Bálint András*, Radovits Tamás*, Dobos Attila Balázs, Kozma Gergely Tibor, Mészáros Tamás, Berényi Petra, Facskó Réka, Fülöp Tamás, Merkely Béla, Szebeni János
Comirnaty-induced cardiopulmonary distress and other symptoms of complement-mediated pseudo-anaphylaxis in a hyperimmune pig model: Causal role of anti-PEG antibodies
VACCINE: X 19 Paper: 100497, 11 p. (2024)
*Shared first authors
IF: 2,2

Oláh A, Barta BA, Ruppert M, Sayour AA, Nagy D, Bálint T, Nagy GV, Puskás I, Szente L, Szőcs L, Sohajda T, Zima E, Merkely B, Radovits T
A Comparative Investigation of the Pulmonary Vasodilating Effects of Inhaled NO Gas Therapy and Inhalation of a New Drug Formulation Containing a NO Donor Metabolite (SIN1A)
INTERNATIONAL JOURNAL OF MOLECULAR SCIENCES 25: 7981, 12 p. (2024)
IF: 4,9

Vogele Daniel, Woehrle Svenja, Saller Benedikt S, Froehlich Klemens, Barta Bálint András, Cosenza-Contreras Miguel, Gross Olaf, Schilling Oliver
Size exclusion chromatography based proteomic and degradomic profiling of inflammasome-activated, murine bone marrow-derived dendritic cells highlights complex retention and release of cleavage products
MOLECULAR OMICS 20: 9 pp. 595–610. (2024)
IF: 2,4

Kökény Gábor, Bakos Tamás, Barta Bálint András, Nagy Georgina Viktória, Mészáros Tamás, Kozma Gergely Tibor, Szabó András, Szebeni János, Merkely Béla, Radovits Tamás
Zymosan Particle-Induced Hemodynamic, Cytokine and Blood Cell Changes in Pigs: An Innate Immune Stimulation Model with Relevance to Cytokine Storm Syndrome and Severe COVID-19
INTERNATIONAL JOURNAL OF MOLECULAR SCIENCES 24: 1138, 18 p. (2023)
IF: 4,9

Kocsmár Éva, Schmid Marlene, Cosenza-Contreras Miguel, Kocsmár Ildikó, Föll Melanie, Krey Leah, Barta Bálint András, Rácz Gergely, Kiss András, Werner Martin, Schilling Oliver, Lotz Gábor, Bronsert Peter
Proteome alterations in human autopsy tissues in relation to time after death
CELLULAR AND MOLECULAR LIFE SCIENCES 80: 117, 15 p. (2023)
IF: 6,2

Oláh A, Sayour AA, Ruppert M, Barta BA, Merkely B, Kovács A, Radovits T
Dynamics of exercise training and detraining induced cardiac adaptations

CURRENT OPINION IN PHYSIOLOGY 33 Paper: 100657, 7 p. (2023)
IF: 2,5

Siegel Patrick Malcolm*, Barta Bálint András*, Orlean Lukas, Steenbuck Ines Derya, Cosenza-Contreras Miguel, Wengenmayer Tobias, Trummer Georg, Wolf Dennis, Westermann Dirk, Schilling Oliver, Diehl Philipp
The serum proteome of VA-ECMO patients changes over time and allows differentiation of survivors and non-survivors: an observational study
JOURNAL OF TRANSLATIONAL MEDICINE 21: 1 Paper: 319, 12 p. (2023)
*Shared first authors
IF: 6,1

Ruppert Mihály, Korkmaz-Icöz Sevil, Benczik Bettina, Ágg Bence, Nagy Dávid, Bálint Tímea, Sayour Alex Ali, Oláh Attila, Barta Bálint András, Benke Kálmán, Ferdinandy Péter, Matthias Karck, Merkely Béla, Radovits Tamás, Szabó Gábor
Pressure overload-induced systolic heart failure is associated with characteristic myocardial microRNA expression signature and post-transcriptional gene regulation in male rats
SCIENTIFIC REPORTS 13: 1 Paper: 16122, 12 p. (2023)
IF: 3,8

Tokodi Márton, Oláh Attila, Fábián Alexandra, Lakatos Bálint Károly, Hizoh István, Ruppert Mihály, Sayour Alex Ali, Barta Bálint András, Kiss Orsolya, Sydó Nóra, Csulak Emese, Ladányi Zsuzsanna, Merkely Béla, Kovács Attila, Radovits Tamás
Novel insights into the athlete’s heart: is myocardial work the new champion of systolic function?
EUROPEAN HEART JOURNAL–CARDIOVASCULAR IMAGING 23: 2 pp. 188–197. (2022)
IF: 6,3

Dézsi László, Mészáros Tamás, Kozma Gergely Tibor, H-Velkei Mária, Oláh Csaba Zs, Szabó Miklós,Patkó Zsófia, Fülöp Tamás, Hennies Mark, Szebeni Miklós, Barta Bálint

András, Merkely Béla, Radovits Tamás, Szebeni János
A naturally hypersensitive porcine model may help understand the mechanism of COVID-19 mRNA vaccine-induced rare (pseudo) allergic reactions: complement activation as a possible contributing factor
GEROSCIENCE 44: 2 pp. 597–618. (2022)
IF: 5,6

Lakatos Bálint Károly, Ruppert Mihály, Tokodi Márton, Oláh Attila, Braun Szilveszter, Karime Christian, Ladányi Zsuzsanna, Sayour Alex Ali, Barta Bálint András, Merkely Béla, Radovits Tamás, Kovács Attila
Myocardial work index: a marker of left ventricular contractility in pressure- or volume overload-induced heart failure
ESC HEART FAILURE 8: 3 pp. 2220–2231. (2021)
IF: 3,612

Oláh Attila, Barta Bálint András, Sayour Alex Ali, Ruppert Mihály, Virág-Tulassay Eszter, Novák Julianna, Varga Zoltán V, Ferdinandy Péter, Merkely Béla, Radovits Tamás
Balanced Intense Exercise Training Induces Atrial Oxidative Stress Counterbalanced by the Antioxidant System and Atrial Hypertrophy That Is Not Associated with Pathological Remodeling or Arrhythmogenicity
ANTIOXIDANTS 10: 3 Paper: 452, 16 p. (2021)
IF: 7,675

Sayour Alex Ali, Ruppert Mihály, Oláh Attila, Benke Kálmán, Barta Bálint András, Zsáry Eszter, Ke Haoran, Horváth Eszter Mária, Merkely Béla, Radovits Tamás
Left Ventricular SGLT1 Protein Expression Correlates with the Extent of Myocardial Nitro-Oxidative Stress in Rats with Pressure and Volume Overload-Induced Heart Failure
ANTIOXIDANTS 10: 8 Paper: 1190, 14 p. (2021)
IF: 7,675

Sayour AA, Ruppert M, Oláh A, Benke K, Barta BA, Zsáry E, Merkely B, Radovits T
Effects of SGLT2 inhibitors beyond glycemic control—focus on myocardial SGLT1

INTERNATIONAL JOURNAL OF MOLECULAR SCIENCES 22: 18 Paper: 9852, 14 p. (2021)
IF: 6,208

Bódi B, Kovács Á, Gulyás H, Mártha L, Tóth A, Mátyás C, Barta BA, Oláh A, Merkely B, Radovits T, Papp Z
Long-term PDE-5A inhibition improves myofilament function in left and right ventricular cardiomyocytes through partially different mechanisms in diabetic rat hearts
ANTIOXIDANTS 10: 11 Paper: 1776, 13 p. (2021)
IF: 7,675

Török Marianna, Monori-Kiss Anna, Pál Éva, Horváth Eszter, Jósvai Attila, Merkely Petra, Barta Bálint András, Mátyás Csaba, Oláh Attila, Radovits Tamás, Merkely Béla, Ács Nándor, Nádasy György László, Várbíró Szabolcs
Long-term exercise results in morphological and biomechanical changes in coronary resistance arterioles in male and female rats
BIOLOGY OF SEX DIFFERENCES 11: 1 Paper: 7, 14 p. (2020)
IF: 5,027

Ruppert Mihály, Lakatos Bálint Károly, Braun Szilveszter, Tokodi Márton, Karime Christian, Oláh Attila, Sayour Alex Ali, Hizoh István, Barta Bálint András, Merkely Béla, Kovács Attila, Radovits Tamás
Longitudinal Strain Reflects Ventriculoarterial Coupling Rather Than Mere Contractility in Rat Models of Hemodynamic Overload–Induced Heart Failure
JOURNAL OF THE AMERICAN SOCIETY OF ECHOCARDIOGRAPHY 33: 10 pp. 1264–1275.e4. (2020)
IF: 5,251

Sayour Alex Ali, Oláh Attila, Ruppert Mihály, Barta Bálint András, Horváth Eszter Mária, Benke Kálmán, Pólos Miklós, Hartyánszky István, Merkely Béla, Radovits Tamás
Characterization of left ventricular myocardial sodium-glucose cotransporter 1 expression in patients with end-stage heart failure
CARDIOVASCULAR DIABETOLOGY 19: 1 Paper: 159, 16 p. (2020)
IF: 9,951

Gazdag Péter, Oravecz Kinga, Acsai Károly, Demeter-Haludka Vivien, Ördög Balázs, Szlovák Jozefina, Kohajda Zsófia, Polyák Alexandra, Barta Bálint András, Oláh Attila, Radovits Tamás, Merkely Béla, Papp Julius Gy, Baczkó István, Varró András, Nagy Norbert, Prorok János
Increased Ca^{2+} content of the sarcoplasmic reticulum provides arrhythmogenic trigger source in swimming-induced rat athlete's heart model
SCIENTIFIC REPORTS 10: 1 Paper: 19596, 13 p. (2020)
IF: 4,380

Oláh Attila, Kovács Attila, Lux Árpád, Tokodi Márton, Braun Szilveszter, Lakatos Bálint Károly, Mátyás Csaba, Kellermayer Dalma, Ruppert Mihály, Sayour Alex Ali, Barta Bálint András, Merkely Béla, Radovits Tamás
Characterization of the dynamic changes in left ventricular morphology and function induced by exercise training and detraining
INTERNATIONAL JOURNAL OF CARDIOLOGY 277 pp. 178–185. (2019)
IF: 3,229

Ruppert M, Korkmaz-Icöz S, Loganathan S, Jiang W, Oláh A, Sayour AA, Barta BA, Karime C, Merkely B, Karck M, Radovits T, Szabó G
Incomplete structural reverse remodeling from late-stage left ventricular hypertrophy impedes the recovery of diastolic but not systolic dysfunction in rats
JOURNAL OF HYPERTENSION 37: 6 pp. 1200–1212. (2019)
IF: 4,171

Ruppert Mihály, Bódi Beáta, Korkmaz-Icöz Sevil, Loganathan Sivakkanan, Jiang Weipeng, Lehmann Lorenz, Oláh Attila, Barta Bálint András, Sayour Alex Ali, Merkely Béla, Matthias Karck, Papp Zoltán, Szabó Gábor, Radovits Tamás
Myofilament Ca^{2+} sensitivity correlates with left ventricular contractility during the progression of pressure overload-induced left ventricular myocardial hypertrophy in rats
JOURNAL OF MOLECULAR AND CELLULAR CARDIOLOGY 129 pp. 208–218. (2019)
IF: 4,133

Oláh Attila, Mátyás Csaba, Kellermayer Dalma, Ruppert Mihály, Barta Bálint András, Sayour Alex Ali, Török Marianna, Koncsos Gábor, Giricz Zoltán, Ferdinandy Péter, Merkely Béla, Radovits Tamás
Sex Differences in Morphological and Functional Aspects of Exercise-Induced Cardiac Hypertrophy in a Rat Model
FRONTIERS IN PHYSIOLOGY 10 Paper: 889, 11 p. (2019)
IF: 3,367

Mátyás C, Kovács A, Németh BT, Oláh A, Braun S, Tokodi M, Barta BA, Benke K, Ruppert M, Lakatos BK, Merkely B, Radovits T
Comparison of speckle-tracking echocardiography with invasive hemodynamics for the detection of characteristic cardiac dysfunction in type-1 and type-2 diabetic rat models
CARDIOVASCULAR DIABETOLOGY 17: 1 Paper: 13, 13 p. (2018)
IF: 5,948

Ruppert M*, Barta BA*, Korkmaz-Icöz S, Li S, Oláh A, Mátyás Cs, Németh BT, Benke K, Sayour AA, Karck M, Merkely B, Radovits T, Szabó G
A hipertrófiás myocardium reverz elektromos remodellációjának vizsgálata patkánymodellben
CARDIOLOGIA HUNGARICA 48: 2 pp. 118–128. (2018)
*Shared first authors

Ruppert M, Korkmaz-Icoz S, Loganathan S, Jiang W, Lehmann LH, Oláh A, Sayour AA, Barta BA, Merkely B, Karck M, Radovits T, Szabó G
Pressure-volume analysis reveals characteristic sex-related differences in cardiac function in a rat model of aortic banding-induced myocardial hypertrophy
AMERICAN JOURNAL OF PHYSIOLOGY: HEART AND CIRCULATORY PHYSIOLOGY 315: 3 pp. H502–H511. (2018)
IF: 4,048

Mátyás C, Németh BT, Oláh A, Török M, Ruppert M, Kellermayer D, Barta BA, Szabó G, Kökény G, Horváth EM, Bódi B, Papp Z, Merkely B, Radovits T
Prevention of the development of heart failure with preserved ejection fraction by the phosphodiesterase-5A inhibitor vardenafil in rats with type 2 diabetes
EUROPEAN JOURNAL OF HEART FAILURE 19: 3 pp. 326–336. (2017)
IF: 10,683

10. Acknowledgements

This PhD thesis would not have been possible without the generous support, guidance, and collegiality of many people at both partner institutions.

At Semmelweis University, Heart and Vascular Center, I am deeply grateful to my Hungarian supervisor, the Head of the Scientific Research Laboratory, Prof. Tamás Radovits, for mentorship, critical feedback, and creating an inspiring research environment; and to the institute director, Prof. Béla Merkely, for supporting this project and hosting my work. I also thank our technical assistants Henriett Biró, Benjamin Prokaj, Gabriella Juhász, Zoltán Manhertz, Dóra Juhász, Dóra Szkrajcsis, Ádám Steiner, Zsombor Fáskerti, Péter Andrássy, Daria Chalkova for their expert help with hemodynamics, histology, and sample preparation. My fellow students and colleagues Dr. Attila Oláh, Dr. Csaba Mátyás, Dr. Mihály Ruppert, Dr. Alex Ali Sayour, Dr. Kálmán Benke, Dr. Tímea Bálint, Dr. Dávid Nagy, Dr. Attila Balázs Dobos, and Dr. Ákos Gergely Tóth made daily lab life productive and enjoyable through thoughtful discussions and constant teamwork.

At Albert-Ludwigs-Universität Freiburg, Institute of Surgical Pathology, I warmly thank my German supervisor, the leader of the Translational Proteomics Laboratory, Prof. Oliver Schilling, for introducing me to proteomics as well as guidance on study design, data interpretation, and manuscript preparation; and the Institute Director, Prof. Martin Werner, for the opportunity to carry out the work. I am indebted to the technical team led by Bettina Wehrle for their meticulous operation of instrumentation and assistance with sample processing and data handling. I am equally grateful to my fellow students and colleagues Dr. Klemens Fröhlich, Dr. Alison Chaves, Dr. Stefan Tholen, Dr. Matthias Fahrner, Dr. Melanie Föll, Dr. Niko Pinter, Dr. Maren Stillger, Dr Thien-Ly Dinh, Dr. Tilman Werner, Dr. Andreas Weber, Dr. Miguel Cosenza-Contreras, Dr. Ada Seredysnka, Dr. Johanna Thiery and Lina Goncharenko for their readiness to teach, support and provide mutual help along the journey.

I would like to acknowledge the students I had the privilege to supervise, Sylvia Spiesshofer, Albert Husznai, Olívia Bottlik, Tracy Kazondanga, and Alina Semenjakin for their curiosity, persistence, and contributions to experiments and analyses included in this thesis. Mentoring you has been one of the most rewarding parts of this journey.

I extend my sincere thanks to both doctoral schools—the Doctoral School of Semmelweis University and the Faculty of Biology at Albert-Ludwigs-Universität Freiburg—for their support in establishing and coordinating the shared cotutelle PhD program. Your help with the cotutelle agreement, administrative procedures, mobility, and joint supervision made this collaboration possible. I gratefully acknowledge the support of the Jellinek Harry Scholarship, which enabled research stays crucial to this thesis. I also thank the International Office of Semmelweis University for their careful guidance with mobility arrangements, documentation, and the countless administrative details between two universities.

Finally, my deepest thanks go to my family for their steady encouragement and patience throughout this journey.

11. Kurze Zusammenfassung auf deutsch

Diese Dissertation verknüpft drei komplementäre Experimente zu einem Gesamtbild darüber, wie sich das Säugerherz strukturell und funktionell umbildet und wieder zurückbildet, wenn es zunächst durch diffuse Ischämie oder chronische Druckbelastung geschädigt wird und diese Last anschließend entfällt. Durch die Kombination von Druck-Volumen-Hämodynamik, Tandem-Mass-Tag-Proteomik und gezielten Steroidprofilen war es möglich, eine direkte Linie von der mechanischen Leistung zu den molekularen Schaltkreisen zu ziehen, welche Erholung ermöglichen oder verhindern.

Im Isoproterenol-Modell der globalen Ischämie wiesen männliche und weibliche Ratten vergleichbare histologische Schäden auf, doch der Verlauf wies entscheidende Unterschiede auf. Weibliche Tiere behielten eine Kontraktilitätsreserve: Druck-/Volumen-Schleifen zeigten erhaltene vorlastrekrutierbare Schlagarbeit und Ejektionsfraktion, während bei männlichen Ratten beide Parameter nachließen. Die Proteomik liefert einen Hinweis auf mögliche Wirkungsmechanismen dieser Resultate: Weibliche Herzen aktivierten einen „Notfall-Werkzeugkasten“ aus Zytoskelett-Reparaturproteinen und Stress-Chaperonen – ACTN2, TPM1, ORP-150, HSP90, CALR – und stabilisierten so die Erregungs-Kontraktions-Kopplung. Männliche Herzen wiesen hingegen eine Downregulation der Schlüsselenzyme des Citratzyklus und der Fettsäure-β-Oxidation auf – ein metabolischer Kollaps, der sich in sinkender kardialer Effizienz widerspiegelte. Dieser frühe Vorteil der Weibchen hatte einen diastolischen Preis: Der enddiastolische Druck und die Relaxationszeitkonstante τ stiegen nur bei Weibchen – parallel zu einem inflammatorischen Proteom, das wahrscheinlich für die langfristige Narbenreifung nötig ist. Geschlechtshormone liefern einen möglichen Erklärungsfaden. Von Dutzenden gemessenen Steroiden stratifizierten die Östron-Metabolite 2-Hydroxy- und 4-Hydroxy-E1 weibliche Tiere in milde versus schwere Funktionsstörungen; ersteres korrelierte mit mitochondrialen Brennstoffenzymen, letzteres mit Aktin-Montage-Modulen – ein Hinweis auf metabolitspezifische Kontrolle der Erholungswege.

Das Aortenbanding rekonstruierte eine Druck-Hypertrophie, das Debanding eine chirurgische Entlastung. Beide Geschlechter entwickelten ähnliche myokardiale Wandverdickungen, doch Männchen verloren ihre anfängliche Kontraktilitätssteigerung bis Woche zwölf, während die diastolische Relaxation sich verschlechterte. Weibchen hielten die Funktion aufrecht.

Nach Bandentfernung besserten sich beide Geschlechter, allerdings auf unterschiedlichen Ebenen. Weibchen zeigten die sauberere strukturelle Umkehr – stärkeren Rückgang der interstitiellen Fibrose, Normalisierung des fetalen myh7/myh6-Verhältnisses und nahezu vollständige Wiederherstellung der Lipid-Oxidations-Proteine. Männchen verzeichneten paradoxerweise die größere funktionelle Erholung in Ejektionsfraktion, Ventrikel-Gefäß-Kopplung und τ; dieser Aufschwung glich jedoch nur einen vorherigen steileren Abfall aus. Proteomisch setzten Männchen auf zytoskelettales Remodeling und gedrosselte Peptidsynthese, während bei Weibchen eine inflammatorisch-metabolische Rückstellung auffiel, welches eine Spiegelung ihres postischämischen Profils darstellt.

Eine fokussierte Re-Analyse der Banding-Daten schloss den Kreis zwischen Mechanik und Molekülen. LASSO-Regression isolierte τ – den Index der aktiven Relaxation – als hämodynamische Variable mit der engsten Verflechtung proteomischer Änderungen. Zweiundzwanzig τ-gekoppelte Proteine, darunter GSTK1, COQ9 und PDLIM5, differenzierten Belastungszustände mit hoher Sensitivität und Spezifität. Netzwerkanalysen ergaben drei dichte Module: kontraktile/antioxidative, nukleo-zytoskelettale/metabolische und Signal-/Chromatin-Cluster. Eine Upstream-Regulator-Analyse hob MYC/MAX, MYOD/MYOG, ATF3 und MAFF als Transkriptionsfaktoren hervor, die mechanische Last, metabolischen Stress und Hormonsignale integrieren.

Biologisches Geschlecht färbt jede Schicht der kardialen Anpassung. Weibchen puffern einen frühen systolischen Verlust ab, zahlen dafür aber einen temporären diastolischen Tribut; Männchen erliegen der Last früher, können jedoch nach Druckentlastung eindrucksvoll zurückkehren. Metabolische Plastizität, welche bei Weibchen erhalten bleibt und bei Männchen brüchig wird – erweist sich als wichtiger Faktor. Östrogen-Metabolite, nicht nur Östradiol, tragen dazu bei, die Zytoskelett-Reparatur und oxidativen Metabolismus zu steuern. Praktisch fungiert τ als molekulares Barometer: Weil es tiefe proteomische Verschiebungen spiegelt, könnten nichtinvasive Surrogate der aktiven Relaxation als Frühmarker für Remodeling und seine Umkehr dienen. Indem die Arbeit geschlechterspezifische therapeutische Fenster und τ-gebundene Proteinpanels als Kandidat-Biomarker hervorhebt, ebnet sie den Weg für metabolit-gezielte Strategien zur präziseren kardialen Erholung.

12. Rövid összefoglalás magyar nyelven

A disszertáció célja, hogy egységes képet nyújtson a patkány miokardium remodellációjáról diffúz iszkémiás károsodás vagy krónikus nyomásterhelés során, valamint reverz remodellációjáról a nyomásterhelés csökkentését követően. Ehhez elsősorban bal kamrai nyomás–térfogat (PV) analízis, exploratív proteomika és keringő szteroid hormonszint mérések módszereit használja fel, majd kísérletet teszt a különböző modalitásokból származó adatok integrációjára.

A globális miokardiális iszkémia isoproterenol indukált patkánymodelljében a hím és a nőstény állatok hasonló mértékű szövettani károsodást szenvedtek, kórlefolyásuk azonban azonnal divergált. A nőstények megőrizték kontraktilis tartalékukat: a PV-hurkok a preload-recruitable stroke work (PRSW) és az ejekciós frakció (EF) megtartottságát mutatták, míg hímekben mindkettő károsodást szenvdett. A proteomikai adatok mechanisztikus magyarázatot kínáltak: a nőstény szívek citoszkeletális és chaperon fehérjéket expresszáltak (ACTN2, TPM1, ORP-150, HSP90, CALR) míg a hím szívekben a trikarboxilsav-ciklus és a zsírsav-β-oxidáció kulcsenzimeinek downregulációja volt megfigyelhető; ez a metabolikus dekompenzáció a szívizom energiahatékonyságának romlásában is tükröződött. Ezzel szemben kizárólag nőstényeknél emelkedett az vég-diasztolés nyomás (EDPVR) és a relaxáció időállandója (τ), melyet a gyulladásos fehérjék expressziójának fokozódása kísért, amely feltehetően a nőstényekre jellemző koncentrikus hipertrófiához is elengedhetetlen lehet. A számos mért keringő szteroid közül az ösztron-metabolitok (2- és 4-hidroxi-E1) alapján tudtuk elkülöníteni legsikeresebben a súlyos valamint mérsékelt miokardiális funkciócsökkenést elszenvedett patkányok csoportjait, mely összefüggést mutatott a mitokondriális enzimek és az aktin citoszkeleton alkotóinak expressziójával.

A sebészi hasi aortaszűkítés (AB) hatására mindkét nemben hasonló falvastagodás alakult ki, a hímek azonban a 12. hétre csökkent kontraktilitással bírtak, melyet a diasztolés relaxáció romlása kísért. A nőstények mindeközben megőrizték eredeti miokardiális funkciójukat. A nyomásterhelés csökkentését (DB) követően mindkét nem javulást mutatott, de eltérő mintázattal. A nőstényeknél volt kifejezettebb a strukturális visszaalakulás: nagyobb mértékben regrediált az intersticiális kollagén, normalizálódott a foetális myh7/myh6 arány, és csaknem teljesen helyreállt a lipid-oxidációs fehérjék expressziója. A hímek paradox módon nagyobb miokardiális funkció javulást mutattak

(EF, kamra–artériás csatolás, τ), ám ez csupán egy korábban meredekebb hanyatlást kompenzált, nem pedig egy magasabb, intrinzikus regenerációs kapacitást jelzett. Proteomikai szinten az AB korai stádiumában mindkét nemben csökkent a lipid és zsírsavoxidáló enzimek expressziója, de DB csoportok közül ez csak a nőstényekben normalizálódott. Az AB késői stádiumában hímekben a citoszkeletális átépülés és a peptid-bioszintézis folyamatai visszaesést mutattak, míg a nőstényekben fokozott gyulladás- és csökkent zsírsav anyagcsere bontakozott ki.

Az AB-DB adatok fókuszált újraelemzése kapcsolatot teremtett a hemodinamika és a proteom között. A LASSO-regresszió a τ-t – az aktív relaxáció indexét – azonosította a proteomikai változásokkal legszorosabban összefüggő hemodinamikai paraméterként. Huszonkét, τ-hoz kapcsolt fehérje – köztük a GSTK1, COQ9 és PDLIM5 – nagy érzékenységgel és specificitással különböztette meg az aktív remodellációt a kontroll állapottól, illetve a reverz remodellációtól. Hálózat analízisünk három, sűrűn kapcsolt modult tárt fel: kontraktilis–antioxidáns, nukleo-citoszkeletális–metabolikus, valamint jelátviteli–kromatin klasztereket. Transzkripciós faktor elemzéssel a MYC/MAX, MYOD/MYOG, ATF3 és MAFF jelátvivőket azonosítottuk, mint olyan integrátorokat, amelyek a mechanikai terhelésre adott expressziós választ vezérelhetik.

A biológiai nem a kardiális adaptáció valamennyi rétegét áthatja. A nőstények tompítják a korai szisztolés veszteséget, ugyanakkor iszkémiát követően már a korai szakban diasztolás funkciókárosodást mutatnak; a hímek miokardiális funkciója korábban csökken, viszont a nyomásterhelés csökkentést követően látványos funkcionális restitúción esnek át. A zsírsavoxidáció enzimei remodelláció során korán csökkennek, de csak nőstényekben mutatnak hajlamot a korai nyomásterhelés csökkentését követő regenerációra. Az ösztrogén-metabolitok (nem pusztán az ösztradiol) funkcionális kapuőrökként irányítják a citoszkeletális átépülést és az oxidatív anyagcserét. Gyakorlati szempontból a τ molekuláris barométerként viselkedik: mivel mély proteomikai átrendeződéseket tükröz, az aktív relaxáció nem invazív markerei érzékenyen jelezhetik a miokardiális remodellációt.